Journal Name

ARTICLE TYPE

Cite this: DOI: 10.1039/xxxxxxxxxx

Strategies for the analysis of the elemental metallic fraction of Ir and Ru oxides via XRD, XANES, and EXAFS†

Anita Hamar Reksten,[a‡] Andrea E. Russell,[b] Peter W. Richardson,[b] Stephen J. Thompson,[b] Karina Mathisen,[c] Frode Seland,[a] and Svein Sunde[d]

Received Date
Accepted Date

DOI: 10.1039/xxxxxxxxxx

www.rsc.org/journalname

Iridium and ruthenium oxide are active electrocatalysts for oxygen evolution. The relation between preparation method, structure, and behavior of mixed oxides of iridium and ruthenium are of interest in order to obtain active and stable catalysts. In this work the structure of mixed Ru-Ir oxides synthesized by the polymeric precursor method, which involves the formation of a gel containing the metal precursors and subsequent heat-treatment in air, was studied for the $Ir_xRu_{1-x}O_2$ system. An in-depth analysis of X-ray diffraction (XRD) and X-ray absorption (XAS) data, including EXAFS and linear combination of XANES, shows that the polymeric precursor synthesis method is capable of providing an intimate mixing of Ir and Ru in the catalyst. In addition to the oxide phase, metal phases, i.e. with Ru or Ir or both in oxidation state zero (Ir(*fcc*) and Ru(*hcp*)), were also found in the product materials. Facing complex structures such as some of those synthesized here, we have shown that a representation of shells with more than one atom type are efficiently represented using mixed sites, i.e. including scattering contributions from several elements in a site corresponding to a partial occupancy of the site by these elements, this method forming a very efficient basis for analyzing EXAFS data.

1 Introduction

Films and powders of Ir and Ru oxides are relevant for a range of applications, such as oxygen-evolving catalysts[1,2], as capacitors[3,4], pH electrodes[5,6], electrodes in waste water treatment[7] and in the chlor-alkali industry[8].

The electrocatalytic activity, selectivity and stability of rutile-type oxide electrocatalysts have been linked to local structure [9–12]. For multicomponent oxides an assessment of the degree of mixing at the atomic level is of particular interest, both for a fundamental understanding of catalytic activity[11,13] and for applications. However, such oxides can be synthesized by a number of methods[14–19], and their structure may vary significantly with preparation method. In this way differences in properties are directly linked to the synthesis methods[20]. The chemical composition and sample structure must therefore be examined critically for each preparation technique.

The polymeric precursor synthesis (PPS) is a method that is particularly well suited for making multicomponent oxides which are well mixed and homogenous at the atomic level[21,22]. It is also a simple and low cost method[23]. However, films and powders produced by the PPS have previously been reported to contain significant fractions of metal phases[23–29], i.e with the metallic elements in oxidation state zero, in addition to the oxides. The metal-phase fraction, which can be significant, is very sensitive to the synthesis conditions[3,23–32]. In addition to investigating the degree to which PPS samples are atomically well mixed it is therefore also necessary to characterize them in terms of any metallic phases in the samples.

X-ray absorption spectroscopy (XAS) and in particular the X-ray absorption near edge structure (XANES) and extended X-ray absorption fine structure (EXAFS) can be used to provide information regarding the oxidation state and coordination chemistry (XANES) and the distances, coordination number and identity of elements immediately surrounding a specific atom (EXAFS)[33]. Chemical state and local atomic structure can therefore be investigated by this method. Since only the local environment of the

[a] Department of Materials Science and Engineering, Norwegian University of Science and Technology (NTNU), NO-7491, Trondheim, Norway.
[b] Department of Chemistry, University of Southampton, Southampton SO17 1BJ, England.
[c] Department of Chemistry, Norwegian University of Science and Technology (NTNU), NO-7491 Trondheim, Norway.
[d] Department of Materials Science and Engineering, Norwegian University of Science and Technology (NTNU), NO-7491, Trondheim, Norway. Fax: +47 7359 1105; Tel: +47 7359 4051; E-mail: svein.sunde@ntnu.no
† Electronic Supplementary Information (ESI) available: [details of any supplementary information available should be included here]. See DOI: 10.1039/b000000x/
‡ Current address: SINTEF Sustainable Energy Technology, NO-0373 Oslo, Norway.

specific atom type is involved, this method can be used to study both crystalline and amorphous samples, and appears particularly well suited to samples in which substantial disorder is expected, such as those described above.

Whereas elaborating the structure of the first shell from EXAFS data refinement is relatively straightforward, samples such as mixed oxides puts more stringent requirements on the analysis because a solid solution implies determining mixed element contribution to more distant shells. Also, because previous experience with the PPS method indicates that several phases may be present in the samples, EXAFS analysis of such samples may prove even more challenging. As data refinement may be performed in several different ways, for example in *k*-space or in real space, using different structural models, and a few more to be detailed below, a range of options exist for how to perform the analysis and on which its outcome may depend. Finally, analysis results will have to be compared to and matched with those of other characterization methods, notably X-ray diffraction (XRD). An investigation of strategies for analysing this relevant class of materials with XANES and EXAFS may seem warranted.

In this work we present results of a thorough structural characterization of ruthenium and iridium oxides and their solid solutions, synthesized by the PPS method. The degree to which the PPS results in the production of well-mixed and homogenous powders at the atomic level is investigated by use of X-ray diffraction (XRD) with Rietveld refinement and X-ray absorption spectroscopy (XAS). Our purpose is to show that with these techniques a consistent set of structural data for pure and mixed oxide phases may be achieved also in the presence of iridium or ruthenium metal phases (Ir(0)(*fcc*) and Ru(0)(*hcp*)), and to analyze quantitatively the fraction of metal phase in the samples with these methods. In particular, below we explore and compare three different approaches to EXAFS refinement, viz. the co-shell approach, the mixed site approach and Fourier filtration, emphasizing the assessment and comparison of these three approaches.

2 Experimental

2.1 Synthesis

$Ir_xRu_{1-x}O_2$ powders were prepared by a polymeric precursor synthesis (PPS). A gel was prepared by dissolving citric acid (CA, Merck 99%) in ethylene glycol (EG, VWR AnalaR Normapur analytical reagent). This mixture was heated at 60 °C for 45 minutes while being stirred. The temperature was raised to 75 °C and the metal precursors, $H_2IrCl_6 \cdot 4H_2O$ (Alfa Aesar 99%, M_w=479 mol g^{-1}) and, or $RuCl_3 \cdot xH_2O$ (Alfa Aesar PMG basis 99.9%, M_w=261 mol g^{-1}) were added to the gel. The total amount of metal added was 0.5 mmol. The ratio between CA, EG and metal was 3:14:1. Stirring was continued for 45 minutes before the gel was transferred to a quartz-tube crucible. The gels were subsequently heat-treated by a three stage temperature program in an atmosphere of stagnant air, all with a heating rate of 1 °C min^{-1} between the stages. The stages were: 30 min at 130 °C, 20 min at 250 °C and finally 20 min at 500 °C. A lid was placed over the crucible, but not fully covering the opening. Three identical syntheses were carried out for each composition x = 0, 0.25, 0.5, 0.75 and 1. We will state the nominal composition of the samples below by the atom fraction of ruthenium, X_{Ru}, or the atom fraction of iridium, X_{Ir}, and $X_{Ir} = 1 - X_{Ru}$.

2.2 X-ray Powder Diffraction, Rietveld Refinement and SEM

XRD measurements for all powders were performed with a Bruker AXS D8Focus diffractometer using Cu $K-\alpha$ radiation source (equipped with a Ni filter that excludes the Cu $K-\beta$ radiation). Zero background silicon sample holders were used. Rietveld analysis was carried out with the Bruker AXS TOPAS version 4.2 software, using a pseudo-Voigt function. The background intensity was accounted for using a Chebychev polynomial of the order 6. Refinements of diffraction patterns were performed within space groups 136 (P42/mnm), and 225 (Fm-3m) or 194(P63/mmc) if metal-phases of iridium or ruthenium (Ir(*fcc*) or Ru(*hcp*)) were present. Unit cell values, the crystallite size and fractions of metal and oxide phases were obtained. The occupancies were set to nominal values, and were not refined.

The sample morphology was studied with FE-SEM, Zeiss Ultra 55 LE, using a high efficiency in-lens secondary electron detector.

2.3 X-ray Absorption Spectroscopy

2.3.1 Data Collection.

The local environment of Ir and Ru was investigated using X-ray absorption spectroscopy (XAS) of one sample of each composition produced. The XAS data were collected at beamline B18-Core XAS of the Diamond Light Source Synchrotron in fluorescence mode. A germanium 9-element detector was used to detect the fluorescence signal. The samples were placed at an angle of 45° to the beam and the detector. The ion chamber before the sample was filled with an appropriate mix of inert gases to optimize sensitivity. A second ion chamber was used for transmission mode data collection for the references foils. Data were collected during a multi-bunch electron filling mode of the Diamond storage ring providing a maximum current of 300 mA. For the measurements of the XAS at the Ru K-edge 0.25 eV steps were used from 21917 to 22917 eV with counting time at each step of 43 ms, applying Si(311) double crystal monochromators and Pt-coated collimating and toroidal focusing mirrors. At the iridium edge a step size of 0.35 eV was used over the energy range 11015-12414 eV, with a counting time of 60 ms at each step, using a Si(111) double crystal monochromator and Cr-coated collimating and toroidal focusing mirrors. Several scans were collected and summed in order to improve the statistics.

Samples of all compositions investigated were supported on carbon paper. Inks of the samples, prepared with 20 mg catalyst, 1 mL deionized water, 200 µL isopropanol (AnalaR Normapure VWR), 228 µL 5 wt.% Nafion (Alfa Aesar) and 4 mg carbon black (Vulcan XC72R), were prepared and painted onto a 0.26 mm thick Toray carbon paper (TGPH-090) until a loading of 0.2-0.3 mg catalyst cm^{-2}. Finally the samples were pressed at 130 °C and ~1 kg cm^{-2} for 3 minutes.

2.3.2 Data Reduction.

The XAS data were binned, summed, normalized, and energy corrected relative to the metal foils (Ru K-edge = 22117 eV at Ru K-edge, and Pt L_{III} edge=11564 eV used for calibration of the Ir-L_{III}-edge) using Athena, a program in the IFEFFIT package[34]. The absorption edge was measured as the first inflection point as identified in the derivative of the spectra. The XANES and EXAFS spectra were normalized from 17 to 90 eV and 150 to 1090 eV above the edge, respectively. The spectra were carefully deglitched and truncated at the end of EXAFS spectra when needed. The linear combination fit (LCF) procedure in the Athena program was used to fit the XANES spectra to the reference material, which were powders of IrO_2 (Aldrich, 99.9 %), $IrCl_3$ (Alfa Aesar, 99.8 %) and Ir black (Alfa Aesar 99.9 %). The linear combination fitting was performed of the XANES spectra over a range from 17 eV below the edge to 70 eV above the edge, always applying the normalization range as described above. The energy shifts of the reference spectra were also fitted, but closely monitored and they were always less than 1.1 eV. The fit parameter for the LCF was reported for each fit, defined in Equation (1),

$$R = \frac{\sum_i^N (|\chi_i^{exp}(k) - \chi_i^{calc}(k)|)^2}{\sum_i^N |\chi_i^{exp}(k)|^2} \quad (1)$$

where $\chi_i^{exp}(k)$ and $\chi_i^{calc}(k)$ are the experimental and theoretical EXFAS fine-structure functions. To distinguish this quantity from bond lengths (see below) we will refer to R in Eq. (1) as the "R-factor".

2.3.3 EXAFS Least-Squares Refinements.

EXAFS least-square refinements were carried out using the DL-EXCURV code, which performs curve fitting of the theoretical $\chi^{th}(k)$ to the experimental $\chi^{exp}(k)$ using curved wave theory[35]. The calculation of ab initio phase shifts for the expected neighboring elements also took place in DL-EXCURV. The least-squares refinements were carried out in the wavenumber k range 2 through 18 eV and 2 through 14 eV respectively for spectra obtained at the Ir- and Ru-edge, using a k^3 weighting scheme.

Whether a solid solution between iridium and ruthenium was obtained was studied by XAS using a range of approaches which we have termed the co-shell approach, the mixed site approach and Fourier filtration. For each of these we employed several strategies and sets of initial values in order to arrive at robust conclusions with respect to the formation of solid solutions. The reference bond lengths and coordination numbers for the pure oxides are reported in Table 1. The mixing was included into the analysis by two distinct methods, the co-shell and mixed site approach, which are summarized in Table 2.

In the co-shell approach two shells, one Ir and one Ru shell, were included for each mixed shell. In the mixed site approach a parameter describing the relative scattering contribution from Ru and Ir in the same site was introduced. We will refer to the relative scattering contribution from a given element as its partial occupancy of the site. In the case of both metal and oxide phases being present, a separate parameter was included for each phase. These were fitted independently. Fourier filtering was performed in order to obtain information of individual shells in the R-space plot by back- transforming the regions of the specific peaks into k-space.

Table 1 Coordination number (N) and bond length (R) of the first four shells in iridium and ruthenium oxide[36]. Me stands for the metal atom, i.e. iridium in IrO_2 and ruthenium in RuO_2. The metal atom in shell 3 is indicated by subscript "Ox1" and that in shell 4 by subscript "Ox2"

Shell	Bond	N	RuO_2 R / Å	IrO_2 R / Å
1	Me-O	2	1.94	1.94
2	Me-O	4	1.98	2.00
3	Me-Me, Ox1	2	3.11	3.15
4	Me-Me, Ox2	8	3.54	3.55

As seen in Table 1 IrO_2 and RuO_2 have two oxygen shells with coordination numbers two and four, in apical and equatorial positions, respectively. In the refinements only one oxygen shell was included, with an initial value for the coordination number equal to six.

Table 2 Overview of the shells included to introduce mixing in the co-shell and mixed site approach, given for the Ir-edge. The metal atom in shell 3 in Table 1 is indicated by subscript "Ox1" and that in shell 4 by subscript "Ox2". $X_{Ru,Ox}$ and $X_{Ru,Met}$ are the partial occupancy of Ru defined for the oxide and metal phase, respectively, in the mixed-site approach.

	Shell	co-shell	Mixed Site
Oxide	Ir-Me_{Ox1}	Ir-Ru_{Ox1} Ir-Ir_{Ox1}	Ir-Me_{Ox1}, $X_{Ru,Ox}$
	Ir-Me_{Ox2}	Ir-Ru_{Ox2} Ir-Ir_{Ox2}	Ir-Me_{Ox2}, $X_{Ru,Ox}$
Metal	Ir-Me_{Met1}	Ir-Ru_{Met1} Ir-Ir_{Met1}	Ir-Me_{Met1}, $X_{Ru,Met}$

For the co-shell method shells of mixed occupancy were modelled by including two shells initially at the same bond lengths, one consisting of iridium and one consisting of ruthenium. Spectra from both edges were refined, and the following description applies to the treatment of both. For X_{Ru}=0.75 and X_{Ru}=0.50 three shells were included. These were the oxygen shell corresponding to a combination of shells 1 and 2 in Table 1, and the two first shells containing metal atoms, corresponding to shells 3 and 4 in Table 1, c. f. Table 2. The initial coordination numbers were set to be the reference coordination number in Table 1, but multiplied by the nominal fraction of ruthenium for the ruthenium shells and with nominal iridium fraction for the iridium shells. First the systems were refined with only iridium or ruthenium in the whole structure, Ru for X_{Ru}=0.75 and X_{Ru}=0.50 and Ir for all except X_{Ru}=0.75. Then the second element was introduced to the first metal oxide shell (shell 3 in Table 1) by adding another shell at the same bond length. Refinements of these shells (combined shells 1 and 2 and shell 3 in Table 1) were performed first in terms of the energy shift, E_F, all bond lengths, R, and Debye-Waller factors (DWFs). Then followed a separate refinement in terms of the coordination numbers, N. These two steps were repeated until convergence. Next, the whole procedure was repeated after the addition of a co-shell for second metal oxide shell (shell 4 in Table 1). For the sample with X_{Ru}=0.25, consisting of both metal and oxide phases, three shells were included,

one oxygen shell, one metal oxide shell (shell 3 in Table 1), and the first metal-phase shell. The same refinement procedure was carried out as for the X_{Ru}=0.75 and 0.50 described above, starting with a pure system and then introducing the other element in the individual shells.

In the mixed site approach an additional parameter describing the partial occupancy of a site was refined. Mixed site is a function in DL-EXCURV where a partial occupancy site is defined and the initial occupancy of up to three elements is specified. The mixed Ir/Ru site is then defined as a new atom type (QA), and atomic potential and phase shifts are calculated for the Ir/Ru pair. Refining QA will then optimize the fractions of the elements defined for the shell. One has the option of including several mixed sites and can therefore have different fractions for different contributions, for instance different phases. The mixed site method was used to find the partial occupancy of Ca and Sr in aragonite structured corals in the work of Finch et al.[37]. In this work the partial occupancy of ruthenium was investigated, for X_{Ru}=0.25 being a mix of an oxide phase and a metal phase. In the latter case one parameter for each phase was defined and were fitted independently of each other, as $X_{Ru,Ox}$ and $X_{Ru,Met}$.

Spectra from both edges were refined with the mixed site approach, and the following description applies to the treatment of both. For X_{Ru}=0.75 and X_{Ru}=0.50 three shells were included in the fit, one oxygen shell and two metal oxide shells (corresponding to the combined 1 and 2 shells, shell 3 and shell 4 in Table 1). Refinement of E_F, all bond lengths, R, and DWFs together, then all N and finally $X_{Ru,Ox}$ were alternated until convergence. For X_{Ru}=0.25 four shells were included, the oxygen shell, the first two metal oxide shells as above, and the first metal-phase shell. The refinements for this sample was not as straightforward as for the pure oxides. In this case refinements of E_F, all R and DWFs together and then refinement of all N were alternated until convergence before all N were left fixed and alternating refinements of E_F, all R, and DWFs together, then $X_{Ru,Ox}$ followed by $X_{Ru,Met}$ were repeated until convergence.

3 Results

3.1 Metal-phase fraction and oxide structure from XRD

X-ray diffractograms, one of each composition, are shown in Figure 1a. A rutile structure is present in all compositions. A shift in peak position can be seen with increasing iridium content from the pure ruthenium oxide, clearly demonstrated by the reflection located in the range 34-36° in Figure 1b. The two diffractograms for X_{Ru}=0 and 0.25 in Figure 1a indicate that metal-phase iridium is present, as can be inferred from the peak at $2\theta \approx 47.5°$. In several of the samples metallic phases, either Ir(*fcc*), Ru(*hcp*), or both, were present. The weight fractions, cell parameters and crystallite sizes of the metal phases are summarized in Table 3. Below we will quantify metal-phase fractions in the samples either by the weight fraction of metal-phase Ru or Ir, wt.% (the mass of Ru or Ir metal divided by the total mass of sample, in percent) or the number of Iror Ru) atoms in oxidation state zero divided by the total number of Ru (or Ru) present in percent as at.%. This corresponds to the at.% as it would have been measured by LCF of XANES. As can be seen the pure iridium samples contained a higher fraction of metal-phase Ir than samples with X_{Ru}=0.25, with an average of 63.2 wt.% and 39.4 wt.% , respectively. This corresponds to 66.6 at.% and 47.5 at.% on average, respectively. (Equations for the conversion are given in the Supplementary Material, section S.4.) Metal-phase Ru was also seen for at least two of the three mixed oxides and the pure ruthenium samples produced. The metal phase fraction was found to be less than 3 wt.% for all samples with the exception of the second sample of X_{Ru}=0.75. This sample contained 14.3 wt.% metal-phase Ru(0), corresponding to 25.5 at.% of the ruthenium atoms being in the metal phase (see Supplementary Material section S.4).

Inclusion of strain in the Rietveld refinements did not affect appreciably the estimates of the fraction of metal-phase in the samples. A detailed discussion is included in Section S.2 of the ESI.

The lattice parameters emerging from the Rietveld analysis are presented as a function of nominal ruthenium fraction in Figure 2. Each data point is an average of the three samples for each composition, and the standard deviation for the set is indicated by error bars. As expected from the shifts in peak positions in Figure 1b, both lattice parameters change with composition. The c lattice parameters decrease linearly as more ruthenium is incorporated into the structure for both synthesis and indicates formation of a solid solution of the two oxides according to Vegard's law. This trend and the values agree well with previously reported lattice parameters[13,38,39]. The a parameter displays considerably less variation, also in agreement with the literature[13,38,39].

3.2 Metal-phase fraction from linear combination fits of XANES.

The fraction of Ir metal-phase was investigated by carrying out linear combination fit (LCF) of the X_{Ru}=0, 0.25, 0.5, and 0.75 samples with spectra of pure metal-phase Ir and IrO_2. Reference samples of oxide and metal-phase Ir with composition equal to the nominal composition of the X_{Ru}=0.25, and X_{Ru}=0.50 and X_{Ru}=0.75 were not available. Instead we performed the LCF of the X_{Ru}=0.25, and X_{Ru}=0.50 and X_{Ru}=0.75 samples with the pure iridium reference. We used $IrCl_3$ in order to evaluate a possible contribution from Ir^{+3}. The $IrCl_3$ has been reported used in several investigations of oxidation state of Ir in anodically formed iridium oxide films (AIROF), electrochemically formed iridium oxide films (EIROF), and sputtered iridium oxide films (SIROF) in an in situ electrochemical cell as function of applied potential[40–42].

Two sets of LCFs were carried out, one with all three reference spectra included (Ir^0, Ir^{+3} and Ir^{+4}), and one which did not include Ir^{+3}. The LCF for X_{Ru}=0 and 0.25 is shown in Figure 3. It was not possible to fit the XANES data for compositions X_{Ru}=0.5 and 0.75 to any linear combination of reference spectra containing metal-phase Ir. The atomic percents of Ir^0 emerging from the LCFs are summarized in Table 4. For X_{Ru} = 0 the LCFs with only Ir^0 and Ir^{+4} (Figure 3a and Table 4) a metal-phase fraction of 77 at.%, equal to 74 wt.%, was obtained, which is 18 percentage points larger than what was found by XRD (55.9 wt.% for this

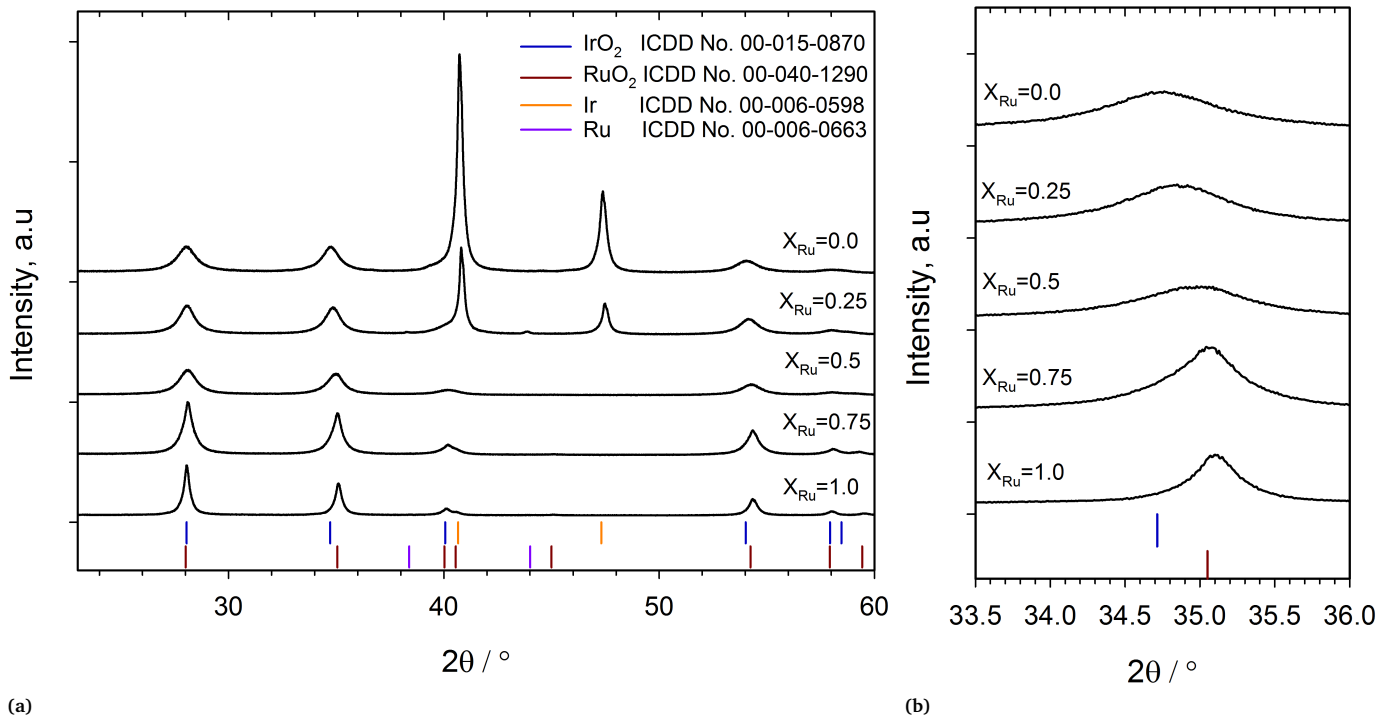

Fig. 1 (a) X-ray diffractogram of $Ir_xRu_{1-x}O_2$ as function of X_{Ru}, and (b) magnification of (101) reflection located at 2θ ~34-35 °.

Table 3 Overview of the metal phases present in the samples as evaluated by XRD Rietveld analysis. The unit cell lengths, a and c, and crystallite diameter, d, for the metal-phase iridium and ruthenium present in the three catalyst powders obtained from Rietveld analysis. Iridium has cubic structure (Fm-3m) and Ru has hexagonal structure (P63/mmc). Data for all the three different samples of each composition, arbitrarily labelled "1", "2", and "3" for distinction, are given

		Ir			Ru			
X_{Ru}		wt.%	a / Å	d / nm	wt.%	a / Å	c /Å	d / nm
0.00	1	55.9(1)	3.84023(7)	16.91(5)	0	-	-	-
	2	75.6(2)	3.83933(7)	25.2(1)	0	-	-	-
	3	58.1(1)	3.83913(7)	16.60(6)	0	-	-	-
0.25	1	42.3(1)	3.83005(8)	23.8(1)	3.01(8)	2.7162(4)	4.3141(1)	24(1)
	2	45.1(1)	3.83116(8)	23.7(1)	3.00(8)	2.7162(4)	4.3141(1)	24(1)
	3	30.91(8)	3.83016(8)	21.4(1)	1.84(7)	2.7161(6)	4.3145(2)	18(1)
0.50	1	0	-	-	0	-	-	-
	2	0	-	-	0.52(8)	2.714(2)	4.326(7)	25(7)
	3	0	-	-	1.36(8)	2.715(2)	4.341(6)	9.3(8)
0.75	1	0	-	-	0	-	-	-
	2	0	-	-	14.3(1)	2.7104(2)	4.2940(4)	16.2(2)
	3	0	-	-	2.17(6)	2.715(2)	4.306(4)	11.0(5)
1.00	1	0	-	-	1.14(7)	2.711(1)	4.273(3)	17(2)
	2	0	-	-	2.00(9)	2.715(1)	4.264(4)	9.4(6)
	3	0	-	-	0	-	-	-

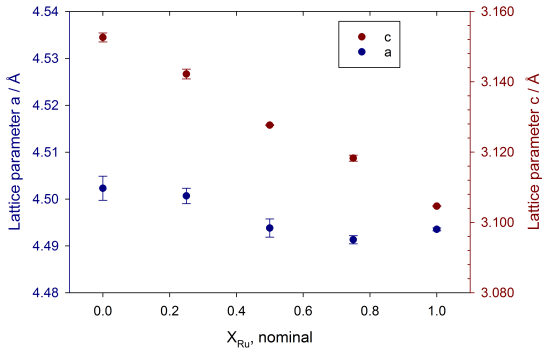

Fig. 2 Lattice parameters a and c for the oxide phase (rutile crystal structure) obtained by Rietveld refinement of X-ray diffractograms as a function of nominal ruthenium fraction. Each data point is an average of the three identical synthesis of each composition and the standard deviation of the three is indicated by error bars.

sample). When the Ir^{+3} spectra was included it was found that 7 at.% of the Ir atoms existed in trivalent state, and the metal-phase fraction was 71 at.%, Figure 3b and Table 5. A slightly improved R-factor is seen with the addition of Ir^{+3} for the pure Ir sample, and it is possible that some of the Ir exist in this oxidation state. A presence of Ir^{+3} could perhaps be due to incomplete decomposition of $IrCl_3$ or formation of intermediate Ir_2O_3 [43,44]. Ir_2O_3 is, however, calculated to be unstable [45] unless the oxygen chemical potential is very low.

The fraction of metal-phase found for the X_{Ru}=0.25 sample was 42 at.% iridium, corresponding to 34 wt.% (c.f. 42.3 wt% for this sample by Rietveld analysis, X_{Ru}=0.25 sample 1 in Table 3). (The Ir^{+3} fraction was found to be zero when included in this fit , Figure 3c.) The LCF of XANES thus predicted a somewhat smaller metal-phase fraction than the Rietveld analysis for the pure Ir sample. However, a small contributing metallic Ru phase (3 wt%) was accounted for in the Rietveld analysis, which can not be included for a LCF carried out in this manner. The weight percentages should therefore in principle not be directly compared. However, since this is quite a small fraction it is therefore not assumed to influence the results substantially. For X_{Ru}=0.25 the metal-phase fraction was found to be similar for the two methods.

3.3 Metal-phase fraction and oxide structure from EXAFS Least-Squares Refinements.

The validity of the mixed site approach was verified by several different procedures. One method was to first perform the refinement of the pure system of either Ru or Ir, viz. the pure iridium system for X_{Ru}=0.25 and 0.50 and the pure ruthenium system for X_{Ru}=0.5 and 0.75, and and then introduce and refine the partial occupancy $X_{Ru,Ox}$, and for X_{Ru}=0.25 also $X_{Ru,Met}$. The values from the first of these refinements served as a set of initial values for the second. This procedure was performed for spectra recorded at both edges.

Refinements were also carried out with the partial occupancies $X_{Ru,Ox}$ (and for X_{Ru}=0.25 $X_{Ru,Met}$) introduced initially and with initial values set to nominal values. The latter procedure was

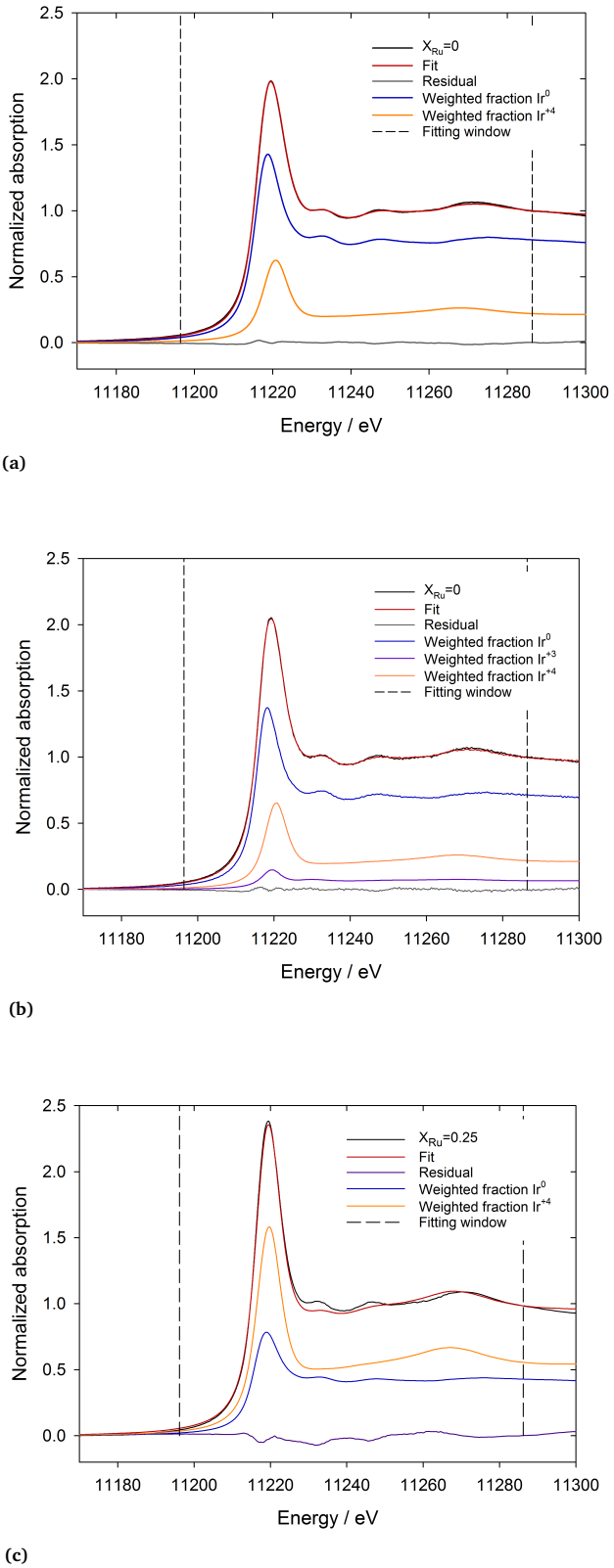

Fig. 3 Linear combination fit of X_{Ru}=0.0 (sample 1 of those with X_{Ru}=0.0, Table 3), with (a) Ir^0 and Ir^{+4} standards and (b) Ir^0, Ir^{+3} and Ir^{+4} standards. (c) linear combination fit of X_{Ru}=0.25 (sample 1 of those with X_{Ru}=0.25,Table 3), with Ir^0 and Ir^{+4}) included. Addition of Ir^{+3} did not change the fit of X_{Ru}=0.25, and the fraction of Ir^{+3} was found to be zero.

Table 4 Atomic percent of Ir^0, the energy shifts, E_F and R-factors obtained in the LCF of the XANES spectra. Fits with reference spectra Ir^0 and Ir^{+4}

X_{Ru}	At.% Ir^0	E_F, Ir^0	E_F, Ir^{+4}	R-factor
0	76.7(2)	-0.14(1)	1.04(2)	4.22E-4
0.25	42(2)	0.3(2)	-0.28(8)	2.39E-3
0.50	0	-	-	-
0.75	0	-	-	-

Table 5 Atomic percent of Ir^0, Ir^{+3} and Ir^{+4}, the energy shifts, E_F and R-factors obtained in the LCF of the XANES spectra. Fit with reference spectra Ir^0, Ir^{+3} and Ir^{+4}

X_{Ru}	At.% Ir^0	E_F, Ir^0	At.% Ir^{+3}	E_F, Ir^{+3}	At.% Ir^{+4}	E_F, Ir^{+4}	R-factor
0	71(3)	-0.23(2)	7(1)	1.1(2)	22(1)	1.01(4)	3.55E-4

carried out three times.

With both strategies (starting with a pure system before refining the partial occupancies and starting with the partial occupancies initally introduced), and for the different refinements, the final ruthenium partial occupancy and bond lengths were always similar. Improved fits were always obtained for the binary oxides when mixing was introduced. The multiplicities of the oxygen shell did not change with the strategy used, but some differences could be seen for shells at longer bond distances.

Finally, refinements including only the oxygen shell (the combined shell 1 and 2 in Table 1) and the first metal-phase shell of samples with X_{Ru}=0.25 from both edges were tested by trying out three different initial values of $X_{Ru,Met}$, 0.10, 0.25 and 0.50. $X_{Ru,Met}$ converged towards the same value for all starting points with highest standard deviation for the Ir-edge at 0.02. A mixed occupancy site was also attempted fitted for the pure Ru sample with various initial values of $X_{Ru,Ox}$, and did result in a ruthenium partial occupancy close to one.

The refinements performed with the mixed site method can be seen in Figure 4 and Figure 5 for Ru-edge and Ir-edge respectively. The results reported in these figures represent fits in which $X_{Ru,Ox}$ and $X_{Ru,Met}$ were introduced initially.

The experimentally obtained ruthenium partial occupancy in the oxide phase, $X_{Ru,Ox}$ fraction from both edges as a function of nominal ruthenium fraction is shown in Figure 6a. The $X_{Ru,Met}$ partial occupancy obtained for the X_{Ru}=0.25 sample from both edges is shown in Figure 6b. A finite ruthenium partial occupancy was obtained for all the mixed samples, both in the oxide and metal phases, indicating a high degree of mixing. Partial occpuancies relatively close to the nominal were obtained, and quite consistently so from both edges, with the exception of X_{Ru}=0.50 and the metal phase for X_{Ru}=0.25, possibly indicating a less homogeneous distribution of the two elements in these phases. For the metal Ir phase it is possible that a more or less pure iridium phase coexists with a phase with some ruthenium incorporated into the structure, reflected by the much lower $X_{Ru,Met}$ found from the Ir edge than from the Ru edge. In addition a small fraction of metal-phase Ru was seen (3 wt.%) for this sample, which may have been partially doped with Ir.

In Figure 7 the coordination numbers obtained from both edges have been plotted as a function nominal ruthenium fraction. To account for the reduction in multiplicity due to presence of several phases in the sample we employed the method of reduced multiplicities by Martens *et al.*[46]. We thus divided the experimentally obtained coordination numbers by the fraction of the respective phase f_{ph}, to obtain the corrected coordination number $N_{corr}=N_{exp}/f_{ph}$.[46] The corrected coordination number expresses what the coordination number would have been if this was the only phase present.[46] In Figure 7 the coordination numbers for oxide and metal-phase shells have been corrected by oxide and metal-phase fractions respectively, which were obtained from LCF of XANES spectra. In Figure 7 we have included the corrected coordination numbers calculated with f_{ph} as obtained for the case in which two reference spectra were employed in the LCF fit and in addition for the case when three reference spectra were included in the fit of X_{Ru}=0.0.

The multiplicities lie close to the reference value for the oxygen shell indicated in Figure 7a when the corrected multiplicities are used to account for the presence of a metal-phase. The corrected multiplicities of the first metal-phase shell, Figure 7b, are smaller than the reference value. Also, a deviation is seen between the two edges for X_{Ru}=0.25, the smaller N appearing for the Ru-edge and the larger for the Ir-edge. For the first metal oxide shell (shell 3 in Table 1, Figure 7c) the multiplicities are in agreement with the reference value, with the exception of the Ru-edge for X_{Ru}=0.25 which is much higher than the reference value.

The second metal oxide shell (shell 4 in Table 1, Figure 7d) demonstrates more variety. The corrected multiplicities from the Ir-edge deviates from reference value, pure Ir being smaller and X_{Ru}=0.25 being larger than the reference value. For X_{Ru}=0.25 at the Ru-edge however, it is much smaller than what was obtained at the Ir-edge. For X_{Ru}=0.5 and 0.75 the values obtained from the two edges are in agreement, and they are either smaller or close to reference value, respectively.

In addition to determining the fractions of metal phase and oxide phases through LCF of XANES and Rietveld analysis, we also estimated the oxide fractions f_{ox} from the formula $f_{ox} = N_{(Ir-O)exp}/6$, where $N_{(Ir-O)exp}$ is the experimentally obtained multiplicity of the oxygen shell (MOS). The metal-phase fractions evaluated for the three methods, the multiplicity of the oxygen shell (MOS), and the quantitative Rietveld analysis of XRD spectra and the LCF of XANES are listed in Table 6.

Both of the two XAS-based methods, LCF of XANES and MOS, result in higher fractions of metal-phase than obtained through the Rietveld refinement for X_{Ru}=0. Quite similar values are found

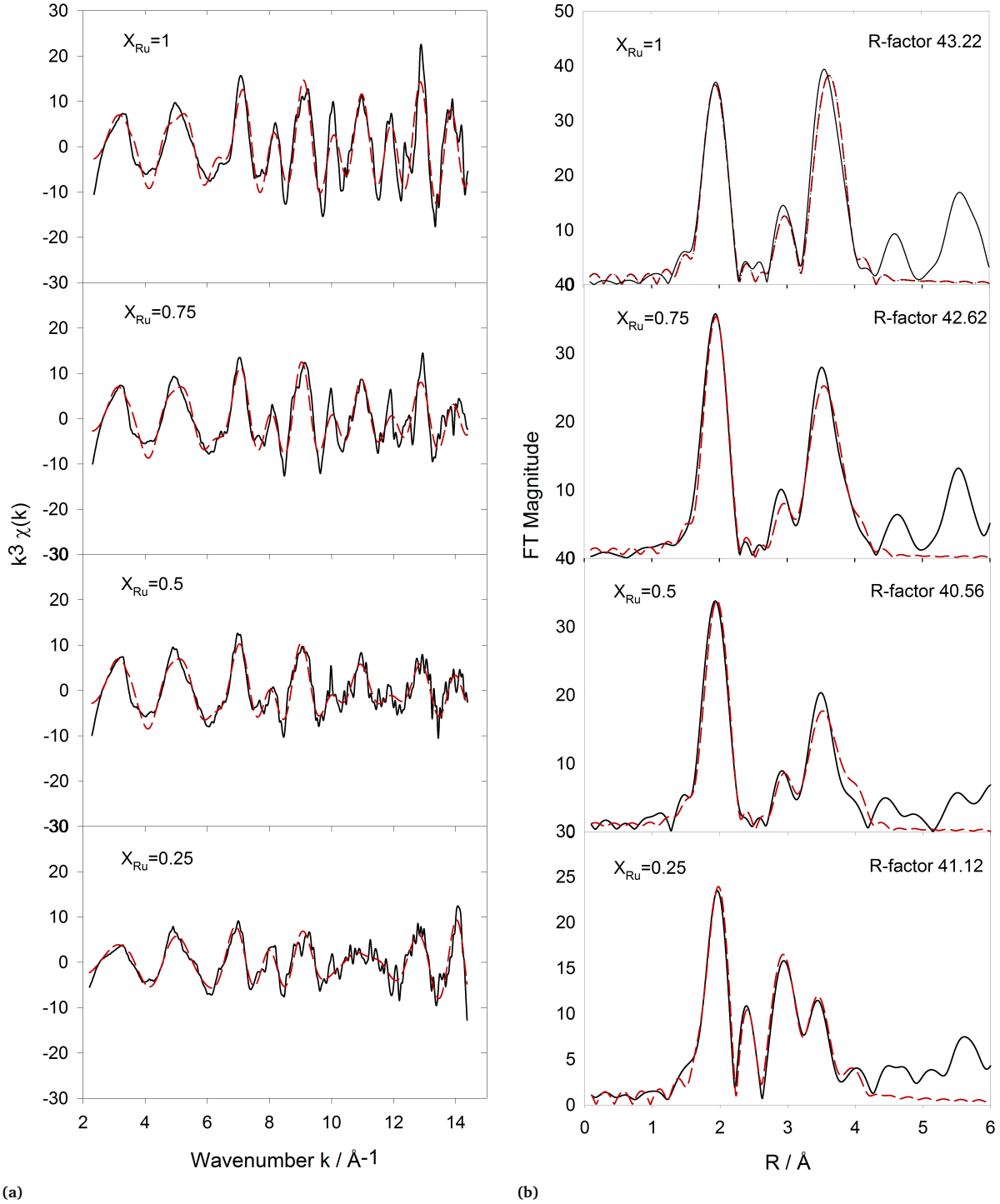

Fig. 4 Experimental (-) and least squares refined (- -) of (a) k^3 χ(k) and (b) EXAFS Fourier transforms of all spectra recorded at the Ru-edge and refined with the mixed-site approach.

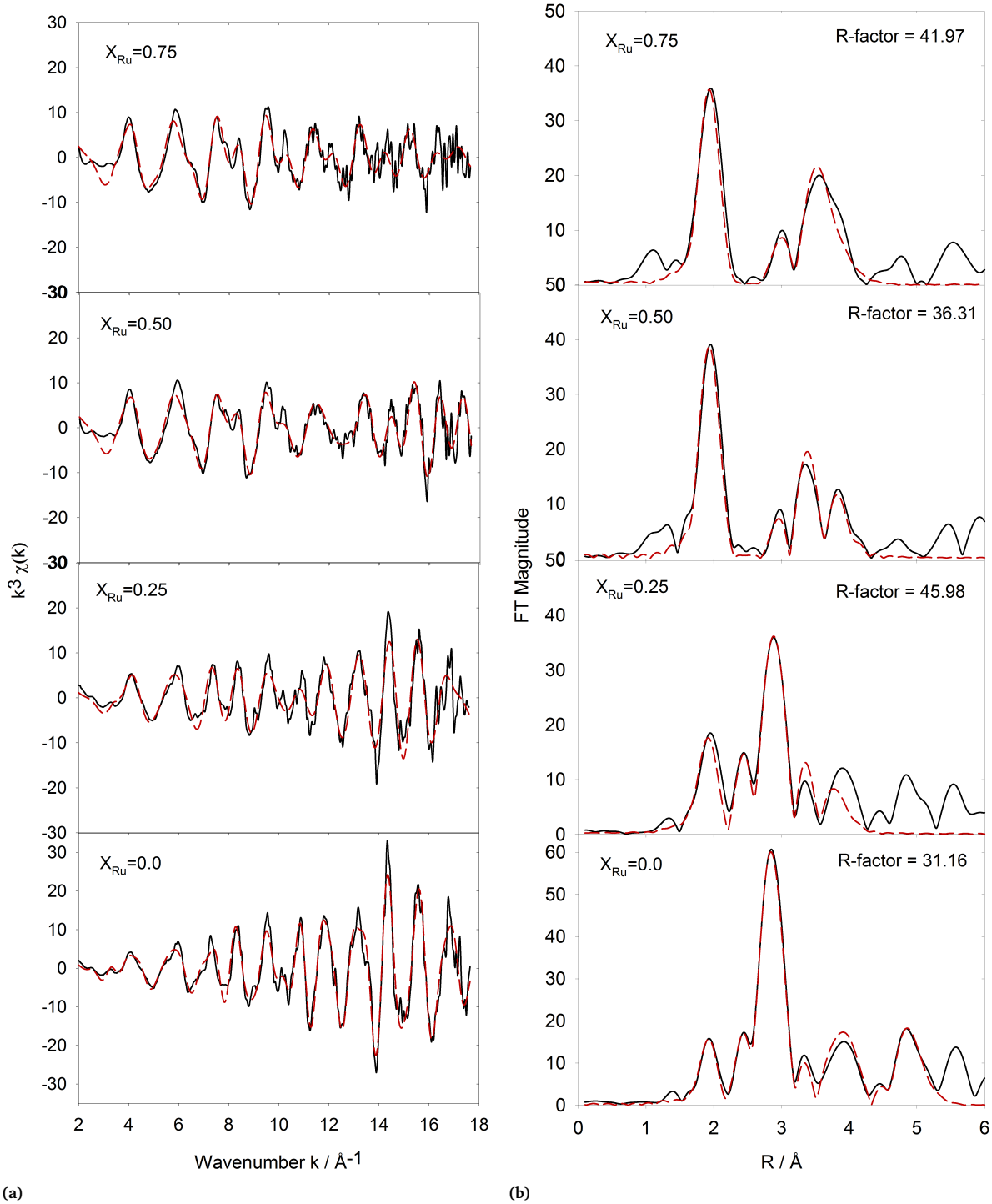

Fig. 5 Experimental (-) and least squares refined (- -) of (a) k^3 χ(k) and (b) EXAFS Fourier transforms of all spectra recorded at the Ir-edge and refined with the mixed-site approach.

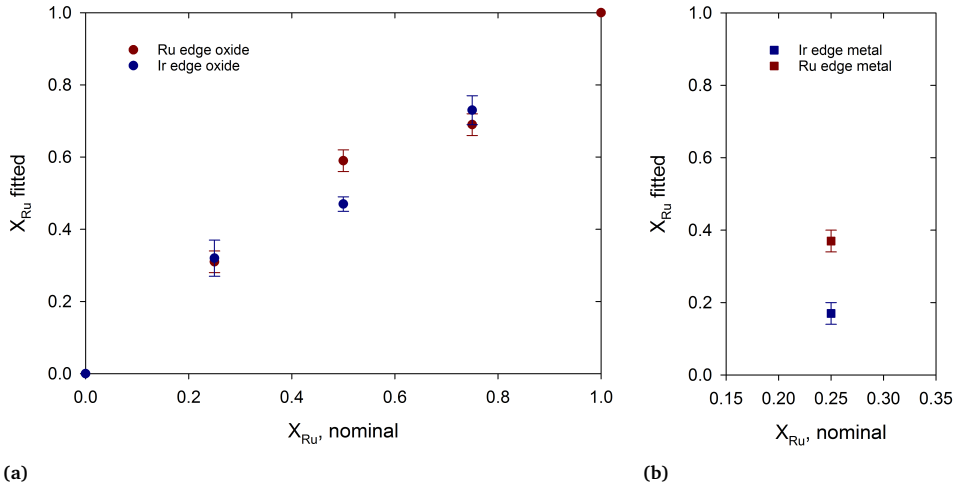

Fig. 6 The obtained partial occupancy as defined in EXCURVE of Ru of (a) the oxide phase and (b) the elemental metal phase evaluated from both Ir- and Ru-edges as function of nominal Ru fraction.

Table 6 Estimation of metal-phase fractions based on quantitative Rietveld analysis of XRD spectra, LCF of XANES spectra and MOS. All fractions are reported in at.% Ir^0. In the final column the coordination numbers used to evaluate the phases fractions with the MOS method are listed. The conversion between wt.% and at.% were performed according to equations in the Supplementary Material section S.4

X_{Ru}	XRD	LCF XANES Ir^{+3} not included	LCF XANES, Ir^{+3} included	MOS, Ir / Ru-edge	$N_{Me-O,exp}$ Ir / Ru-edge
0	59.7(1)	76.7(2)	71(3)	72(5) / -	1.7(3)/ -
0.25	50.6(1)	42(2)	-	53(8) / 42(5)	2.8(5) / 3.5(3)

from MOS and LCF of XANES spectra if Ir^{+3} is included in the LCF fit. For X_{Ru}=0.75 less variation is seen, with the exception of MOS method evaluated from Ir-edge. However, in spite of significant differences between the MOS results from the Ir and Ru edges, an overlap exists within the uncertainties. Since smaller uncertainties were found for LCF of XANES than from MOS, Figure 7 has been been based on the former.

The experimentally obtained bond lengths as function of nominal X_{Ru} are shown in Figure 8. Some deviation between the bond lengths obtained from the two edges is apparent. The bond lengths obtained at the Ru-edge are in general longer than the ones obtained from the Ir-edge, and with a few exceptions show the highest uncertainties. Decreasing bond lengths are seen for the oxygen shell at Ru-edge (although not the Ir-edge), the metal-phase shell at the Ir-edge and the first metal oxide shell at both edges. For the second metal oxide shell small changes are expected since the difference in bond length for this shell in IrO_2 and RuO_2 is quite small in value (Table 1), consistent with the data in Fig. (8d).

Fourier filtration of the EXAFS was another strategy applied in order to investigate the degree of mixing. Using Fourier filtration it can be possible to investigate the contribution to each shell separately. This was however difficult due to the large degree of overlap between the individual shells in the structure. This is illustrated for Ir-edge X_{Ru}=0.75 in Figure 9 where the contribution from the individual shells has been plotted. As can be seen the two metal oxide shells overlap. The results from the Fourier filtration were therefore inconclusive, and was not further explored.

EXAFS analysis of data for the mixed oxides with the co-shell approach demonstrated a decrease of the R-factor and even visually better fits as a second element was introduced in the first shell and improved for each shell which was modeled as a mixture. This confirms that a high degree of element mixing was indeed obtained for this synthesis procedure. However, this method quickly required a large number of parameters. In order to describe the mixing of a singe shell an additional three parameters had to be included, whereas introduction of mixing for a single phase required one single parameter in the mixed site approach. In addition, Ir and Ru in these co-shells were often at different bond lengths, and from the two edges both elements could be found to have the shortest bond length. The coordination number summed for the two shells often exceeded or was much smaller than the reference occupancy for the shell it was simulating. The result of the co-shell method was not satisfactory, and thus the mixed site approach became the primary method of EXAFS spectra analysis, for which results are presented above (Figures 4 through 8).

4 Discussion

The XRD and XAS results consistently indicate a high degree of mixing between Ir and Ru in the obtained oxides. A linear contraction of the cell volume was obtained as function of ruthenium fraction, see Figure 2, as expected when a solid solution is obtained. This is further supported by the close to equal partial

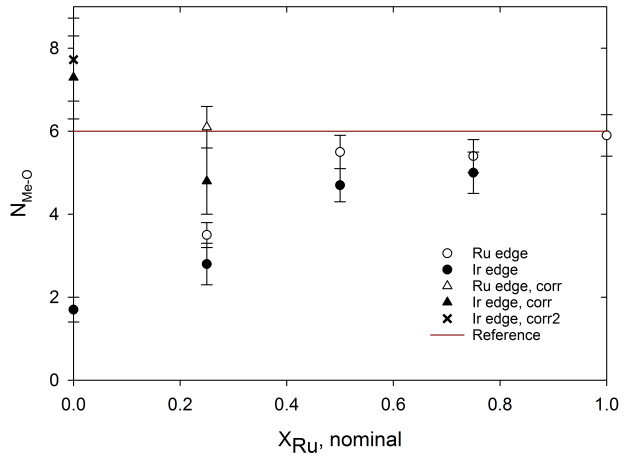

(a) N_{Me-O}

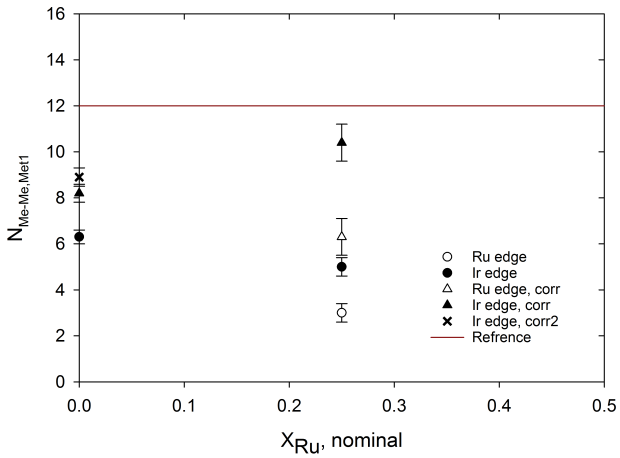

(b) $N_{Me-Me,Met1}$

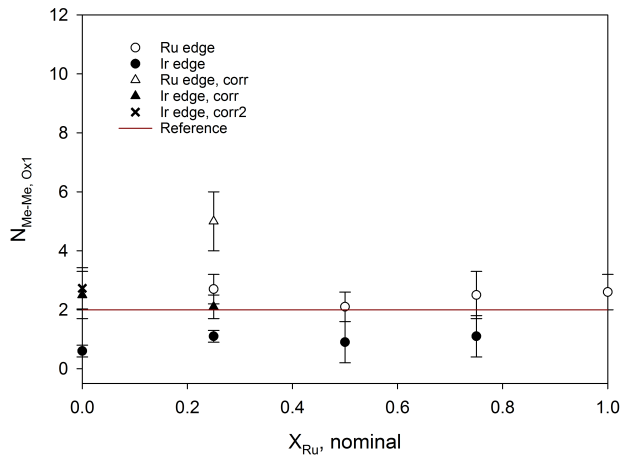

(c) $N_{Me-Me,Ox1}$

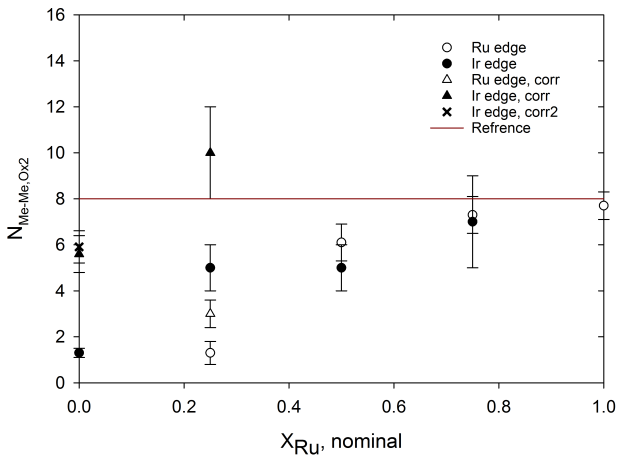

(d) $N_{Me-Me,Ox2}$

Fig. 7 Experimentally obtained coordination numbers for (a) the oxygen shell, N_{Me-O}, (b) the first metal-phase shell, $N_{Me-Me,Met1}$, (c) the first metal oxide shell, $N_{Me-Me,Ox1}$ (shell 3 in Table 1), and (d) the second metal oxide shell, $N_{Me-Me,Ox2}$ (shell 4 in Table 1), as function of nominal ruthenium fraction. The reference coordination numbers are indicated with red lines in the figures. For phases which are mixes of oxide and metal-phases the corrected multiplicities are also included. For X_{Ru}=0 different metal-phase fractions were obtained whether Ir^{+3} was included in the LCF of XANES or not, both are indicated. Fractions obtained without Ir^{+3} are named "corr" (triangles), and with named "corr2" (crosses).

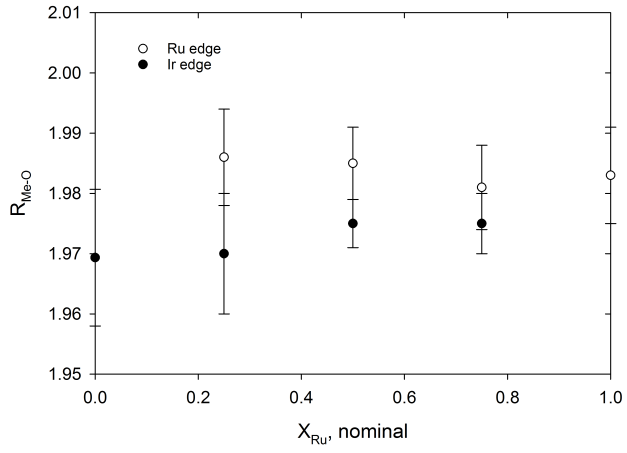

(a) R_{Me-O}

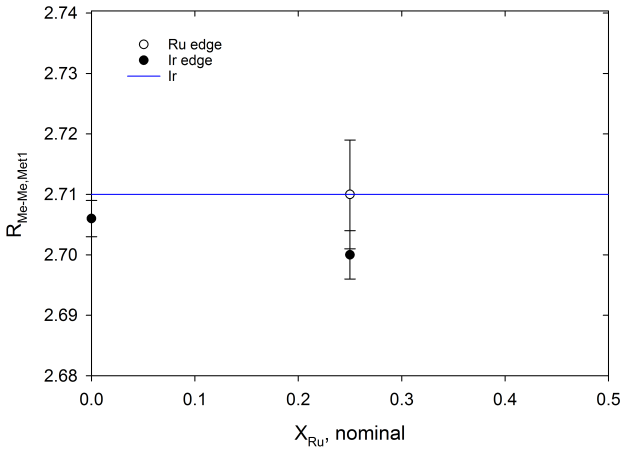

(b) $R_{Me-Met1}$

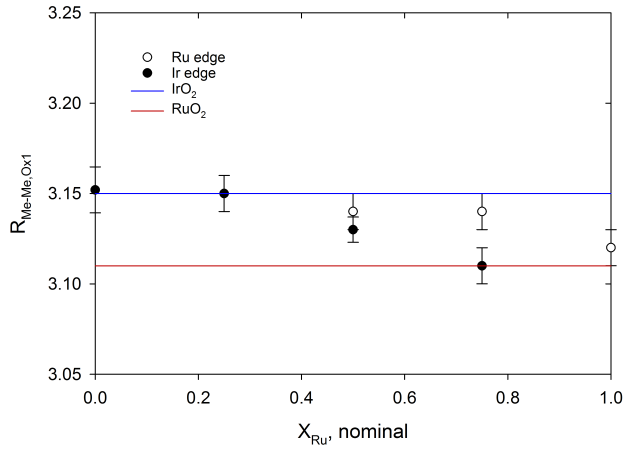

(c) R_{Me-Ox1}

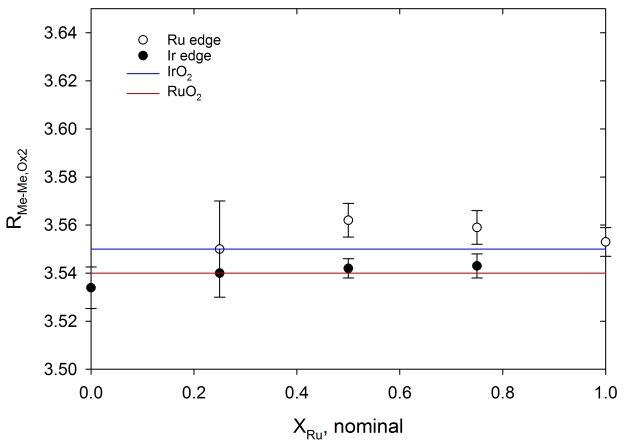

(d) R_{Me-Ox2}

Fig. 8 Experimentally obtained bond lengths in Å for the (a) oxygen shell ,R_{Me-O}, (b) first metal-phase shell, $R_{Me-Met1}$, (c) first metal oxide shell, R_{Me-Ox1}, and (d) second metal oxide shell, R_{Me-Ox2}, as function of nominal ruthenium fraction. The reference bond length is indicated in the figures for IrO_2 and Ir in blue and RuO_2 in red.

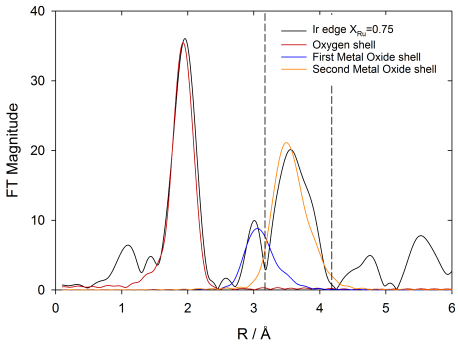

Fig. 9 Contributions from individual shells for X_{Ru}=0.75 recoded at Ir-edge.

occupancy of Ru found from both Ir- and Ru-edges in the EXAFS refinement of the X_{Ru}=0.25 and 0.75 spectra, Fig. 6. However, for X_{Ru}=0.50 the value differed from the two edges indicating that the distribution of Ru was not completely homogeneous.

The bond lengths in Figure 8c for shell 3 in Table 1 ("Me-Me, Ox1") are consistent with the linear lattice contraction inferred from the X-ray diffractograms. The bond length for shell 3 decreases with increasing ruthenium fraction as assessed from both edges and as expected for formation of solid solution. The decrease is the same as that obtained by Rietveld refinement, Fig. 2.

The other EXAFS-based bond lengths in Figure 8 are also consistent with what would be expected from the XRD results within the uncertainties. The average bond-length for the six oxygen atoms is expected to change from 1.980 Å in IrO_2 to 1.967 Å in RuO_2. This is in the range of the smallest uncertainties in the estimated bond length for this shell. Also, this shell was fitted as six oxygen atoms at an equal distance and not as two separate oxygen shells for the oxygen atoms in equatorial position and for the oxygen atoms in apical positions (i.e. shells 1 and 2 in Table 1 combined), which may have contributed adversely to the accuracy. The expected change in bond distance for the second metal oxide shell (shell 4 in Table 1, "Me-Me, Ox2") is 0.01 Å, which is clearly beyond the resolution limit of the methods employed.

The EXAFS data in Fig. 6a help to rationalise why the oxide lattice contracts linearly in Fig. 2 in spite of the sizeable metallic fraction in this material. The X_{Ru}=0.25 samples contain a rather large amount of iridium metal (i.e. Ir(0)). It is therefore perhaps somewhat unexpected that the c lattice parameter of the oxide phase of this composition complies so well with the linear contraction in Fig. 2, and that an $X_{Ru,Ox}$ close to nominal value is evaluated by XAS for this composition. If formation of a pure metallic iridium phase is assumed, and that the balance of the Ir forms a binary oxide with Ru, the ruthenium fraction of this oxide would be 0.41(4) if averaged over the three samples. The c lattice parameter data point for a nominal value of X_{Ru}=0.25 would therefore, if shifted to X_{Ru}=0.41, be well above the expected linear trend for a binary mixture[38]. This apparent inconsistency arises, however, from the fact that a substantial amount of ruthenium is incorporated into the Ir metal structure and that a small separate Ru metal phase was also formed.

Both the XRD and the EXAFS data consistently indicate the inclusion of ruthenium in the metallic iridium phase of the X_{Ru}=0.25 material. The lattice parameter of the metallic Ir has decreased from an average value of 3.839 Å for the X_{Ru}=0 samples to 3.830 Å for X_{Ru}=0.25, as can be seen in Table 3. Alloying of ruthenium into cubic iridium metal is normally associated with a decreasing lattice parameter with increasing ruthenium fraction[47]. A lattice constant of 3.830 Å is expected at an atomic fraction of ruthenium of ~19 at.%[47]. This is in agreement with the ruthenium partial occupancy found in the Ir metal by EXAFS evaluation at the Ir-edge, 0.17(3). However, this was smaller than the value obtained at the Ru-edge; 0.37(3). Formation of a metallic ruthenium phase and alloying of Ru into the Ir metal phase account for the close to nominal ruthenium partial occupancy obtained for the oxide phase, and explain why the c parameter for this oxide also complies with the linear trend in Figure 2.

The formation of metal phases does therefore not necessarily indicate inhomogeneous mixing of the elements in the oxide phase. A degree of alloying of Ru into the Ir metal, and possibly Ir into the Ru metal, is an expression of the ability of the PPS method to produce high degrees of elemental mixing, and appears to be the case for the metal phases as well although this phase appears to be somewhat less homogeneous.

The small fraction of a metallic Ru phase, ~3 wt.% metallic Ru (Table 3) is a likely cause for the differences seen for ruthenium partial occupancy found from the two edges. The first three shells of metallic Ru are located at 2.65, 2.71 and 3.79 Å, each with a multiplicity of six, according to the published crystal structure (ICDD Card no. 00-006-0663). The first two of these shells will therefore overlap with the first metallic Ir shell (at 2.71 Å) for the refinement at the Ru-edge. The metallic Ru phase was too small to be resolved in the EXAFS analysis, but its effect on the fitted metallic Ir structure may explain some of the differences seen for the properties of the Ir metallic phase as observed from the two edges.

The metallic Ru phase may exist as a pure metal, or it can be partially doped with Ir. An average increase of the c lattice parameter of the Ru metal phase is seen for X_{Ru}=0.25 compared to X_{Ru}=1 (Table 3), which indicates that Ir alloying into the Ru metal actually has occurred. However, the lattice parameter of Ru found for the pure ruthenium samples are larger than reported by Okamoto[47]. The hexagonal metallic ruthenium phase can support up to 44 at.% Ir before a transition to cubic Ir metal phase is expected[47]. The presence of both Ir and Ru metal phases, each with the possibility of being more or less phase pure and being alloyed with the other element homogeneously or in a varying degree throughout the structure may therefore well be the cause for the difference seen in ruthenium partial occupancy for the cubic Ir phase from the two edges.

The three methods of evaluating the atomic percentage of metallic Ir, Rietveld refinement, LCF of XANES and multiplicity of the oxygen shell (MOS), are in the same range, but with some deviations for the X_{Ru}=0.25 sample. The Rietveld refinement method and LCF of XANES are in better agreement for X_{Ru}=0. Since XRD requires some long-range order whereas XAS does not, a possible explanation behind the discrepancy seen for the pure Ir

sample might therefore be that small metallic Ir crystallites contribute to XAS measurements but are invisible in the XRD spectra. Differences can arise due to the probing scales not overlapping and the presence of phases of only limited or no long-range order in the samples. With these aspects of the measurement methods in mind we conclude that a set of likely models for the composition and structure of the polymeric-precursor synthesized $Ir_xRu_{1-x}O_2$ powders has been established.

For electrocatalytic applications an assessment of the mixing at the atomic level in multicomponent oxides is particularly important, both for fundamental understanding [13] and for practical applications. For example, results of Kötz and Stucki [11] indicate that for sputtered Ir-Ru mixed oxides, iridium and ruthenium interact synergistically to give a catalytic activity which is different from the sum of the catalytic activities of the two component oxides. For other types of samples the opposite is the case; Owe *et al.* [13] showed that in oxides synthesized by the hydrolysis method and verified to be solid solutions by pair-distribution analysis of high-resolution XRD data, the electrocatalytic activity is a simple superposition of the activities of the component oxides. A detailed structural characterization for the sputtered oxides reported by Kötz and Stucki [11] is not available, and a resolution of these conflicting reports is currently not possible. Therefore, if metal-metal interaction and catalytic properties of oxides are to be assessed experimentally, a good knowledge of the makeup and structure of the catalyst is essential. This goes well beyond the fundamental understanding of the electrocatalytic process and will have applied ramifications. If there is no synergistic interaction, optimization of catalysts should concentrate on maximising surface to volume ratio rather than composition, whereas also composition will be critical if such an interaction is present.

5 Conclusions

The extent of mixing and formation of solid solution in $Ir_xRu_{1-x}O_2$ powders prepared by a polymeric precursor method were evaluated by Rietveld refinement of XRD spectra and refinements of EXAFS spectra. Introduction of a mixed site describing the partial occupancy of ruthenium relative to iridium in both oxide and metal-phase shells was successfully applied in order to evaluate the degree of element mixing. Close to nominal ruthenium partial occupancy was found from both Ru- and Ir-edge for the oxide phase. However, the distribution of ruthenium and iridium was not completely homogeneous for all compositions. The X_{Ru}=0.50 oxide phase demonstrated different ruthenium partial occupancy obtained from the EXAFS spectra at the Ir- and Ru-edge, respectively. This was also the case for the cubic Ir metal phase produced in the X_{Ru}=0.25 sample, although this showed that an alloy was produced even for the metal phase. The presence of metal phases of both cubic Ir and hexagonal Ru, which are both likely to be mixtures of pure metals and alloys, is probably the cause for the difference seen in the Ru-partial occupancy from EXAFS at the two edges.

The metal-phase content of the Ir and Ru samples produced by polymeric precursor synthesis is highly sensitive to the synthesis conditions, and a consistent characterization of their structure required a concerted analysis based on several methods based on XRD and XAS. The presence of metal phases does not appear to implicate a low extent of element mixing of the oxide phase.

Conflicts of interest

There are no conflicts to declare.

Acknowledgements

The funding for this research was provided by Faculty of Natural Sciences and Technology at NTNU (project no. 81730900), and was greatly appreciated. We thank Diamond Light Source for providing access to synchrotron beam-time on B18 (proposal 8591) and synchrotron technician Diego Gianolio for help during the recording of the X-ray absorption spectroscopy data.

Notes and references

1 M. Carmo, D. L. Fritz, J. M. Mergel and D. Stolten, *International Journal of Hydrogen Energy*, 2013, **38**, 4901 – 4934.
2 E. Fabbri, A. Habereder, K. Waltar, R. Kotz and T. J. Schmidt, *Catal. Sci. Technol.*, 2014, **4**, 3800–3821.
3 L. A. Pocrifka, R. G. Freitas, A. V. Rosario and E. C. Pereira, *Journal of Solid State Electrochemistry*, 2011, **15**, 1109–1113.
4 Y.-T. Shih, K.-Y. Lee and Y.-S. Huang, *Journal of Alloys and Compounds*, 2015, **619**, 131 – 137.
5 W.-D. Huang, H. Cao, S. Deb, M. Chiao and J. Chiao, *Sensors and Actuators A: Physical*, 2011, **169**, 1 – 11.
6 K. Kreider, M. Tarlov and J. Cline, *Sensors and Actuators: B. Chemical*, 1995, **28**, 167–172.
7 C. R. Costa, C. M. Botta, E. L. Espindola and P. Olivi, *Journal of Hazardous Materials*, 2008, **153**, 616 – 627.
8 R. Chen, V. Trieu, B. Schley, H. Natter, J. Kintrup, A. Bulan, R. Weber and R. Hempelmann, *Zeitschrift fur Physikalische Chemie*, 2013, **227**, 651–666.
9 E. Kuznetsova, V. Petrykin, S. Sunde and P. Krtil, *Electrocatalysis*, 2015, **6**, 198–210.
10 V. Petrykin, K. Macounova, M. Okube, S. Mukerjee and P. Krtil, *Catalysis Today*, 2013, **202**, 63–69.
11 R. Kötz and S. Stucki, *Electrochimica Acta*, 1986, **31**, 1311 – 1316.
12 N. Halck, V. Petrykin, P. Krtil and J. Rossmeisl, *Physical Chemistry Chemical Physics*, 2014, **16**, 13682–13688.
13 L.-E. Owe, M. Tsypkin, K. S. Wallwork, R. G. Haverkamp and S. Sunde, *Electrochimica Acta*, 2012, **70**, 158 – 164.
14 E. Rasten, G. Hagen and R. Tunold, *Electrochimica Acta*, 2003, **48**, 3945 – 3952.
15 A. Marshall, B. Børresen, G. Hagen, M. Tsypkin and R. Tunold, *Electrochimica Acta*, 2006, **51**, 3161–3167.
16 A. Marshall, B. Børresen, G. Hagen, M. Tsypkin and R. Tunold, *Materials Chemistry and Physics*, 2005, **94**, 226 – 232.
17 A. Marshall and R. Haverkamp, *Electrochimica Acta*, 2010, **55**, 1978–1984.
18 R. Tunold, A. T. Marshall, E. Rasten, M. Tsypkin, L. E. Owe and S. Sunde, *ECS Transactions*, 2010, **25**, 103–117.
19 A. Reksten, F. Moradi, F. Seland and S. Sunde, *ECS Transactions*, 2013, **58**, 39–50.

20 C. Angelinetta, S. Trasatti, L. Atanososka and R. Atanasoski, *Journal of Electroanalytical Chemistry and Interfacial Electrochemistry*, 1986, **214**, 535 – 546.

21 M. Kakihana and M. Yoshimura, *Bulletin of the Chemical Society of Japan*, 1999, **72**, 1427–1443.

22 J. Lin, M. Yu, C. Lin and X. Liu, *The Journal of Physical Chemistry C*, 2007, **111**, 5835–5845.

23 A. V. Rosario, L. O. Bulhoes and E. C. Pereira, *Journal of Power Sources*, 2006, **158**, 795 – 800.

24 A. Terezo and E. Pereira, *Electrochimica Acta*, 2000, **45**, 4351–4358.

25 A. J. Terezo and E. C. Pereira, *Materials Letters*, 2002, **53**, 339–345.

26 M. Santos, A. Terezo, V. Fernandes, E. Pereira and L. Bulhões, *Journal of Solid State Electrochemistry*, 2005, **9**, 91–95.

27 L. Profeti, F. Simões, P. Olivi, K. Kokoh, C. Coutanceau, J.-M. Léger and C. Lamy, *Journal of Power Sources*, 2006, **158**, 1195 – 1201.

28 N. Mamaca, E. Mayousse, S. Arrii-Clacens, T. Napporn, K. Servat, N. Guillet and K. Kokoh, *Applied Catalysis B: Environmental*, 2012, **111-112**, 376 – 380.

29 D. Von Dreifus, A. J. A. de Oliveira, A. V. do Rosario and E. C. Pereira, *Journal of Superconductivity and Novel Magnetism*, 2013, **26**, 2319–2321.

30 R. G. Freitas, L. R. Marchesi, R. T. S. Oliveira, F. I. Mattos-Costa, E. C. Pereira, L. O. S. Bulhões and M. C. Santos, *JOURNAL OF POWER SOURCES*, 2007, **171**, 373–380.

31 O. Kahvecioglu and S. Timur, Advances in Energy Materials, 2009, pp. 77–86.

32 X. Yonglei, X. Likun, W. Juntao and L. Xiangbo, *RARE METAL MATERIALS AND ENGINEERING*, 2010, **39**, 1903–1907.

33 M. Newville, *Fundamentals of XAFS*, 2004.

34 B. Ravel and M. Newville, Physica Scripta T, 2005, pp. 1007–1010.

35 S. Tomic, B. Searle, A. Wander, N. Harrison, A. Dent, J. Mosselmans and J. Inglesfield, *New Tools for the Analysis of EXAFS: The DL EXCURV Package*, Council for the central laboratory of the research councils technical report, 2005.

36 T. Arikawa, Y. Takasu, Y. Murakami, K. Asakura and Y. Iwasawa, *Journal of Physical Chemistry B*, 1998, **102**, 3736–3741.

37 A. Finch, N. Allison, S. Sutton and M. Newville, *Geochimica et Cosmochimica Acta*, 2003, **67**, 1189–1194.

38 C. Georg, P. Triggs and F. Lévy, *Materials Research Bulletin*, 1982, **17**, 105 – 110.

39 E. Balko and C. Davidson, *Journal of Inorganic and Nuclear Chemistry*, 1980, **42**, 1778 – 1781.

40 A. R. Hillman, M. A. Skopek and S. J. Gurman, *Physical Chemistry Chemical Physics (Incorporating Faraday Transactions)*, 2011, **13**, 5252.

41 M. Hüppauff and B. Lengeler, *Journal of The Electrochemical Society*, 1993, **140**, 598–602.

42 T. Pauporté, D. Aberdam, J.-L. Hazemann, R. Faure and R. Durand, *Journal of Electroanalytical Chemistry*, 1999, **465**, 88 – 95.

43 R. Kawar, P. Chigare and P. Patil, *Applied Surface Science*, 2003, **206**, 90 – 101.

44 O. Gencyilmaz, F. Atay and I. Akyuz, *Journal of optoelectronics and advanced materials*, 2015, **17**, 395–402.

45 M.-S. Miao and R. Seshadri, *Journal of Physics: Condensed Matter*, 2012, **24**, 215503.

46 J. H. A. Martens, R. Prins and D. C. Koningsberger, *The Journal of Physical Chemistry*, 1989, **93**, 3179–3185.

47 H. Okamoto, *Journal of Phase Equilibria*, 1992, **13**, 565–567.

Journal Name

ARTICLE TYPE

Cite this: DOI: 10.1039/xxxxxxxxxx

Strategies for the analysis of the elemental metallic fraction of Ir and Ru oxides via XRD, XANES, and EXAFS†

Anita Hamar Reksten,[a‡] Andrea E. Russell,[b] Peter W. Richardson,[b] Stephen J. Thompson,[b] Karina Mathisen,[c] Frode Seland,[a] and Svein Sunde[d]

Received Date
Accepted Date

DOI: 10.1039/xxxxxxxxxx

www.rsc.org/journalname

Iridium and ruthenium oxide are active electrocatalysts for oxygen evolution. The relation between preparation method, structure, and behavior of mixed oxides of iridium and ruthenium are of interest in order to obtain active and stable catalysts. In this work the structure of mixed Ru-Ir oxides synthesized by the polymeric precursor method, which involves the formation of a gel containing the metal precursors and subsequent heat-treatment in air, was studied for the $Ir_xRu_{1-x}O_2$ system. An in-depth analysis of X-ray diffraction (XRD) and X-ray absorption (XAS) data, including EXAFS and linear combination of XANES, shows that the polymeric precursor synthesis method is capable of providing an intimate mixing of Ir and Ru in the catalyst. In addition to the oxide phase, metal phases, i.e. with Ru or Ir or both in oxidation state zero (Ir(*fcc*) and Ru(*hcp*)), were also found in the product materials. Facing complex structures such as some of those synthesized here, we have shown that a representation of shells with more than one atom type are efficiently represented using mixed sites, i.e. including scattering contributions from several elements in a site corresponding to a partial occupancy of the site by these elements, this method forming a very efficient basis for analyzing EXAFS data.

1 Introduction

Films and powders of Ir and Ru oxides are relevant for a range of applications, such as oxygen-evolving catalysts[1,2], as capacitors[3,4], pH electrodes[5,6], electrodes in waste water treatment[7] and in the chlor-alkali industry[8].

The electrocatalytic activity, selectivity and stability of rutile-type oxide electrocatalysts have been linked to local structure [9–12]. For multicomponent oxides an assessment of the degree of mixing at the atomic level is of particular interest, both for a fundamental understanding of catalytic activity[11,13] and for applications. However, such oxides can be synthesized by a number of methods[14–19], and their structure may vary significantly with preparation method. In this way differences in properties are directly linked to the synthesis methods[20]. The chemical composition and sample structure must therefore be examined critically for each preparation technique.

The polymeric precursor synthesis (PPS) is a method that is particularly well suited for making multicomponent oxides which are well mixed and homogenous at the atomic level[21,22]. It is also a simple and low cost method[23]. However, films and powders produced by the PPS have previously been reported to contain significant fractions of metal phases[23–29], i.e with the metallic elements in oxidation state zero, in addition to the oxides. The metal-phase fraction, which can be significant, is very sensitive to the synthesis conditions[3,23–32]. In addition to investigating the degree to which PPS samples are atomically well mixed it is therefore also necessary to characterize them in terms of any metallic phases in the samples.

X-ray absorption spectroscopy (XAS) and in particular the X-ray absorption near edge structure (XANES) and extended X-ray absorption fine structure (EXAFS) can be used to provide information regarding the oxidation state and coordination chemistry (XANES) and the distances, coordination number and identity of elements immediately surrounding a specific atom (EXAFS)[33]. Chemical state and local atomic structure can therefore be investigated by this method. Since only the local environment of the

[a] *Department of Materials Science and Engineering, Norwegian University of Science and Technology (NTNU), NO-7491, Trondheim, Norway.*
[b] *Department of Chemistry, University of Southampton, Southampton SO17 1BJ, England.*
[c] *Department of Chemistry, Norwegian University of Science and Technology (NTNU), NO-7491 Trondheim, Norway.*
[d] *Department of Materials Science and Engineering, Norwegian University of Science and Technology (NTNU), NO-7491, Trondheim, Norway. Fax: +47 7359 1105; Tel: +47 7359 4051; E-mail: svein.sunde@ntnu.no*
† Electronic Supplementary Information (ESI) available: [details of any supplementary information available should be included here]. See DOI: 10.1039/b000000x/
‡ Current address: SINTEF Sustainable Energy Technology, NO-0373 Oslo, Norway.

specific atom type is involved, this method can be used to study both crystalline and amorphous samples, and appears particularly well suited to samples in which substantial disorder is expected, such as those described above.

Whereas elaborating the structure of the first shell from EXAFS data refinement is relatively straightforward, samples such as mixed oxides puts more stringent requirements on the analysis because a solid solution implies determining mixed element contribution to more distant shells. Also, because previous experience with the PPS method indicates that several phases may be present in the samples, EXAFS analysis of such samples may prove even more challenging. As data refinement may be performed in several different ways, for example in *k*-space or in real space, using different structural models, and a few more to be detailed below, a range of options exist for how to perform the analysis and on which its outcome may depend. Finally, analysis results will have to be compared to and matched with those of other characterization methods, notably X-ray diffraction (XRD). An investigation of strategies for analysing this relevant class of materials with XANES and EXAFS may seem warranted.

In this work we present results of a thorough structural characterization of ruthenium and iridium oxides and their solid solutions, synthesized by the PPS method. The degree to which the PPS results in the production of well-mixed and homogenous powders at the atomic level is investigated by use of X-ray diffraction (XRD) with Rietveld refinement and X-ray absorption spectroscopy (XAS). Our purpose is to show that with these techniques a consistent set of structural data for pure and mixed oxide phases may be achieved also in the presence of iridium or ruthenium metal phases (Ir(0)(*fcc*) and Ru(0)(*hcp*)), and to analyze quantitatively the fraction of metal phase in the samples with these methods. In particular, below we explore and compare three different approaches to EXAFS refinement, viz. the co-shell approach, the mixed site approach and Fourier filtration, emphasizing the assessment and comparison of these three approaches.

2 Experimental

2.1 Synthesis

$Ir_xRu_{1-x}O_2$ powders were prepared by a polymeric precursor synthesis (PPS). A gel was prepared by dissolving citric acid (CA, Merck 99%) in ethylene glycol (EG, VWR AnalaR Normapur analytical reagent). This mixture was heated at 60 °C for 45 minutes while being stirred. The temperature was raised to 75 °C and the metal precursors, $H_2IrCl_6 \cdot 4H_2O$ (Alfa Aesar 99%, M_w=479 mol g^{-1}) and, or $RuCl_3 \cdot xH_2O$ (Alfa Aesar PMG basis 99.9%, M_w=261 mol g^{-1}) were added to the gel. The total amount of metal added was 0.5 mmol. The ratio between CA, EG and metal was 3:14:1. Stirring was continued for 45 minutes before the gel was transferred to a quartz-tube crucible. The gels were subsequently heat-treated by a three stage temperature program in an atmosphere of stagnant air, all with a heating rate of 1 °C min^{-1} between the stages. The stages were: 30 min at 130 °C, 20 min at 250 °C and finally 20 min at 500 °C. A lid was placed over the crucible, but not fully covering the opening. Three identical syntheses were carried out for each composition x = 0, 0.25, 0.5, 0.75 and 1. We will state the nominal composition of the samples below by the atom fraction of ruthenium, X_{Ru}, or the atom fraction of iridium, X_{Ir}, and $X_{Ir} = 1 - X_{Ru}$.

2.2 X-ray Powder Diffraction, Rietveld Refinement and SEM

XRD measurements for all powders were performed with a Bruker AXS D8Focus diffractometer using Cu $K-\alpha$ radiation source (equipped with a Ni filter that excludes the Cu $K-\beta$ radiation). Zero background silicon sample holders were used. Rietveld analysis was carried out with the Bruker AXS TOPAS version 4.2 software, using a pseudo-Voigt function. The background intensity was accounted for using a Chebychev polynomial of the order 6. Refinements of diffraction patterns were performed within space groups 136 (P42/mnm), and 225 (Fm-3m) or 194(P63/mmc) if metal-phases of iridium or ruthenium (Ir(*fcc*) or Ru(*hcp*)) were present. Unit cell values, the crystallite size and fractions of metal and oxide phases were obtained. The occupancies were set to nominal values, and were not refined.

The sample morphology was studied with FE-SEM, Zeiss Ultra 55 LE, using a high efficiency in-lens secondary electron detector.

2.3 X-ray Absorption Spectroscopy

2.3.1 Data Collection.

The local environment of Ir and Ru was investigated using X-ray absorption spectroscopy (XAS) of one sample of each composition produced. The XAS data were collected at beamline B18-Core XAS of the Diamond Light Source Synchrotron in fluorescence mode. A germanium 9-element detector was used to detect the fluorescence signal. The samples were placed at an angle of 45° to the beam and the detector. The ion chamber before the sample was filled with an appropriate mix of inert gases to optimize sensitivity. A second ion chamber was used for transmission mode data collection for the references foils. Data were collected during a multi-bunch electron filling mode of the Diamond storage ring providing a maximum current of 300 mA. For the measurements of the XAS at the Ru K-edge 0.25 eV steps were used from 21917 to 22917 eV with counting time at each step of 43 ms, applying Si(311) double crystal monochromators and Pt-coated collimating and toroidal focusing mirrors. At the iridium edge a step size of 0.35 eV was used over the energy range 11015-12414 eV, with a counting time of 60 ms at each step, using a Si(111) double crystal monochromator and Cr-coated collimating and toroidal focusing mirrors. Several scans were collected and summed in order to improve the statistics.

Samples of all compositions investigated were supported on carbon paper. Inks of the samples, prepared with 20 mg catalyst, 1 mL deionized water, 200 μL isopropanol (AnalaR Normapure VWR), 228 μL 5 wt.% Nafion (Alfa Aesar) and 4 mg carbon black (Vulcan XC72R), were prepared and painted onto a 0.26 mm thick Toray carbon paper (TGPH-090) until a loading of 0.2-0.3 mg catalyst cm^{-2}. Finally the samples were pressed at 130 °C and ∼1 kg cm^{-2} for 3 minutes.

2.3.2 Data Reduction.

The XAS data were binned, summed, normalized, and energy corrected relative to the metal foils (Ru K-edge = 22117 eV at Ru K-edge, and Pt L_{III} edge=11564 eV used for calibration of the Ir-L_{III}-edge) using Athena, a program in the IFEFFIT package[34]. The absorption edge was measured as the first inflection point as identified in the derivative of the spectra. The XANES and EXAFS spectra were normalized from 17 to 90 eV and 150 to 1090 eV above the edge, respectively. The spectra were carefully deglitched and truncated at the end of EXAFS spectra when needed. The linear combination fit (LCF) procedure in the Athena program was used to fit the XANES spectra to the reference material, which were powders of IrO_2 (Aldrich, 99.9 %), $IrCl_3$ (Alfa Aesar, 99.8 %) and Ir black (Alfa Aesar 99.9 %). The linear combination fitting was performed of the XANES spectra over a range from 17 eV below the edge to 70 eV above the edge, always applying the normalization range as described above. The energy shifts of the reference spectra were also fitted, but closely monitored and they were always less than 1.1 eV. The fit parameter for the LCF was reported for each fit, defined in Equation (1),

$$R = \frac{\sum_i^N (|\chi_i^{exp}(k) - \chi_i^{calc}(k)|)^2}{\sum_i^N |\chi_i^{exp}(k)|^2} \quad (1)$$

where $\chi_i^{exp}(k)$ and $\chi_i^{calc}(k)$ are the experimental and theoretical EXFAS fine-structure functions. To distinguish this quantity from bond lengths (see below) we will refer to R in Eq. (1) as the "R-factor".

2.3.3 EXAFS Least-Squares Refinements.

EXAFS least-square refinements were carried out using the DL-EXCURV code, which performs curve fitting of the theoretical $\chi^{th}(k)$ to the experimental $\chi^{exp}(k)$ using curved wave theory[35]. The calculation of ab initio phase shifts for the expected neighboring elements also took place in DL-EXCURV. The least-squares refinements were carried out in the wavenumber k range 2 through 18 eV and 2 through 14 eV respectively for spectra obtained at the Ir- and Ru-edge, using a k^3 weighting scheme.

Whether a solid solution between iridium and ruthenium was obtained was studied by XAS using a range of approaches which we have termed the co-shell approach, the mixed site approach and Fourier filtration. For each of these we employed several strategies and sets of initial values in order to arrive at robust conclusions with respect to the formation of solid solutions. The reference bond lengths and coordination numbers for the pure oxides are reported in Table 1. The mixing was included into the analysis by two distinct methods, the co-shell and mixed site approach, which are summarized in Table 2.

In the co-shell approach two shells, one Ir and one Ru shell, were included for each mixed shell. In the mixed site approach a parameter describing the relative scattering contribution from Ru and Ir in the same site was introduced. We will refer to the relative scattering contribution from a given element as its partial occupancy of the site. In the case of both metal and oxide phases being present, a separate parameter was included for each phase. These were fitted independently. Fourier filtering was performed in order to obtain information of individual shells in the R-space plot by back- transforming the regions of the specific peaks into k-space.

Table 1 Coordination number (N) and bond length (R) of the first four shells in iridium and ruthenium oxide[36]. Me stands for the metal atom, i.e. iridium in IrO_2 and ruthenium in RuO_2. The metal atom in shell 3 is indicated by subscript "Ox1" and that in shell 4 by subscript "Ox2"

Shell	Bond	N	RuO_2 R / Å	IrO_2 R / Å
1	Me-O	2	1.94	1.94
2	Me-O	4	1.98	2.00
3	Me-Me, Ox1	2	3.11	3.15
4	Me-Me, Ox2	8	3.54	3.55

As seen in Table 1 IrO_2 and RuO_2 have two oxygen shells with coordination numbers two and four, in apical and equatorial positions, respectively. In the refinements only one oxygen shell was included, with an initial value for the coordination number equal to six.

Table 2 Overview of the shells included to introduce mixing in the co-shell and mixed site approach, given for the Ir-edge. The metal atom in shell 3 in Table 1 is indicated by subscript "Ox1" and that in shell 4 by subscript "Ox2". $X_{Ru,Ox}$ and $X_{Ru,Met}$ are the partial occupancy of Ru defined for the oxide and metal phase, respectively, in the mixed-site approach.

	Shell	co-shell	Mixed Site
Oxide	Ir-Me_{Ox1}	Ir-Ru_{Ox1} Ir-Ir_{Ox1}	Ir-Me_{Ox1}, $X_{Ru,Ox}$
	Ir-Me_{Ox2}	Ir-Ru_{Ox2} Ir-Ir_{Ox2}	Ir-Me_{Ox2}, $X_{Ru,Ox}$
Metal	Ir-Me_{Met1}	Ir-Ru_{Met1} Ir-Ir_{Met1}	Ir-Me_{Met1}, $X_{Ru,Met}$

For the co-shell method shells of mixed occupancy were modelled by including two shells initially at the same bond lengths, one consisting of iridium and one consisting of ruthenium. Spectra from both edges were refined, and the following description applies to the treatment of both. For X_{Ru}=0.75 and X_{Ru}=0.50 three shells were included. These were the oxygen shell corresponding to a combination of shells 1 and 2 in Table 1, and the two first shells containing metal atoms, corresponding to shells 3 and 4 in Table 1, c. f. Table 2. The initial coordination numbers were set to be the reference coordination number in Table 1, but multiplied by the nominal fraction of ruthenium for the ruthenium shells and with nominal iridium fraction for the iridium shells. First the systems were refined with only iridium or ruthenium in the whole structure, Ru for X_{Ru}=0.75 and X_{Ru}=0.50 and Ir for all except X_{Ru}=0.75. Then the second element was introduced to the first metal oxide shell (shell 3 in Table 1) by adding another shell at the same bond length. Refinements of these shells (combined shells 1 and 2 and shell 3 in Table 1) were performed first in terms of the energy shift, E_F, all bond lengths, R, and Debye-Waller factors (DWFs). Then followed a separate refinement in terms of the coordination numbers, N. These two steps were repeated until convergence. Next, the whole procedure was repeated after the addition of a co-shell for second metal oxide shell (shell 4 in Table 1). For the sample with X_{Ru}=0.25, consisting of both metal and oxide phases, three shells were included,

one oxygen shell, one metal oxide shell (shell 3 in Table 1), and the first metal-phase shell. The same refinement procedure was carried out as for the X_{Ru}=0.75 and 0.50 described above, starting with a pure system and then introducing the other element in the individual shells.

In the mixed site approach an additional parameter describing the partial occupancy of a site was refined. Mixed site is a function in DL-EXCURV where a partial occupancy site is defined and the initial occupancy of up to three elements is specified. The mixed Ir/Ru site is then defined as a new atom type (QA), and atomic potential and phase shifts are calculated for the Ir/Ru pair. Refining QA will then optimize the fractions of the elements defined for the shell. One has the option of including several mixed sites and can therefore have different fractions for different contributions, for instance different phases. The mixed site method was used to find the partial occupancy of Ca and Sr in aragonite structured corals in the work of Finch et al.[37]. In this work the partial occupancy of ruthenium was investigated, for X_{Ru}=0.25 being a mix of an oxide phase and a metal phase. In the latter case one parameter for each phase was defined and were fitted independently of each other, as $X_{Ru,Ox}$ and $X_{Ru,Met}$.

Spectra from both edges were refined with the mixed site approach, and the following description applies to the treatment of both. For X_{Ru}=0.75 and X_{Ru}=0.50 three shells were included in the fit, one oxygen shell and two metal oxide shells (corresponding to the combined 1 and 2 shells, shell 3 and shell 4 in Table 1). Refinement of E_F, all bond lengths, R, and DWFs together, then all N and finally $X_{Ru,Ox}$ were alternated until convergence. For X_{Ru}=0.25 four shells were included, the oxygen shell, the first two metal oxide shells as above, and the first metal-phase shell. The refinements for this sample was not as straightforward as for the pure oxides. In this case refinements of E_F, all R and DWFs together and then refinement of all N were alternated until convergence before all N were left fixed and alternating refinements of E_F, all R, and DWFs together, then $X_{Ru,Ox}$ followed by $X_{Ru,Met}$ were repeated until convergence.

3 Results

3.1 Metal-phase fraction and oxide structure from XRD

X-ray diffractograms, one of each composition, are shown in Figure 1a. A rutile structure is present in all compositions. A shift in peak position can be seen with increasing iridium content from the pure ruthenium oxide, clearly demonstrated by the reflection located in the range 34-36° in Figure 1b. The two diffractograms for X_{Ru}=0 and 0.25 in Figure 1a indicate that metal-phase iridium is present, as can be inferred from the peak at $2\theta \approx 47.5°$. In several of the samples metallic phases, either Ir(*fcc*), Ru(*hcp*), or both, were present. The weight fractions, cell parameters and crystallite sizes of the metal phases are summarized in Table 3. Below we will quantify metal-phase fractions in the samples either by the weight fraction of metal-phase Ru or Ir, wt.% (the mass of Ru or Ir metal divided by the total mass of sample, in percent) or the number of Iror Ru) atoms in oxidation state zero divided by the total number of Ru (or Ru) present in percent as at.%. This corresponds to the at.% as it would have been measured by LCF of XANES. As can be seen the pure iridium samples contained a higher fraction of metal-phase Ir than samples with X_{Ru}=0.25, with an average of 63.2 wt.% and 39.4 wt.% , respectively. This corresponds to 66.6 at.% and 47.5 at.% on average, respectively. (Equations for the conversion are given in the Supplementary Material, section S.4.) Metal-phase Ru was also seen for at least two of the three mixed oxides and the pure ruthenium samples produced. The metal phase fraction was found to be less than 3 wt.% for all samples with the exception of the second sample of X_{Ru}=0.75. This sample contained 14.3 wt.% metal-phase Ru(0), corresponding to 25.5 at.% of the ruthenium atoms being in the metal phase (see Supplementary Material section S.4).

Inclusion of strain in the Rietveld refinements did not affect appreciably the estimates of the fraction of metal-phase in the samples. A detailed discussion is included in Section S.2 of the ESI.

The lattice parameters emerging from the Rietveld analysis are presented as a function of nominal ruthenium fraction in Figure 2. Each data point is an average of the three samples for each composition, and the standard deviation for the set is indicated by error bars. As expected from the shifts in peak positions in Figure 1b, both lattice parameters change with composition. The c lattice parameters decrease linearly as more ruthenium is incorporated into the structure for both synthesis and indicates formation of a solid solution of the two oxides according to Vegard's law. This trend and the values agree well with previously reported lattice parameters[13,38,39]. The a parameter displays considerably less variation, also in agreement with the literature[13,38,39].

3.2 Metal-phase fraction from linear combination fits of XANES.

The fraction of Ir metal-phase was investigated by carrying out linear combination fit (LCF) of the X_{Ru}=0, 0.25, 0.5, and 0.75 samples with spectra of pure metal-phase Ir and IrO_2. Reference samples of oxide and metal-phase Ir with composition equal to the nominal composition of the X_{Ru}=0.25, and X_{Ru}=0.50 and X_{Ru}=0.75 were not available. Instead we performed the LCF of the X_{Ru}=0.25, and X_{Ru}=0.50 and X_{Ru}=0.75 samples with the pure iridium reference. We used $IrCl_3$ in order to evaluate a possible contribution from Ir^{+3}. The $IrCl_3$ has been reported used in several investigations of oxidation state of Ir in anodically formed iridium oxide films (AIROF), electrochemically formed iridium oxide films (EIROF), and sputtered iridium oxide films (SIROF) in an in situ electrochemical cell as function of applied potential[40–42].

Two sets of LCFs were carried out, one with all three reference spectra included (Ir^0, Ir^{+3} and Ir^{+4}), and one which did not include Ir^{+3}. The LCF for X_{Ru}=0 and 0.25 is shown in Figure 3. It was not possible to fit the XANES data for compositions X_{Ru}=0.5 and 0.75 to any linear combination of reference spectra containing metal-phase Ir. The atomic percents of Ir^0 emerging from the LCFs are summarized in Table 4. For X_{Ru} = 0 the LCFs with only Ir^0 and Ir^{+4} (Figure 3a and Table 4) a metal-phase fraction of 77 at.%, equal to 74 wt.%, was obtained, which is 18 percentage points larger than what was found by XRD (55.9 wt.% for this

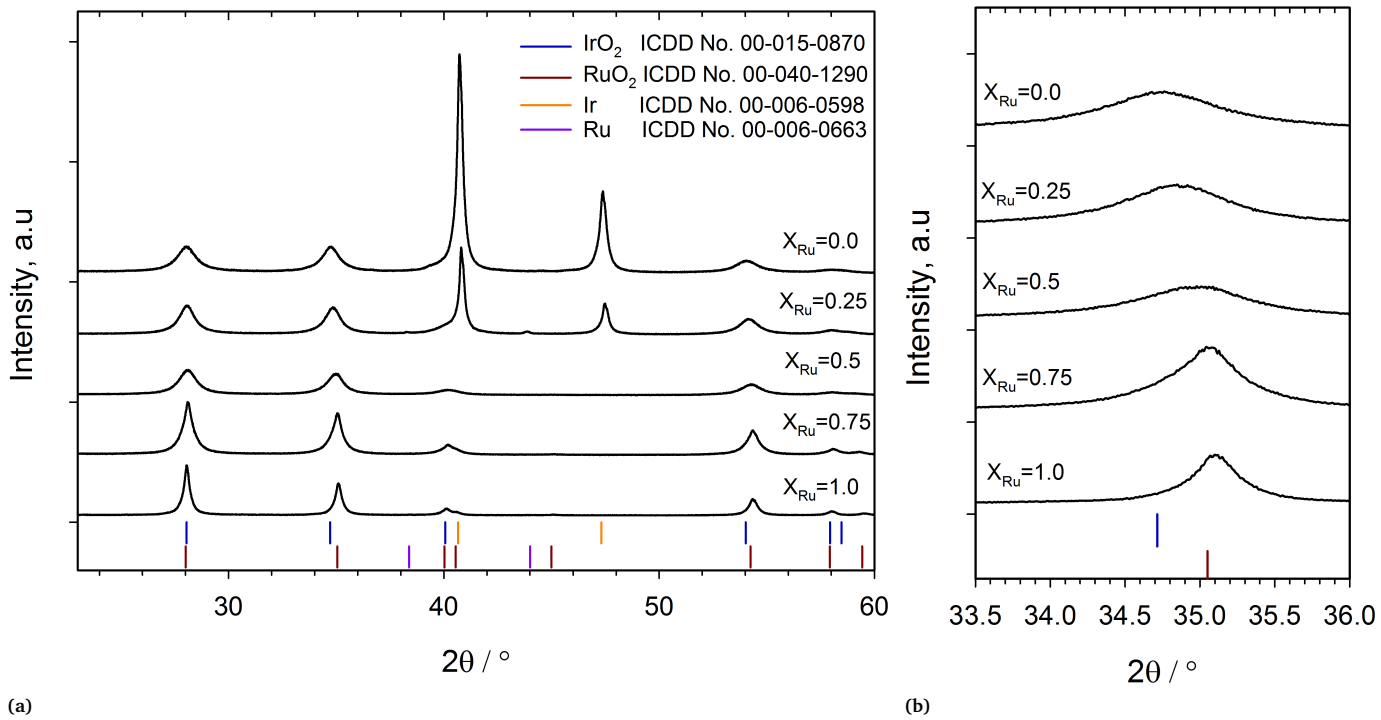

Fig. 1 (a) X-ray diffractogram of $Ir_xRu_{1-x}O_2$ as function of X_{Ru}, and (b) magnification of (101) reflection located at 2θ ~34-35 °.

Table 3 Overview of the metal phases present in the samples as evaluated by XRD Rietveld analysis. The unit cell lengths, a and c, and crystallite diameter, d, for the metal-phase iridium and ruthenium present in the three catalyst powders obtained from Rietveld analysis. Iridium has cubic structure (Fm-3m) and Ru has hexagonal structure (P63/mmc). Data for all the three different samples of each composition, arbitrarily labelled "1", "2", and "3" for distinction, are given

		Ir			Ru			
X_{Ru}		wt.%	a / Å	d / nm	wt.%	a / Å	c /Å	d / nm
0.00	1	55.9(1)	3.84023(7)	16.91(5)	0	-	-	-
	2	75.6(2)	3.83933(7)	25.2(1)	0	-	-	-
	3	58.1(1)	3.83913(7)	16.60(6)	0	-	-	-
0.25	1	42.3(1)	3.83005(8)	23.8(1)	3.01(8)	2.7162(4)	4.3141(1)	24(1)
	2	45.1(1)	3.83116(8)	23.7(1)	3.00(8)	2.7162(4)	4.3141(1)	24(1)
	3	30.91(8)	3.83016(8)	21.4(1)	1.84(7)	2.7161(6)	4.3145(2)	18(1)
0.50	1	0	-	-	0	-	-	-
	2	0	-	-	0.52(8)	2.714(2)	4.326(7)	25(7)
	3	0	-	-	1.36(8)	2.715(2)	4.341(6)	9.3(8)
0.75	1	0	-	-	0	-	-	-
	2	0	-	-	14.3(1)	2.7104(2)	4.2940(4)	16.2(2)
	3	0	-	-	2.17(6)	2.715(2)	4.306(4)	11.0(5)
1.00	1	0	-	-	1.14(7)	2.711(1)	4.273(3)	17(2)
	2	0	-	-	2.00(9)	2.715(1)	4.264(4)	9.4(6)
	3	0	-	-	0	-	-	-

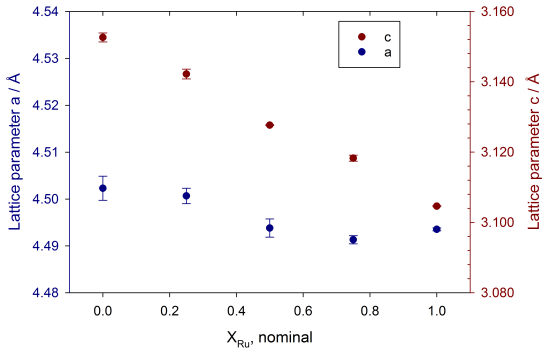

Fig. 2 Lattice parameters a and c for the oxide phase (rutile crystal structure) obtained by Rietveld refinement of X-ray diffractograms as a function of nominal ruthenium fraction. Each data point is an average of the three identical synthesis of each composition and the standard deviation of the three is indicated by error bars.

sample). When the Ir^{+3} spectra was included it was found that 7 at.% of the Ir atoms existed in trivalent state, and the metal-phase fraction was 71 at.%, Figure 3b and Table 5. A slightly improved R-factor is seen with the addition of Ir^{+3} for the pure Ir sample, and it is possible that some of the Ir exist in this oxidation state. A presence of Ir^{+3} could perhaps be due to incomplete decomposition of $IrCl_3$ or formation of intermediate Ir_2O_3 [43,44]. Ir_2O_3 is, however, calculated to be unstable[45] unless the oxygen chemical potential is very low.

The fraction of metal-phase found for the $X_{Ru}=0.25$ sample was 42 at.% iridium, corresponding to 34 wt.% (c.f. 42.3 wt% for this sample by Rietveld analysis, $X_{Ru}=0.25$ sample 1 in Table 3). (The Ir^{+3} fraction was found to be zero when included in this fit , Figure 3c.) The LCF of XANES thus predicted a somewhat smaller metal-phase fraction than the Rietveld analysis for the pure Ir sample. However, a small contributing metallic Ru phase (3 wt%) was accounted for in the Rietveld analysis, which can not be included for a LCF carried out in this manner. The weight percentages should therefore in principle not be directly compared. However, since this is quite a small fraction it is therefore not assumed to influence the results substantially. For $X_{Ru}=0.25$ the metal-phase fraction was found to be similar for the two methods.

3.3 Metal-phase fraction and oxide structure from EXAFS Least-Squares Refinements.

The validity of the mixed site approach was verified by several different procedures. One method was to first perform the refinement of the pure system of either Ru or Ir, viz. the pure iridium system for $X_{Ru}=0.25$ and 0.50 and the pure ruthenium system for $X_{Ru}=0.5$ and 0.75, and and then introduce and refine the partial occupancy $X_{Ru,Ox}$, and for $X_{Ru}=0.25$ also $X_{Ru,Met}$. The values from the first of these refinements served as a set of initial values for the second. This procedure was performed for spectra recorded at both edges.

Refinements were also carried out with the partial occupancies $X_{Ru,Ox}$ (and for $X_{Ru}=0.25$ $X_{Ru,Met}$) introduced initially and with initial values set to nominal values. The latter procedure was

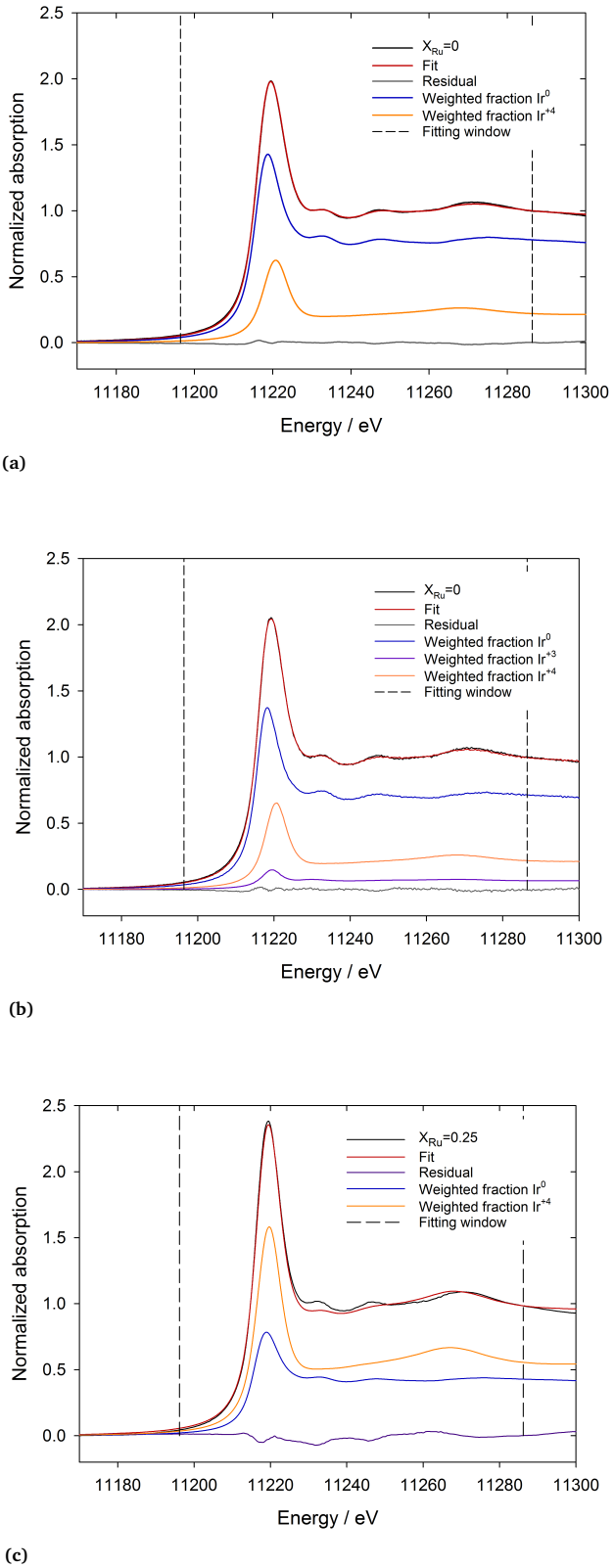

Fig. 3 Linear combination fit of $X_{Ru}=0.0$ (sample 1 of those with $X_{Ru}=0.0$, Table 3), with (a) Ir^0 and Ir^{+4} standards and (b) Ir^0, Ir^{+3} and Ir^{+4} standards. (c) linear combination fit of $X_{Ru}=0.25$ (sample 1 of those with $X_{Ru}=0.25$,Table 3), with Ir^0 and Ir^{+4}) included. Addition of Ir^{+3} did not change the fit of $X_{Ru}=0.25$, and the fraction of Ir^{+3} was found to be zero.

Table 4 Atomic percent of Ir^0, the energy shifts, E_F and R-factors obtained in the LCF of the XANES spectra. Fits with reference spectra Ir^0 and Ir^{+4}

X_{Ru}	At.% Ir^0	E_F, Ir^0	E_F, Ir^{+4}	R-factor
0	76.7(2)	-0.14(1)	1.04(2)	4.22E-4
0.25	42(2)	0.3(2)	-0.28(8)	2.39E-3
0.50	0	-	-	-
0.75	0	-	-	-

Table 5 Atomic percent of Ir^0, Ir^{+3} and Ir^{+4}, the energy shifts, E_F and R-factors obtained in the LCF of the XANES spectra. Fit with reference spectra Ir^0, Ir^{+3} and Ir^{+4}

X_{Ru}	At.% Ir^0	E_F, Ir^0	At.% Ir^{+3}	E_F, Ir^{+3}	At.% Ir^{+4}	E_F, Ir^{+4}	R-factor
0	71(3)	-0.23(2)	7(1)	1.1(2)	22(1)	1.01(4)	3.55E-4

carried out three times.

With both strategies (starting with a pure system before refining the partial occupancies and starting with the partial occupancies initally introduced), and for the different refinements, the final ruthenium partial occupancy and bond lengths were always similar. Improved fits were always obtained for the binary oxides when mixing was introduced. The multiplicities of the oxygen shell did not change with the strategy used, but some differences could be seen for shells at longer bond distances.

Finally, refinements including only the oxygen shell (the combined shell 1 and 2 in Table 1) and the first metal-phase shell of samples with $X_{Ru}=0.25$ from both edges were tested by trying out three different initial values of $X_{Ru,Met}$, 0.10, 0.25 and 0.50. $X_{Ru,Met}$ converged towards the same value for all starting points with highest standard deviation for the Ir-edge at 0.02. A mixed occupancy site was also attempted fitted for the pure Ru sample with various initial values of $X_{Ru,Ox}$, and did result in a ruthenium partial occupancy close to one.

The refinements performed with the mixed site method can be seen in Figure 4 and Figure 5 for Ru-edge and Ir-edge respectively. The results reported in these figures represent fits in which $X_{Ru,Ox}$ and $X_{Ru,Met}$ were introduced initially.

The experimentally obtained ruthenium partial occupancy in the oxide phase, $X_{Ru,Ox}$ fraction from both edges as a function of nominal ruthenium fraction is shown in Figure 6a. The $X_{Ru,Met}$ partial occupancy obtained for the $X_{Ru}=0.25$ sample from both edges is shown in Figure 6b. A finite ruthenium partial occupancy was obtained for all the mixed samples, both in the oxide and metal phases, indicating a high degree of mixing. Partial occpuancies relatively close to the nominal were obtained, and quite consistently so from both edges, with the exception of $X_{Ru}=0.50$ and the metal phase for $X_{Ru}=0.25$, possibly indicating a less homogeneous distribution of the two elements in these phases. For the metal Ir phase it is possible that a more or less pure iridium phase coexists with a phase with some ruthenium incorporated into the structure, reflected by the much lower $X_{Ru,Met}$ found from the Ir edge than from the Ru edge. In addition a small fraction of metal-phase Ru was seen (3 wt.%) for this sample, which may have been partially doped with Ir.

In Figure 7 the coordination numbers obtained from both edges have been plotted as a function nominal ruthenium fraction. To account for the reduction in multiplicity due to presence of several phases in the sample we employed the method of reduced multiplicities by Martens *et al.*[46]. We thus divided the experimentally obtained coordination numbers by the fraction of the respective phase f_{ph}, to obtain the corrected coordination number $N_{corr}=N_{exp}/f_{ph}$.[46] The corrected coordination number expresses what the coordination number would have been if this was the only phase present.[46] In Figure 7 the coordination numbers for oxide and metal-phase shells have been corrected by oxide and metal-phase fractions respectively, which were obtained from LCF of XANES spectra. In Figure 7 we have included the corrected coordination numbers calculated with f_{ph} as obtained for the case in which two reference spectra were employed in the LCF fit and in addition for the case when three reference spectra were included in the fit of $X_{Ru}=0.0$.

The multiplicities lie close to the reference value for the oxygen shell indicated in Figure 7a when the corrected multiplicities are used to account for the presence of a metal-phase. The corrected multiplicities of the first metal-phase shell, Figure 7b, are smaller than the reference value. Also, a deviation is seen between the two edges for $X_{Ru}=0.25$, the smaller N appearing for the Ru-edge and the larger for the Ir-edge. For the first metal oxide shell (shell 3 in Table 1, Figure 7c) the multiplicities are in agreement with the reference value, with the exception of the Ru-edge for $X_{Ru}=0.25$ which is much higher than the reference value.

The second metal oxide shell (shell 4 in Table 1, Figure 7d) demonstrates more variety. The corrected multiplicities from the Ir-edge deviates from reference value, pure Ir being smaller and $X_{Ru}=0.25$ being larger than the reference value. For $X_{Ru}=0.25$ at the Ru-edge however, it is much smaller than what was obtained at the Ir-edge. For $X_{Ru}=0.5$ and 0.75 the values obtained from the two edges are in agreement, and they are either smaller or close to reference value, respectively.

In addition to determining the fractions of metal phase and oxide phases through LCF of XANES and Rietveld analysis, we also estimated the oxide fractions f_{ox} from the formula $f_{ox} = N_{(Ir-O)exp}/6$, where $N_{(Ir-O)exp}$ is the experimentally obtained multiplicity of the oxygen shell (MOS). The metal-phase fractions evaluated for the three methods, the multiplicity of the oxygen shell (MOS), and the quantitative Rietveld analysis of XRD spectra and the LCF of XANES are listed in Table 6.

Both of the two XAS-based methods, LCF of XANES and MOS, result in higher fractions of metal-phase than obtained through the Rietveld refinement for $X_{Ru}=0$. Quite similar values are found

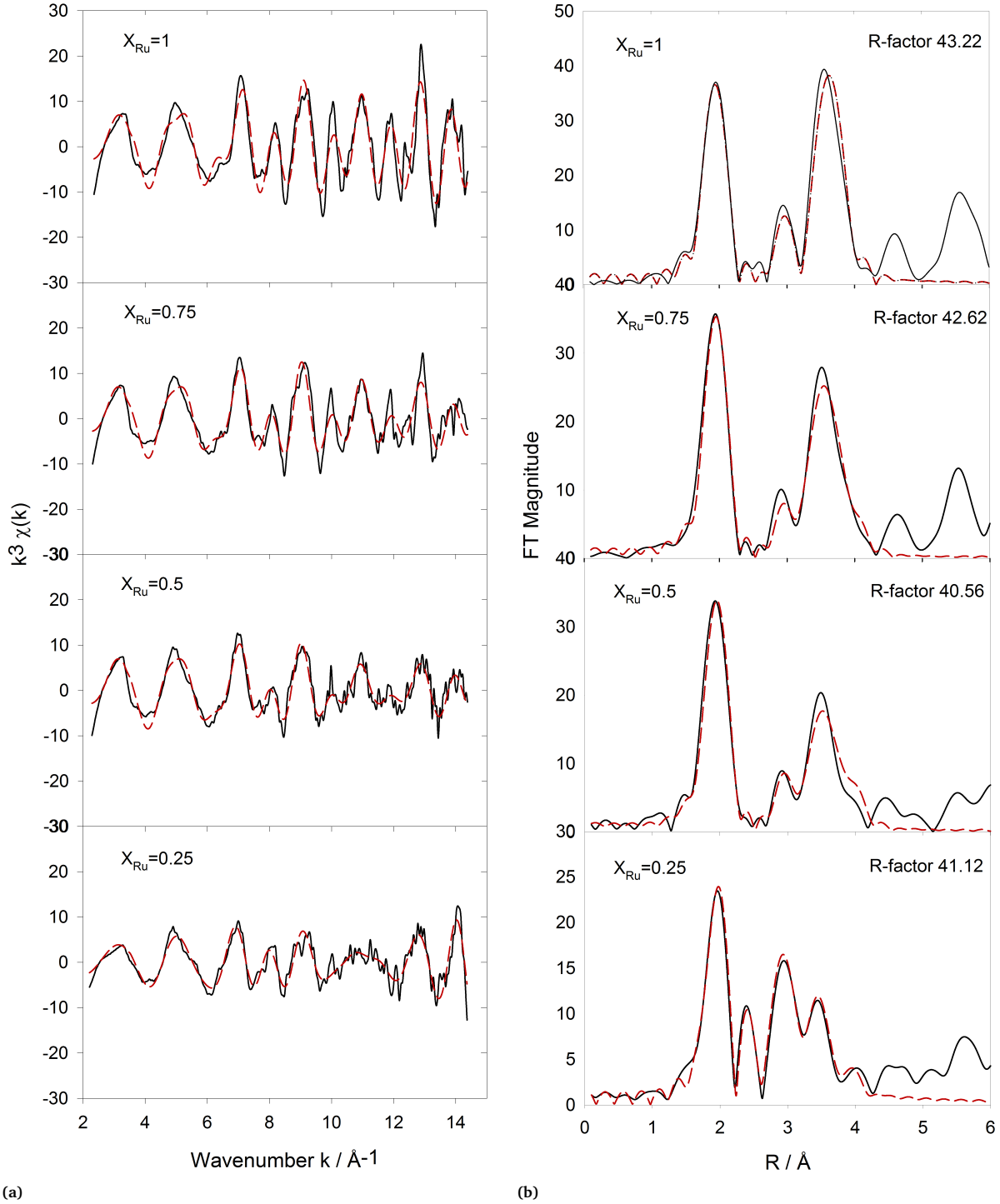

Fig. 4 Experimental (-) and least squares refined (- -) of (a) k^3 χ(k) and (b) EXAFS Fourier transforms of all spectra recorded at the Ru-edge and refined with the mixed-site approach.

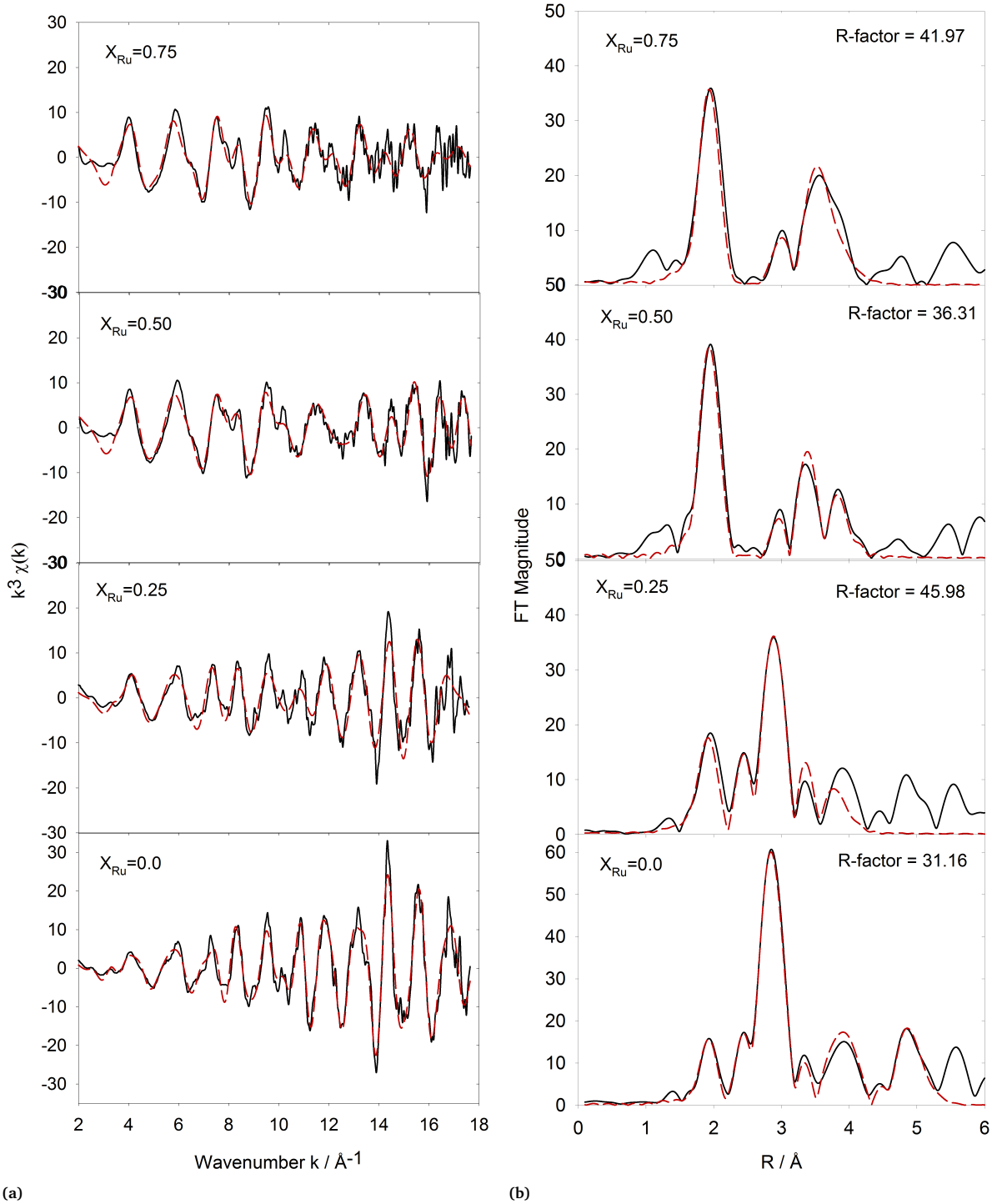

Fig. 5 Experimental (-) and least squares refined (- -) of (a) k^3 χ(k) and (b) EXAFS Fourier transforms of all spectra recorded at the Ir-edge and refined with the mixed-site approach.

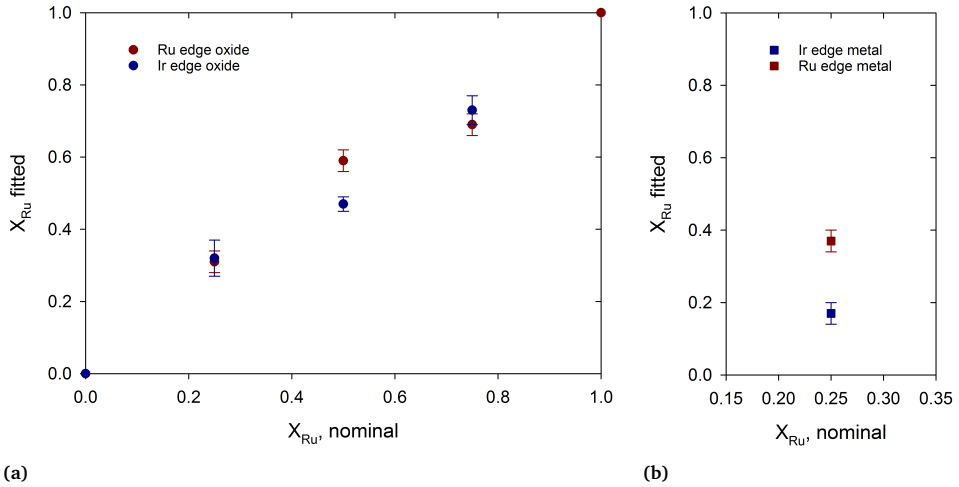

Fig. 6 The obtained partial occupancy as defined in EXCURVE of Ru of (a) the oxide phase and (b) the elemental metal phase evaluated from both Ir- and Ru-edges as function of nominal Ru fraction.

Table 6 Estimation of metal-phase fractions based on quantitative Rietveld analysis of XRD spectra, LCF of XANES spectra and MOS. All fractions are reported in at.% Ir^0. In the final column the coordination numbers used to evaluate the phases fractions with the MOS method are listed. The conversion between wt.% and at.% were performed according to equations in the Supplementary Material section S.4

X_{Ru}	XRD	LCF XANES Ir^{+3} not included	LCF XANES, Ir^{+3} included	MOS, Ir / Ru-edge	$N_{Me-O,exp}$ Ir / Ru-edge
0	59.7(1)	76.7(2)	71(3)	72(5) / -	1.7(3)/ -
0.25	50.6(1)	42(2)	-	53(8) / 42(5)	2.8(5) / 3.5(3)

from MOS and LCF of XANES spectra if Ir^{+3} is included in the LCF fit. For X_{Ru}=0.75 less variation is seen, with the exception of MOS method evaluated from Ir-edge. However, in spite of significant differences between the MOS results from the Ir and Ru edges, an overlap exists within the uncertainties. Since smaller uncertainties were found for LCF of XANES than from MOS, Figure 7 has been been based on the former.

The experimentally obtained bond lengths as function of nominal X_{Ru} are shown in Figure 8. Some deviation between the bond lengths obtained from the two edges is apparent. The bond lengths obtained at the Ru-edge are in general longer than the ones obtained from the Ir-edge, and with a few exceptions show the highest uncertainties. Decreasing bond lengths are seen for the oxygen shell at Ru-edge (although not the Ir-edge), the metal-phase shell at the Ir-edge and the first metal oxide shell at both edges. For the second metal oxide shell small changes are expected since the difference in bond length for this shell in IrO_2 and RuO_2 is quite small in value (Table 1), consistent with the data in Fig. (8d).

Fourier filtration of the EXAFS was another strategy applied in order to investigate the degree of mixing. Using Fourier filtration it can be possible to investigate the contribution to each shell separately. This was however difficult due to the large degree of overlap between the individual shells in the structure. This is illustrated for Ir-edge X_{Ru}=0.75 in Figure 9 where the contribution from the individual shells has been plotted. As can be seen the two metal oxide shells overlap. The results from the Fourier filtration were therefore inconclusive, and was not further explored.

EXAFS analysis of data for the mixed oxides with the co-shell approach demonstrated a decrease of the R-factor and even visually better fits as a second element was introduced in the first shell and improved for each shell which was modeled as a mixture. This confirms that a high degree of element mixing was indeed obtained for this synthesis procedure. However, this method quickly required a large number of parameters. In order to describe the mixing of a singe shell an additional three parameters had to be included, whereas introduction of mixing for a single phase required one single parameter in the mixed site approach. In addition, Ir and Ru in these co-shells were often at different bond lengths, and from the two edges both elements could be found to have the shortest bond length. The coordination number summed for the two shells often exceeded or was much smaller than the reference occupancy for the shell it was simulating. The result of the co-shell method was not satisfactory, and thus the mixed site approach became the primary method of EXAFS spectra analysis, for which results are presented above (Figures 4 through 8).

4 Discussion

The XRD and XAS results consistently indicate a high degree of mixing between Ir and Ru in the obtained oxides. A linear contraction of the cell volume was obtained as function of ruthenium fraction, see Figure 2, as expected when a solid solution is obtained. This is further supported by the close to equal partial

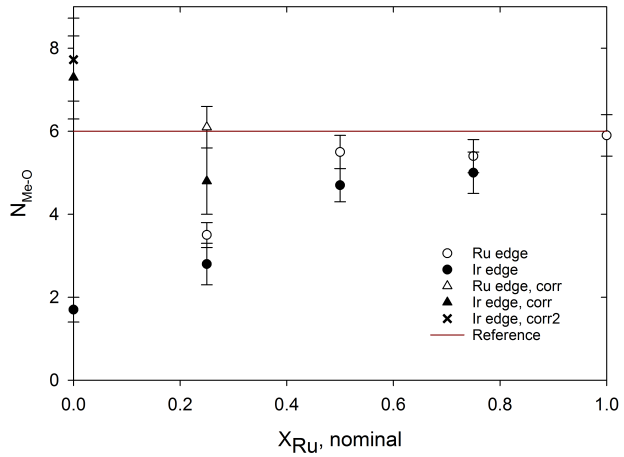

(a) N_{Me-O}

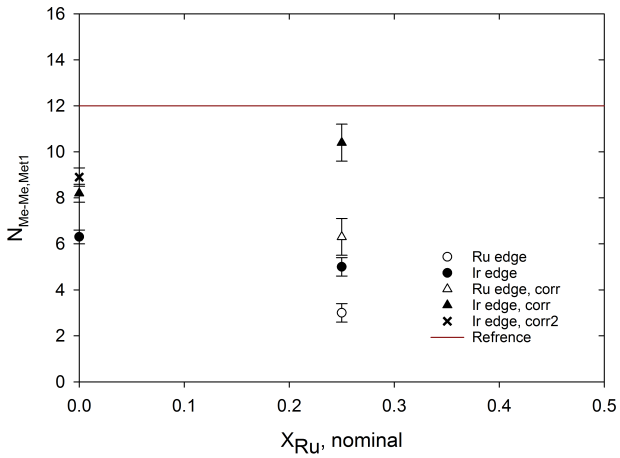

(b) $N_{Me-Me,Met1}$

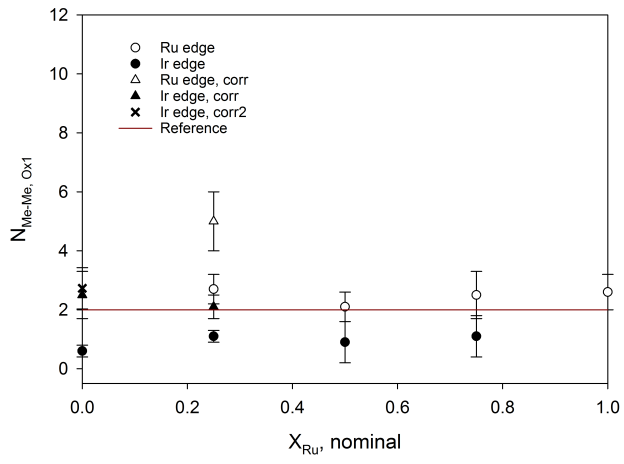

(c) $N_{Me-Me,Ox1}$

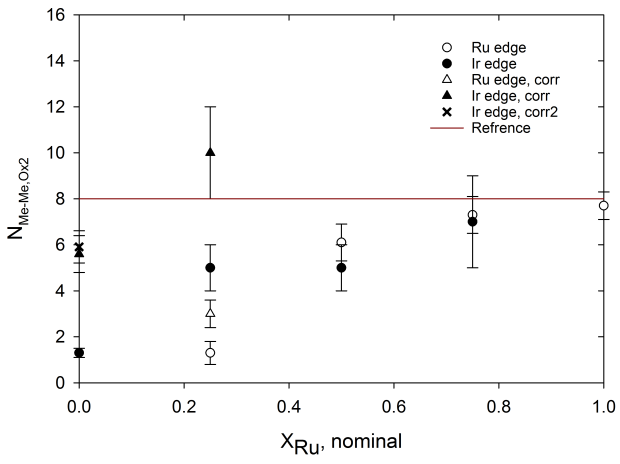

(d) $N_{Me-Me,Ox2}$

Fig. 7 Experimentally obtained coordination numbers for (a) the oxygen shell, N_{Me-O}, (b) the first metal-phase shell, $N_{Me-Me,Met1}$, (c) the first metal oxide shell, $N_{Me-Me,Ox1}$ (shell 3 in Table 1), and (d) the second metal oxide shell, $N_{Me-Me,Ox2}$ (shell 4 in Table 1), as function of nominal ruthenium fraction. The reference coordination numbers are indicated with red lines in the figures. For phases which are mixes of oxide and metal-phases the corrected multiplicities are also included. For X_{Ru}=0 different metal-phase fractions were obtained whether Ir^{+3} was included in the LCF of XANES or not, both are indicated. Fractions obtained without Ir^{+3} are named "corr" (triangles), and with named "corr2" (crosses).

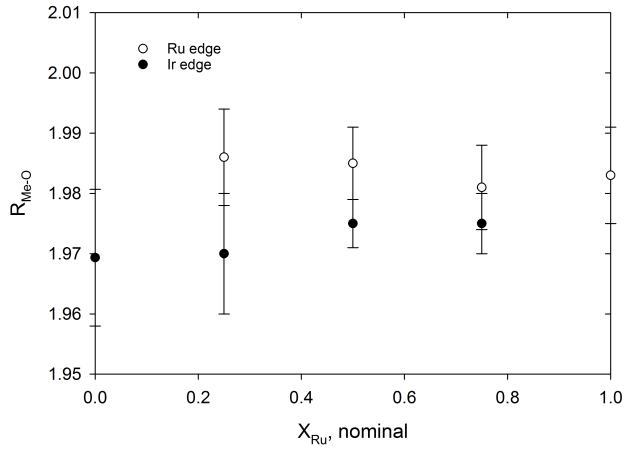

(a) R_{Me-O}

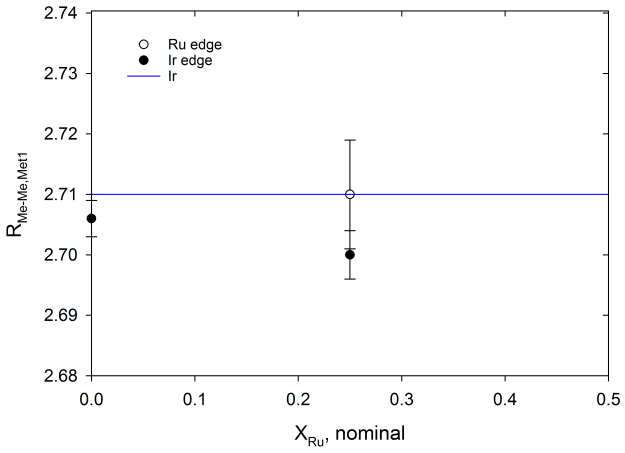

(b) $R_{Me-Met1}$

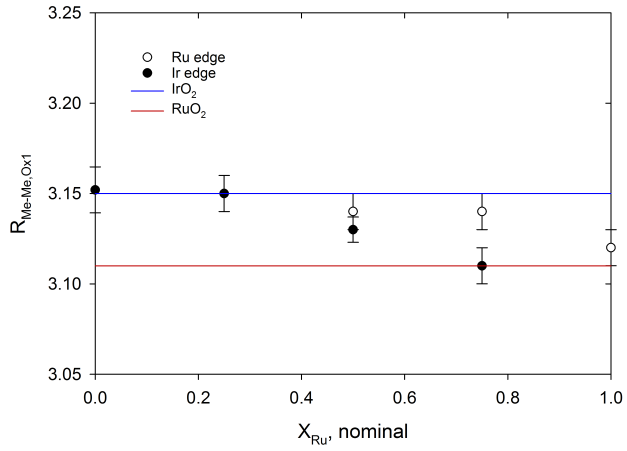

(c) R_{Me-Ox1}

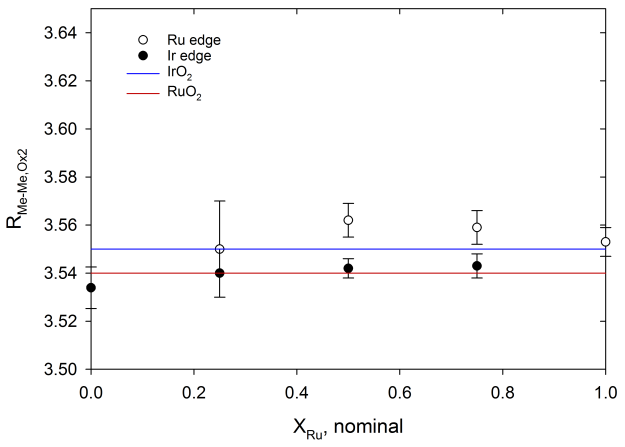

(d) R_{Me-Ox2}

Fig. 8 Experimentally obtained bond lengths in Å for the (a) oxygen shell ,R_{Me-O}, (b) first metal-phase shell, $R_{Me-Met1}$, (c) first metal oxide shell, R_{Me-Ox1}, and (d) second metal oxide shell, R_{Me-Ox2}, as function of nominal ruthenium fraction. The reference bond length is indicated in the figures for IrO_2 and Ir in blue and RuO_2 in red.

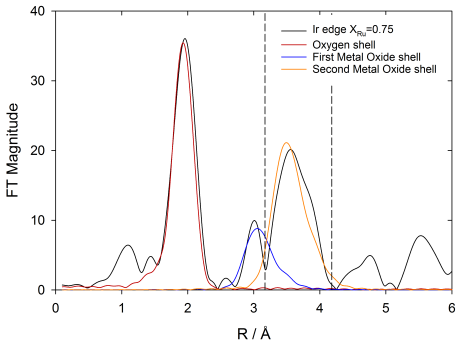

Fig. 9 Contributions from individual shells for X_{Ru}=0.75 recoded at Ir-edge.

occupancy of Ru found from both Ir- and Ru-edges in the EXAFS refinement of the X_{Ru}=0.25 and 0.75 spectra, Fig. 6. However, for X_{Ru}=0.50 the value differed from the two edges indicating that the distribution of Ru was not completely homogeneous.

The bond lengths in Figure 8c for shell 3 in Table 1 ("Me-Me, Ox1") are consistent with the linear lattice contraction inferred from the X-ray diffractograms. The bond length for shell 3 decreases with increasing ruthenium fraction as assessed from both edges and as expected for formation of solid solution. The decrease is the same as that obtained by Rietveld refinement, Fig. 2.

The other EXAFS-based bond lengths in Figure 8 are also consistent with what would be expected from the XRD results within the uncertainties. The average bond-length for the six oxygen atoms is expected to change from 1.980 Å in IrO_2 to 1.967 Å in RuO_2. This is in the range of the smallest uncertainties in the estimated bond length for this shell. Also, this shell was fitted as six oxygen atoms at an equal distance and not as two separate oxygen shells for the oxygen atoms in equatorial position and for the oxygen atoms in apical positions (i.e. shells 1 and 2 in Table 1 combined), which may have contributed adversely to the accuracy. The expected change in bond distance for the second metal oxide shell (shell 4 in Table 1, "Me-Me, Ox2") is 0.01 Å, which is clearly beyond the resolution limit of the methods employed.

The EXAFS data in Fig. 6a help to rationalise why the oxide lattice contracts linearly in Fig. 2 in spite of the sizeable metallic fraction in this material. The X_{Ru}=0.25 samples contain a rather large amount of iridium metal (i.e. Ir(0)). It is therefore perhaps somewhat unexpected that the c lattice parameter of the oxide phase of this composition complies so well with the linear contraction in Fig. 2, and that an $X_{Ru,Ox}$ close to nominal value is evaluated by XAS for this composition. If formation of a pure metallic iridium phase is assumed, and that the balance of the Ir forms a binary oxide with Ru, the ruthenium fraction of this oxide would be 0.41(4) if averaged over the three samples. The c lattice parameter data point for a nominal value of X_{Ru}=0.25 would therefore, if shifted to X_{Ru}=0.41, be well above the expected linear trend for a binary mixture[38]. This apparent inconsistency arises, however, from the fact that a substantial amount of ruthenium is incorporated into the Ir metal structure and that a small separate Ru metal phase was also formed.

Both the XRD and the EXAFS data consistently indicate the inclusion of ruthenium in the metallic iridium phase of the X_{Ru}=0.25 material. The lattice parameter of the metallic Ir has decreased from an average value of 3.839 Å for the X_{Ru}=0 samples to 3.830 Å for X_{Ru}=0.25, as can be seen in Table 3. Alloying of ruthenium into cubic iridium metal is normally associated with a decreasing lattice parameter with increasing ruthenium fraction[47]. A lattice constant of 3.830 Å is expected at an atomic fraction of ruthenium of ~19 at.%[47]. This is in agreement with the ruthenium partial occupancy found in the Ir metal by EXAFS evaluation at the Ir-edge, 0.17(3). However, this was smaller than the value obtained at the Ru-edge; 0.37(3). Formation of a metallic ruthenium phase and alloying of Ru into the Ir metal phase account for the close to nominal ruthenium partial occupancy obtained for the oxide phase, and explain why the c parameter for this oxide also complies with the linear trend in Figure 2.

The formation of metal phases does therefore not necessarily indicate inhomogeneous mixing of the elements in the oxide phase. A degree of alloying of Ru into the Ir metal, and possibly Ir into the Ru metal, is an expression of the ability of the PPS method to produce high degrees of elemental mixing, and appears to be the case for the metal phases as well although this phase appears to be somewhat less homogeneous.

The small fraction of a metallic Ru phase, ~3 wt.% metallic Ru (Table 3) is a likely cause for the differences seen for ruthenium partial occupancy found from the two edges. The first three shells of metallic Ru are located at 2.65, 2.71 and 3.79 Å, each with a multiplicity of six, according to the published crystal structure (ICDD Card no. 00-006-0663). The first two of these shells will therefore overlap with the first metallic Ir shell (at 2.71 Å) for the refinement at the Ru-edge. The metallic Ru phase was too small to be resolved in the EXAFS analysis, but its effect on the fitted metallic Ir structure may explain some of the differences seen for the properties of the Ir metallic phase as observed from the two edges.

The metallic Ru phase may exist as a pure metal, or it can be partially doped with Ir. An average increase of the c lattice parameter of the Ru metal phase is seen for X_{Ru}=0.25 compared to X_{Ru}=1 (Table 3), which indicates that Ir alloying into the Ru metal actually has occurred. However, the lattice parameter of Ru found for the pure ruthenium samples are larger than reported by Okamoto[47]. The hexagonal metallic ruthenium phase can support up to 44 at.% Ir before a transition to cubic Ir metal phase is expected[47]. The presence of both Ir and Ru metal phases, each with the possibility of being more or less phase pure and being alloyed with the other element homogeneously or in a varying degree throughout the structure may therefore well be the cause for the difference seen in ruthenium partial occupancy for the cubic Ir phase from the two edges.

The three methods of evaluating the atomic percentage of metallic Ir, Rietveld refinement, LCF of XANES and multiplicity of the oxygen shell (MOS), are in the same range, but with some deviations for the X_{Ru}=0.25 sample. The Rietveld refinement method and LCF of XANES are in better agreement for X_{Ru}=0. Since XRD requires some long-range order whereas XAS does not, a possible explanation behind the discrepancy seen for the pure Ir

sample might therefore be that small metallic Ir crystallites contribute to XAS measurements but are invisible in the XRD spectra. Differences can arise due to the probing scales not overlapping and the presence of phases of only limited or no long-range order in the samples. With these aspects of the measurement methods in mind we conclude that a set of likely models for the composition and structure of the polymeric-precursor synthesized $Ir_xRu_{1-x}O_2$ powders has been established.

For electrocatalytic applications an assessment of the mixing at the atomic level in multicomponent oxides is particularly important, both for fundamental understanding[13] and for practical applications. For example, results of Kötz and Stucki[11] indicate that for sputtered Ir-Ru mixed oxides, iridium and ruthenium interact synergistically to give a catalytic activity which is different from the sum of the catalytic activities of the two component oxides. For other types of samples the opposite is the case; Owe *et al.*[13] showed that in oxides synthesized by the hydrolysis method and verified to be solid solutions by pair-distribution analysis of high-resolution XRD data, the electrocatalytic activity is a simple superposition of the activities of the component oxides. A detailed structural characterization for the sputtered oxides reported by Kötz and Stucki[11] is not available, and a resolution of these conflicting reports is currently not possible. Therefore, if metal-metal interaction and catalytic properties of oxides are to be assessed experimentally, a good knowledge of the makeup and structure of the catalyst is essential. This goes well beyond the fundamental understanding of the electrocatalytic process and will have applied ramifications. If there is no synergistic interaction, optimization of catalysts should concentrate on maximising surface to volume ratio rather than composition, whereas also composition will be critical if such an interaction is present.

5 Conclusions

The extent of mixing and formation of solid solution in $Ir_xRu_{1-x}O_2$ powders prepared by a polymeric precursor method were evaluated by Rietveld refinement of XRD spectra and refinements of EXAFS spectra. Introduction of a mixed site describing the partial occupancy of ruthenium relative to iridium in both oxide and metal-phase shells was successfully applied in order to evaluate the degree of element mixing. Close to nominal ruthenium partial occupancy was found from both Ru- and Ir-edge for the oxide phase. However, the distribution of ruthenium and iridium was not completely homogeneous for all compositions. The $X_{Ru}=0.50$ oxide phase demonstrated different ruthenium partial occupancy obtained from the EXAFS spectra at the Ir- and Ru-edge, respectively. This was also the case for the cubic Ir metal phase produced in the $X_{Ru}=0.25$ sample, although this showed that an alloy was produced even for the metal phase. The presence of metal phases of both cubic Ir and hexagonal Ru, which are both likely to be mixtures of pure metals and alloys, is probably the cause for the difference seen in the Ru-partial occupancy from EXAFS at the two edges.

The metal-phase content of the Ir and Ru samples produced by polymeric precursor synthesis is highly sensitive to the synthesis conditions, and a consistent characterization of their structure required a concerted analysis based on several methods based on XRD and XAS. The presence of metal phases does not appear to implicate a low extent of element mixing of the oxide phase.

Conflicts of interest

There are no conflicts to declare.

Acknowledgements

The funding for this research was provided by Faculty of Natural Sciences and Technology at NTNU (project no. 81730900), and was greatly appreciated. We thank Diamond Light Source for providing access to synchrotron beam-time on B18 (proposal 8591) and synchrotron technician Diego Gianolio for help during the recording of the X-ray absorption spectroscopy data.

Notes and references

1 M. Carmo, D. L. Fritz, J. M. Mergel and D. Stolten, *International Journal of Hydrogen Energy*, 2013, **38**, 4901 – 4934.
2 E. Fabbri, A. Habereder, K. Waltar, R. Kotz and T. J. Schmidt, *Catal. Sci. Technol.*, 2014, **4**, 3800–3821.
3 L. A. Pocrifka, R. G. Freitas, A. V. Rosario and E. C. Pereira, *Journal of Solid State Electrochemistry*, 2011, **15**, 1109–1113.
4 Y.-T. Shih, K.-Y. Lee and Y.-S. Huang, *Journal of Alloys and Compounds*, 2015, **619**, 131 – 137.
5 W.-D. Huang, H. Cao, S. Deb, M. Chiao and J. Chiao, *Sensors and Actuators A: Physical*, 2011, **169**, 1 – 11.
6 K. Kreider, M. Tarlov and J. Cline, *Sensors and Actuators: B. Chemical*, 1995, **28**, 167–172.
7 C. R. Costa, C. M. Botta, E. L. Espindola and P. Olivi, *Journal of Hazardous Materials*, 2008, **153**, 616 – 627.
8 R. Chen, V. Trieu, B. Schley, H. Natter, J. Kintrup, A. Bulan, R. Weber and R. Hempelmann, *Zeitschrift fur Physikalische Chemie*, 2013, **227**, 651–666.
9 E. Kuznetsova, V. Petrykin, S. Sunde and P. Krtil, *Electrocatalysis*, 2015, **6**, 198–210.
10 V. Petrykin, K. Macounova, M. Okube, S. Mukerjee and P. Krtil, *Catalysis Today*, 2013, **202**, 63–69.
11 R. Kötz and S. Stucki, *Electrochimica Acta*, 1986, **31**, 1311 – 1316.
12 N. Halck, V. Petrykin, P. Krtil and J. Rossmeisl, *Physical Chemistry Chemical Physics*, 2014, **16**, 13682–13688.
13 L.-E. Owe, M. Tsypkin, K. S. Wallwork, R. G. Haverkamp and S. Sunde, *Electrochimica Acta*, 2012, **70**, 158 – 164.
14 E. Rasten, G. Hagen and R. Tunold, *Electrochimica Acta*, 2003, **48**, 3945 – 3952.
15 A. Marshall, B. Børresen, G. Hagen, M. Tsypkin and R. Tunold, *Electrochimica Acta*, 2006, **51**, 3161–3167.
16 A. Marshall, B. Børresen, G. Hagen, M. Tsypkin and R. Tunold, *Materials Chemistry and Physics*, 2005, **94**, 226 – 232.
17 A. Marshall and R. Haverkamp, *Electrochimica Acta*, 2010, **55**, 1978–1984.
18 R. Tunold, A. T. Marshall, E. Rasten, M. Tsypkin, L. E. Owe and S. Sunde, *ECS Transactions*, 2010, **25**, 103–117.
19 A. Reksten, F. Moradi, F. Seland and S. Sunde, *ECS Transactions*, 2013, **58**, 39–50.

20 C. Angelinetta, S. Trasatti, L. Atanososka and R. Atanasoski, *Journal of Electroanalytical Chemistry and Interfacial Electrochemistry*, 1986, **214**, 535 – 546.

21 M. Kakihana and M. Yoshimura, *Bulletin of the Chemical Society of Japan*, 1999, **72**, 1427–1443.

22 J. Lin, M. Yu, C. Lin and X. Liu, *The Journal of Physical Chemistry C*, 2007, **111**, 5835–5845.

23 A. V. Rosario, L. O. Bulhoes and E. C. Pereira, *Journal of Power Sources*, 2006, **158**, 795 – 800.

24 A. Terezo and E. Pereira, *Electrochimica Acta*, 2000, **45**, 4351–4358.

25 A. J. Terezo and E. C. Pereira, *Materials Letters*, 2002, **53**, 339–345.

26 M. Santos, A. Terezo, V. Fernandes, E. Pereira and L. Bulhões, *Journal of Solid State Electrochemistry*, 2005, **9**, 91–95.

27 L. Profeti, F. Simões, P. Olivi, K. Kokoh, C. Coutanceau, J.-M. Léger and C. Lamy, *Journal of Power Sources*, 2006, **158**, 1195 – 1201.

28 N. Mamaca, E. Mayousse, S. Arrii-Clacens, T. Napporn, K. Servat, N. Guillet and K. Kokoh, *Applied Catalysis B: Environmental*, 2012, **111-112**, 376 – 380.

29 D. Von Dreifus, A. J. A. de Oliveira, A. V. do Rosario and E. C. Pereira, *Journal of Superconductivity and Novel Magnetism*, 2013, **26**, 2319–2321.

30 R. G. Freitas, L. R. Marchesi, R. T. S. Oliveira, F. I. Mattos-Costa, E. C. Pereira, L. O. S. Bulhões and M. C. Santos, *JOURNAL OF POWER SOURCES*, 2007, **171**, 373–380.

31 O. Kahvecioglu and S. Timur, Advances in Energy Materials, 2009, pp. 77–86.

32 X. Yonglei, X. Likun, W. Juntao and L. Xiangbo, *RARE METAL MATERIALS AND ENGINEERING*, 2010, **39**, 1903–1907.

33 M. Newville, *Fundamentals of XAFS*, 2004.

34 B. Ravel and M. Newville, Physica Scripta T, 2005, pp. 1007–1010.

35 S. Tomic, B. Searle, A. Wander, N. Harrison, A. Dent, J. Mosselmans and J. Inglesfield, *New Tools for the Analysis of EXAFS: The DL EXCURV Package*, Council for the central laboratory of the research councils technical report, 2005.

36 T. Arikawa, Y. Takasu, Y. Murakami, K. Asakura and Y. Iwasawa, *Journal of Physical Chemistry B*, 1998, **102**, 3736–3741.

37 A. Finch, N. Allison, S. Sutton and M. Newville, *Geochimica et Cosmochimica Acta*, 2003, **67**, 1189–1194.

38 C. Georg, P. Triggs and F. Lévy, *Materials Research Bulletin*, 1982, **17**, 105 – 110.

39 E. Balko and C. Davidson, *Journal of Inorganic and Nuclear Chemistry*, 1980, **42**, 1778 – 1781.

40 A. R. Hillman, M. A. Skopek and S. J. Gurman, *Physical Chemistry Chemical Physics (Incorporating Faraday Transactions)*, 2011, **13**, 5252.

41 M. Hüppauff and B. Lengeler, *Journal of The Electrochemical Society*, 1993, **140**, 598–602.

42 T. Pauporté, D. Aberdam, J.-L. Hazemann, R. Faure and R. Durand, *Journal of Electroanalytical Chemistry*, 1999, **465**, 88 – 95.

43 R. Kawar, P. Chigare and P. Patil, *Applied Surface Science*, 2003, **206**, 90 – 101.

44 O. Gencyilmaz, F. Atay and I. Akyuz, *Journal of optoelectronics and advanced materials*, 2015, **17**, 395–402.

45 M.-S. Miao and R. Seshadri, *Journal of Physics: Condensed Matter*, 2012, **24**, 215503.

46 J. H. A. Martens, R. Prins and D. C. Koningsberger, *The Journal of Physical Chemistry*, 1989, **93**, 3179–3185.

47 H. Okamoto, *Journal of Phase Equilibria*, 1992, **13**, 565–567.

Supplementary Material for Strategies for the analysis of the metallic fraction of Ir and Ru oxides via XRD, XANES, and EXAFS

Anita Hamar Reksten* Frode Seland
Svein Sunde†
Department of Materials Science and Engineering, Norwegian University of Science and Technology (NTNU) NO-7491 Trondheim, Norway

Andrea E. Russell and Peter W. Richardson
Stephen J. Thompson
Department of Chemistry, University of Southampton
Southampton SO17 1BJ, England

Karina Mathisen
Department of Chemistry, Norwegian University of Science and Technology (NTNU), NO-7491 Trondheim, Norway

May 23, 2019

S.1 Effect of strain on Rietveld refinements

The Rietveld refinements may overestimate the metallic Ru fraction. For the ruthenium-rich samples, especially pure ruthenium, well described peak shapes in the refinements were not obtained. A super-Lorentzian contribution to the peaks was seen which could not be included in the fit. There

*Current address: SINTEF Sustainable Energy Technology, NO-0373 Oslo, Norway
†Corresponding author. Tel.: +47 73594051; fax: +47 73591105, *E-mail address:* Svein.Sunde@material.ntnu.no

are several origins to peak broadening; any lattice imperfection will cause diffraction-line broadening, and domain-size broadening can occur if the powder consist of incoherent diffraction domains, such as dislocation arrays, stacking faults, twins or any other extended imperfections [1]. Investigation of the exact cause for the broadening seen in these samples was not performed. However, misfitting of the high intensity region of the peaks has consequences for the quantification. A strain parameter was added in order to include more of these areas. However, the omitted areas were small, and changes in fraction were insignificant (always < 0.4 wt.%) when strain was included in the fit. The contributions from the omitted high intensity peak region is therefore believed to be negligible in the phase quantification. The addition of the strain parameter did not effect the cell parameters. An example of refinement of X_{Ru}=1 is shown with and without strain added in Figure S.1. As can be seen the inclusion of strain improves the fit, however still a complete description of the most intense peaks is not obtained (Figure S.1b). Omitting the super-Lorentizan portion will also have consequences for the crystallite sizes obtained from the fit, and would be larger than indicated if these peak regions were well described. The sizes reported here are based on refinement carried out without added strain parameter, and can be looked upon as a lower limit of the crystallite size.

S.2 Microstructure

The morphology was investigated with SEM, and images of X_{Ru}=0, 0.5 and 1 are shown in Figure S.2. The samples contain large particles with diameter of several hundreds of nm, and smaller particles down to a few tenths of nm in diameter. The larger structures are in general larger for the Ru samples of both series, and smaller for Ir and the mixtures. The powders are in general agglomerated.

S.3 Crystallite size

In parallel to the increasing average particle diameter with ruthenium fraction, the crystallite sizes evaluated by Rietveld analysis were also found to increase with X_{Ru}, Figure S.3. Due to the broad structure and misfit of a super-Lorenzian part of the peaks (see ESI, Section S.1) of ruthenium-rich

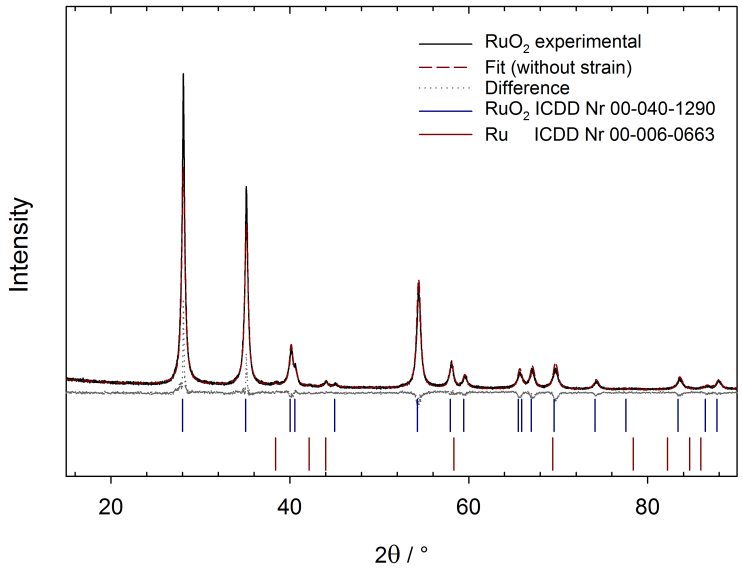

(a) RuO_2 without strain parameter

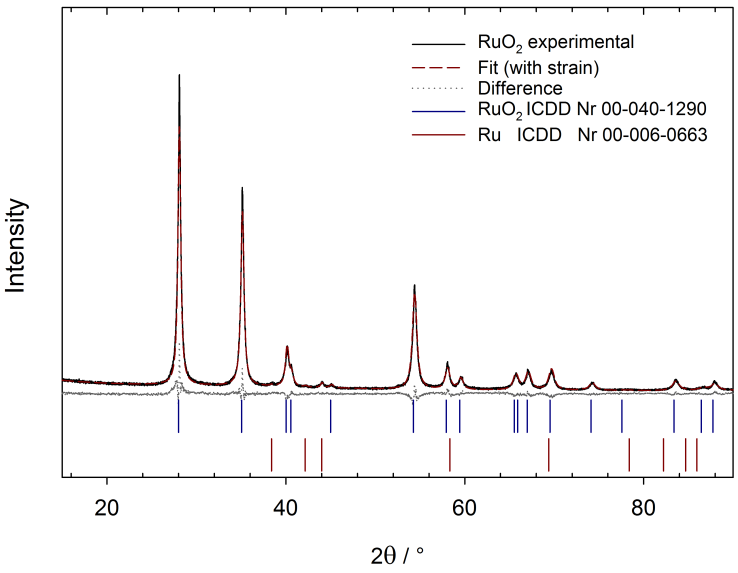

(b) RuO_2 with strain parameter

Figure S.1: Rietveld refinement of XRD data for a RuO_2 sample refined without (a) and with (b) added strain parameter.

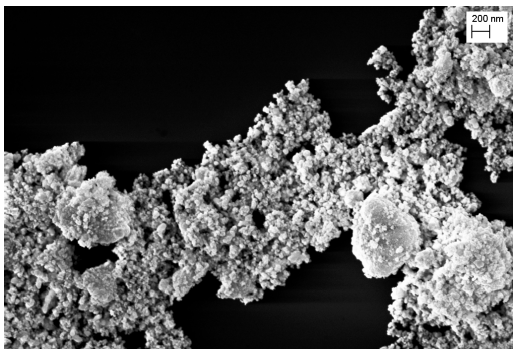

(a) X_{Ru}=0.0

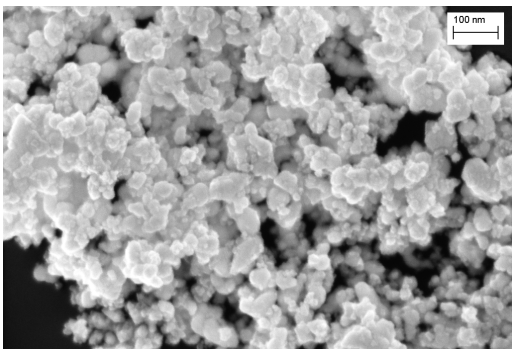

(b) X_{Ru}=0.0

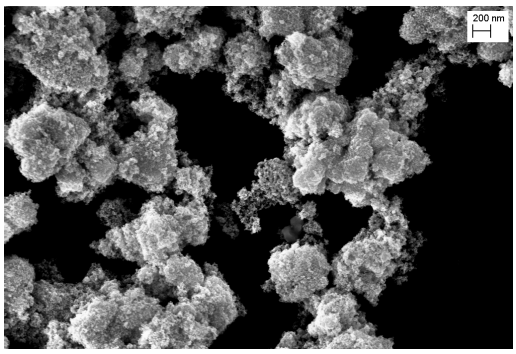

(c) X_{Ru}=0.5

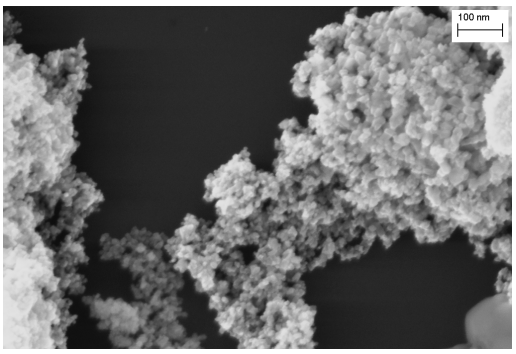

(d) X_{Ru}=0.5

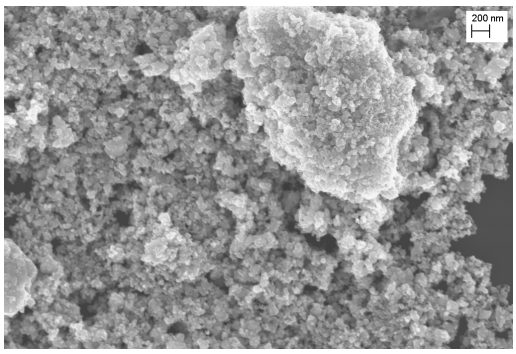

(e) X_{Ru}=1.0

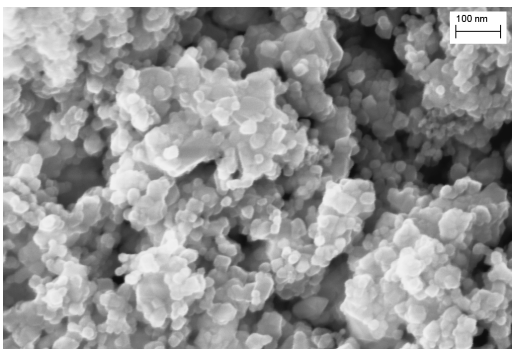

(f) X_{Ru}=1.0

Figure S.2: SEM images of (a), (b) X_{Ru}=0.0, (c), (d) X_{Ru}=0.5 and (e), (f) X_{Ru}=1.0 .

samples, the obtained and reported diameters can at best be looked upon as representing the smallest crystallites present. The diameters obtained increase with increasing ruthenium content. The increasing crystallite size with ruthenium fraction can be explained by lower crystallization temperature of ruthenium oxide and has been reported previously [2, 4].

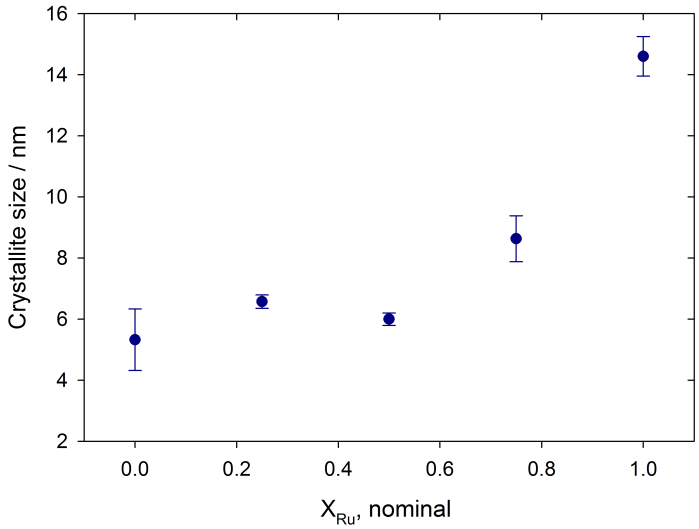

Figure S.3: Crystallite size of the oxide phase obtained by Rietveld refinement of X-ray diffractograms as a function of ruthenium fraction. Each data point is an average of the three samples of each composition, and the standard deviation of the three is indicated by error bars.

S.4 Conversion between atom percent and weight percent

The at.% iridium as obtained by linear-combination fitting of XANES is the number of iridium atoms in the metal reference sample Ir(0), n_{Ir}, divided by the total number of atoms in the two references Ir(0) and IrO_2 ($n_{\mathrm{IrO_2}}$). Thus

$$\text{at.\%(Ir)} = 100 \times \frac{n_{\mathrm{Ir}}}{n_{\mathrm{Ir}} + n_{\mathrm{IrO_2}}} \tag{S.1}$$

The wt.% iridium metal as computed in the Rietveld analysis was [3, 5]

$$\text{wt.\%(Ir)} = 100 S_{\text{Ir}} Z_{\text{Ir}} M_{\text{Ir}} V_{\text{Ir}} \times [S_{\text{Ir}} Z_{\text{Ir}} M_{\text{Ir}} V_{\text{Ir}} + S_{\text{Ir}_x\text{Ru}_{1-x}\text{O}_2} Z_{\text{Ir}_x\text{Ru}_{1-x}\text{O}_2} M_{\text{Ir}_x\text{Ru}_{1-x}\text{O}_2} V_{\text{Ir}_x\text{Ru}_{1-x}\text{O}_2} + S_{\text{Ru}} Z_{\text{Ru}} M_{\text{Ru}} V_{\text{Ru}}]^{-1} \quad \text{(S.2)}$$

where Z_{i} is the number of formula units in the unit cell, S_{i} are scale factors adjusted during the refinement, M_{i} the molar mass, and V_{i} the unit cell volume in the phase of composition i. We use the convention here that i = Ir refers elemental iridium (metal) and i = Ru to elemental ruthenium. For ruthenium the wt.% metal was correspondingly

$$\text{wt.\%(Ru)} = 100 S_{\text{Ru}} Z_{\text{Ru}} M_{\text{Ir}} V_{\text{Ru}} \times [S_{\text{Ir}} Z_{\text{Ir}} M_{\text{Ir}} V_{\text{Ir}} + S_{\text{Ir}_x\text{Ru}_{1-x}\text{O}_2} Z_{\text{Ir}_x\text{Ru}_{1-x}\text{O}_2} M_{\text{Ir}_x\text{Ru}_{1-x}\text{O}_2} V_{\text{Ir}_x\text{Ru}_{1-x}\text{O}_2} + S_{\text{Ru}} Z_{\text{Ru}} M_{\text{Ru}} V_{\text{Ru}}]^{-1} \quad \text{(S.3)}$$

We let the scale factors correspond to the (relative) number of unit cells so that the number of iridium atoms n_{Ir} in the sample is proportional to $S_{\text{Ir}} Z_{\text{Ir}}$ etc. with the same proportionality factor for all phases. From (S.2) we obtain

$$\text{wt.\%(Ir)} = 100 n_{\text{Ir}} M_{\text{Ir}} \times [n_{\text{Ir}} M_{\text{Ir}} + n_{\text{Ir}_x\text{Ru}_{1-x}\text{O}_2} M_{\text{Ir}_x\text{Ru}_{1-x}\text{O}_2} V_{\text{Ir}_x\text{Ru}_{1-x}\text{O}_2}/V_{\text{Ir}} + n_{\text{Ru}} M_{\text{Ru}} V_{\text{Ru}}/V_{\text{Ir}}]^{-1} \quad \text{(S.4)}$$

where $n_{\text{Ir}_x\text{Ru}_{1-x}\text{O}_2}$ is the number of formula units of $\text{Ir}_x\text{Ru}_{1\text{-}x}\text{O}_2$ and $M_{\text{Ir}_x\text{Ru}_{1-x}\text{O}_2}$ its molar weight. Since the number of iridium atoms in the oxide phase, $n_{\text{Ir,Ox}}$, is $n_{\text{Ir,Ox}} = x n_{\text{Ir}_x\text{Ru}_{1-x}\text{O}_2}$, we may write Eq. (S.4) as

$$\text{wt.\%} = 100 n_{\text{Ir}} M_{\text{Ir}} \left[n_{\text{Ir}} M_{\text{Ir}} + \frac{n_{\text{Ir,Ox}}}{x} M_{\text{Ir}_x\text{Ru}_{1-x}\text{O}_2} V_{\text{Ir}_x\text{Ru}_{1-x}\text{O}_2}/V_{\text{Ir}} + n_{\text{Ru}} M_{\text{Ru}} V_{\text{Ru}}/V_{\text{Ir}}\right]^{-1} \quad \text{(S.5)}$$

We divide numerator and denominator with $n_{\text{Ir}} + n_{\text{Ir,Ox}}$ and use Eq. (S.1) to obtain

$$\text{wt.\%(Ir)} = 100 \left[\text{at.\%(Ir)}/100\right] M_{\text{Ir}} \times \left\{ \left[\text{at.\%(Ir)}/100\right] M_{\text{Ir}} + \frac{1 - \text{at.\%(Ir)}/100}{x} M_{\text{Ir}_x\text{Ru}_{1-x}\text{O}_2} V_{\text{Ir}_x\text{Ru}_{1-x}\text{O}_2}/V_{\text{Ir}} + \frac{n_{\text{Ru}}}{n_{\text{Ir}} + n_{\text{Ir,Ox}}} M_{\text{Ru}} V_{\text{Ru}}/V_{\text{Ir}} \right\}^{-1} \quad \text{(S.6)}$$

For the samples with $X_{Ru} = 0$, the last term in the denominator of Eq. (S.4) is zero. For the samples with $X_{Ru} = 0.25$ we observe that dividing Eq. (S.2) by Eq. (S.3) gives

$$\frac{\text{wt.\%(Ir)}}{\text{wt.\%(Ru)}} = \frac{S_{Ir} Z_{Ir} M_{Ir} V_{Ir}}{S_{Ru} Z_{Ru} M_{Ir} V_{Ru}} = \frac{n_{Ir} M_{Ir} V_{Ir}}{n_{Ru} M_{Ru} V_{Ru}} \tag{S.7}$$

Using this result in Eq. (S.6) we obtain

$$\begin{aligned}\text{wt.\%(Ir)} = 100 \times [\text{at.\%(Ir)}/100]\, M_{Ir} \times \\ \left\{ [\text{at.\%(Ir)}/100]\, M_{Ir} + \frac{1 - at.\%/100}{x} M_{Ir_xRu_{1-x}O_2} V_{Ir_xRu_{1-x}O_2}/V_{Ir} \right. \\ \left. + \frac{1}{\text{wt.\%(Ru)} M_{Ru} V_{Ru}/\text{wt.\%(Ru)} M_{Ir} V_{Ir} + n_{Ir,Ox}/n_{Ru}} M_{Ru} V_{Ru}/V_{Ir} \right\}^{-1}\end{aligned} \tag{S.8}$$

Since wt.%(Ir) $\sim$ 40% and wt.%(Ru) $\sim$ 3% in this sample,

$$\begin{aligned}\frac{1}{\text{wt.\%(Ir)} M_{Ru} V_{Ru}/\text{wt.\%(Ru)} M_{Ir} V_{Ir} + n_{Ir,Ox}/n_{Ru}} \\ < \frac{1}{\text{wt.\%(Ir)} M_{Ru} V_{Ru}/\text{wt.\%(Ru)} M_{Ir} V_{Ir}} \approx 0.1\end{aligned}$$

The factors multiplying the molar masses in the first two terms of the denominator of Eq. (S.7) are expected to be in the order of 0.5 and 2, respectively, which can be checked for consistency (see below). Also, the molar mass of ruthenium is approximately half of that of iridium. Whereas this is offset slightly by the volume ratios ($V_{Ru} = 81$ Å^3,$V_{Ir} = 56.6$ Å^3,$V_{IrO_2} = 63.3$ Å^3 $V_{RuO_2} = 63.3$ Å^3 for the conventional unit cells), the last term in the denominator of Eq. (S.4) is to a good approximation negligible. Therefore,

$$\text{wt.\%(Ir)} \approx \frac{100 \times [\text{at.\%(Ir)}/100]\, M_{Ir}}{[\text{at.\%(Ir)}/100]\, M_{Ir} + \frac{1 - \text{at.\%(Ir)}/100}{x} M_{Ir_xRu_{1-x}O_2}} \tag{S.9}$$

in which we have also neglected the volume ratios being different from one, and from which we in turn obtain,

$$\begin{aligned}\text{at.\%(Ir)} \approx \\ 100 \times \frac{[\text{wt.\%(Ir)}/100]\, M_{Ir_xRu_xO_2}/x}{M_{Ir}\,(1 - \text{wt.\%(Ir)}/100) + [\text{wt.\%(Ir)}/100]\, M_{Ir_xRu_{1-x}O_2}/x}\end{aligned} \tag{S.10}$$

For ruthenium the equations become

$$\text{wt.\%(Ru)} \approx 100 \times \frac{[\text{at.\%(Ru)}/100]\, M_{\text{Ru}}}{[\text{at.\%(Ru)}/100]\, M_{\text{Ru}} + \dfrac{1 - \text{at.\%(Ru)}/100}{1-x} M_{\text{Ir}_x\text{Ru}_{1-x}\text{O}_2}} \quad \text{(S.11)}$$

$$\text{at.\%(Ru)} \approx 100 \times \frac{[\text{wt.\%(Ru)}/100]\, M_{\text{Ir}_x\text{Ru}_{1-x}\text{O}_2}/\,(1-x)}{M_{\text{Ru}}\,[1 - \text{wt.\%(Ru)}/100] + [\text{wt.\%(Ru)}/100]\, M_{\text{Ir}_x\text{Ru}_{1-x}\text{O}_2}/\,(1-x)} \quad \text{(S.12)}$$

for samples with no iridium metal in them.

X_{Ru} (nominal)	wt. Ir%	at.% Ir	wt. Ru%	at.% Ru
0	55.9	59.7		
0	75.6	78.3		
0	58.1	61.8		
0.25	42.3	50.6		
0.25	45.1	53.4		
0.25	30.9	38.5		
0	73.8	76.7		
0	67.7	71		
0.25	34.1	42		
0.75			14.3	25.5

Table S.1: Conversion of wt.% to at.% for various samples described in the main article as computed by Eqs. (S.9) through (S.12).

References

[1] D. Balzar. *J. Research of the National Institute of Standards and Technology*, 98:321–353, 1993.

[2] J. Cheng, H. Zhang, G. Chen, and Y. Zhang. *Electrochimica Acta*, 54(26):6250 – 6256, 2009.

[3] RJ Hill and CJ Howard. Quantitative Phase-Analysis From Neutron Powder Diffraction Data Using the Rietveld Method. *Journal of Applied Crystallography*, 20(6):467–474, DEC 1 1987.

[4] A. Marshall, B. Børresen, G. Hagen, M. Tsypkin, and R. Tunold. *Energy*, 32(4):431 – 436, 2007.

[5] JC Taylor and CE Matulis. Absorption Contrast Effects in the Quantitative XRD Analysis of Powders by Full Multiphase Profile Refinement. *Journal of Applied Crystallography*, 24(1):14–17, FEB 1 1991.

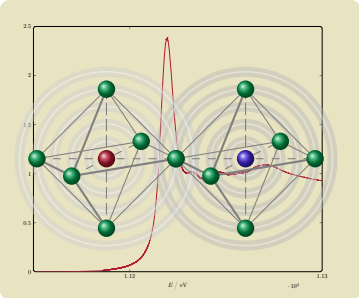

X-ray absorption spectroscopy reveals separately the structures of metal and oxide phases of iridium and ruthenium electrocatalysts containing both.

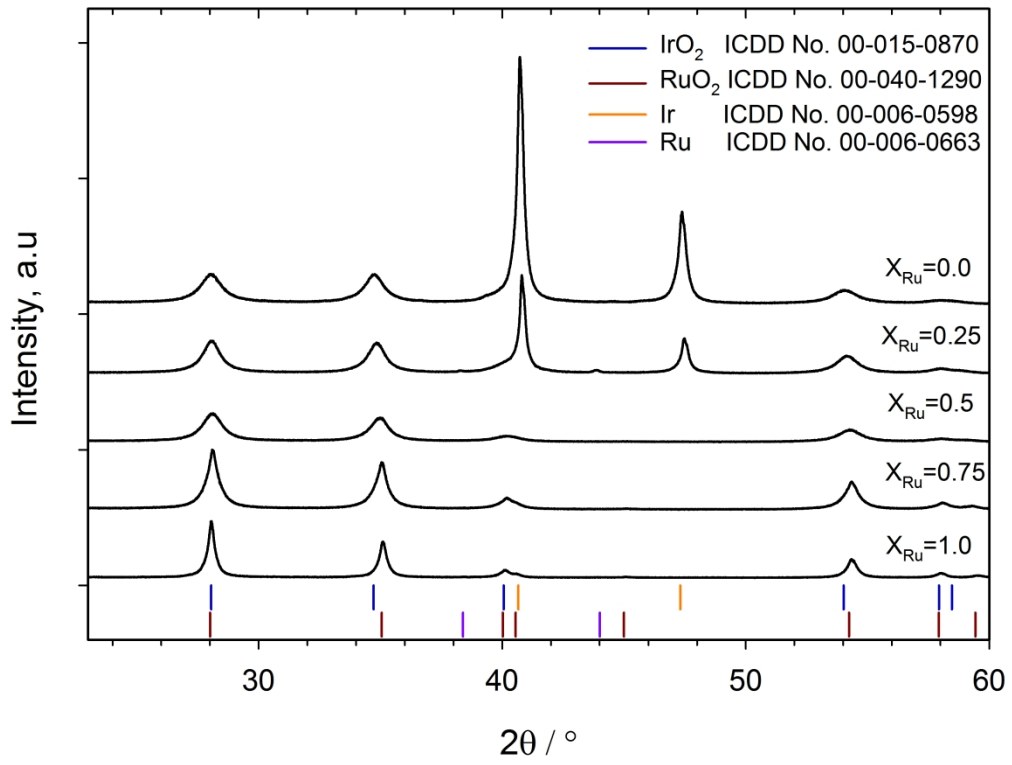

X-ray diffractogram of Ir$_x$Ru$_\mathrm{1-x}$O$_2$ as function of X$_\mathrm{Ru}$

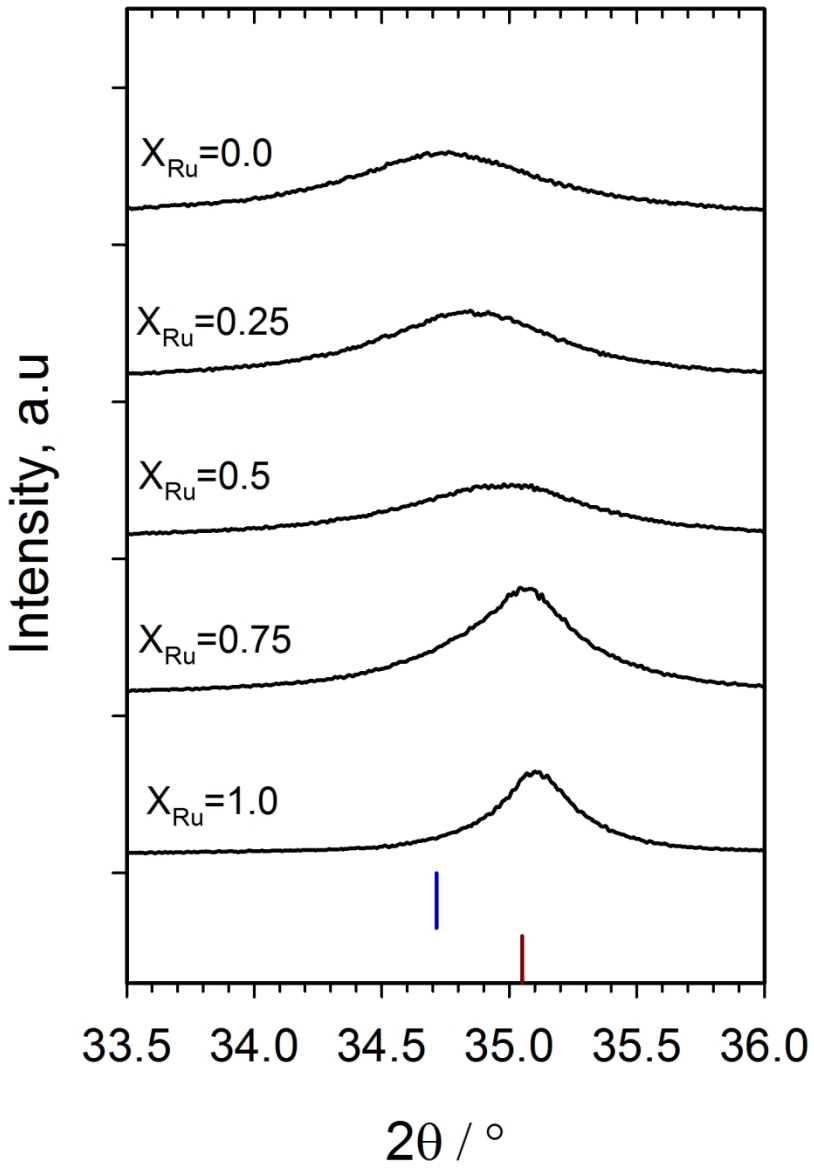

magnification of (101) reflection located at 2$\theta\sim$34-35\,$^\circ$

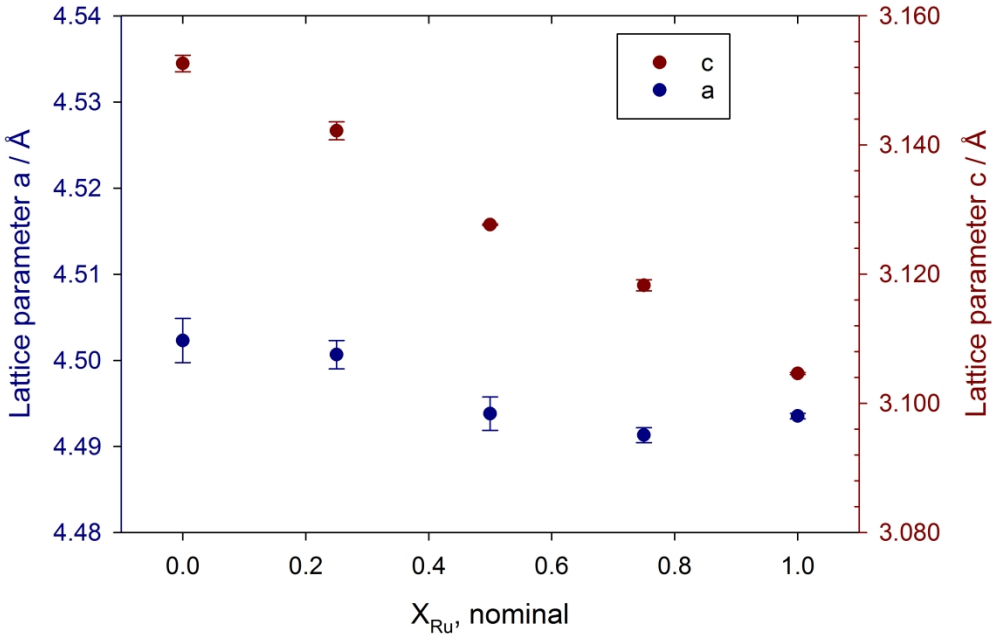

Lattice parameters a and c for the oxide phase (rutile crystal structure) obtained by Rietveld refinement of X-ray diffractograms as a function of
ruthenium fraction. Each data point is an average of the three identical synthesis of each composition and the standard deviation of the three is indicated by error bars.

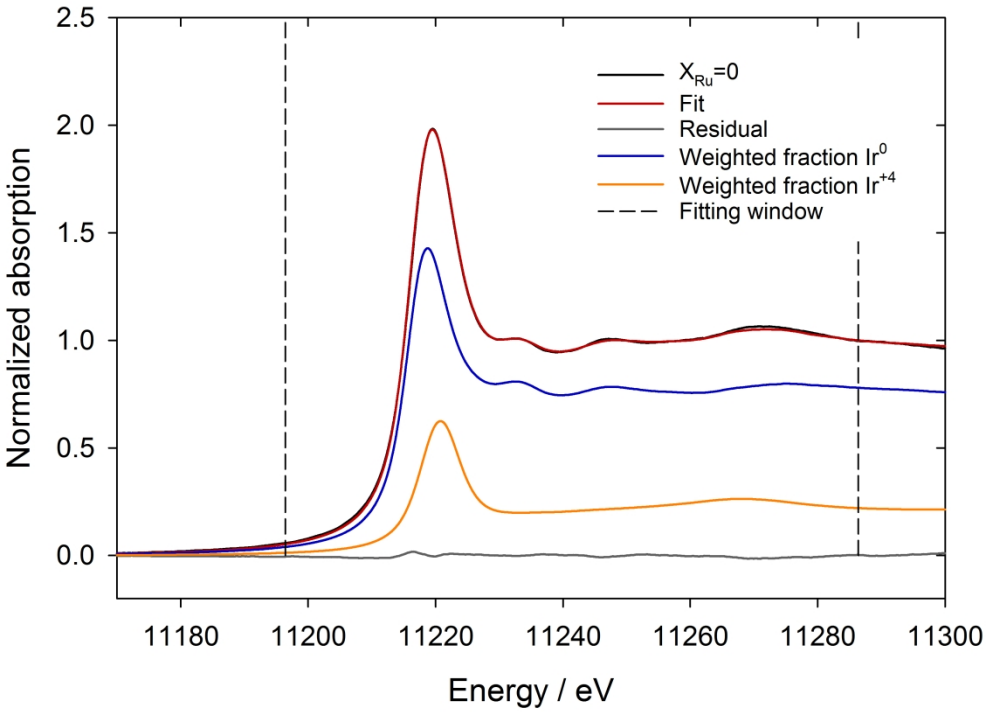

Linear combination fit of X$_\mathrm{Ru}$=0.0 (sample 1 of those with X$_\mathrm{Ru}$=0.0, Table~\ref{tab:metalphasesPolymeric Precursor A}), with (a) Ir^0 and Ir^{+4} standards

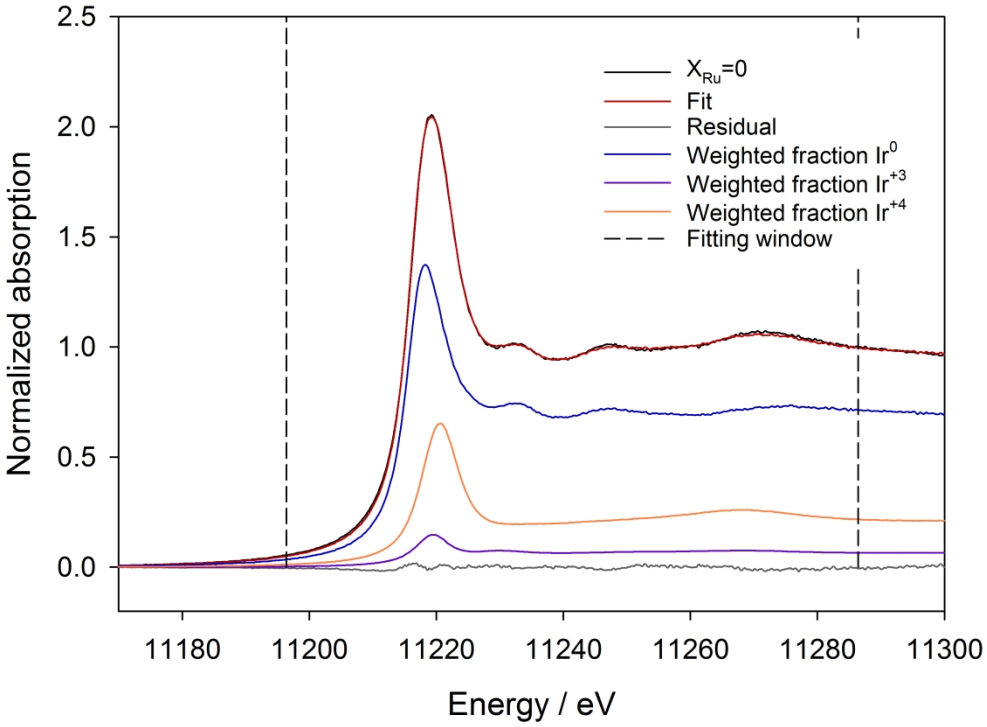

Ir^0, Ir^{+3} and Ir^{+4} standards.

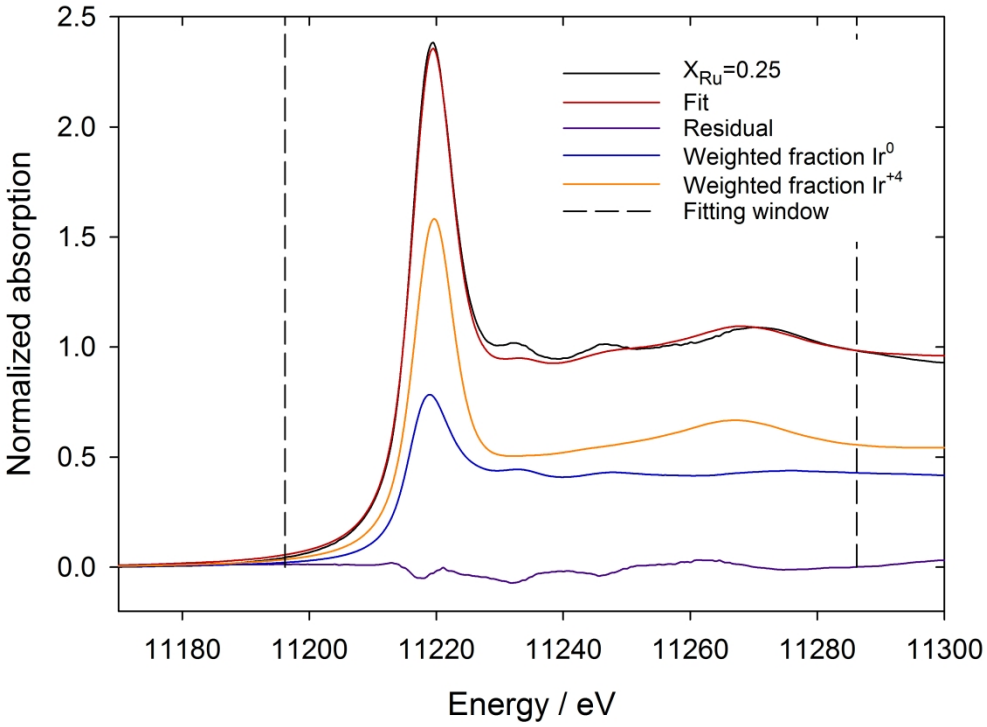

linear combination fit of X$_\mathrm{Ru}$=0.25 (sample 1 of those with X$_\mathrm{Ru}$=0.25,Table~\ref{tab:metalphasesPolymeric Precursor A}), with Ir^0 and Ir^{+4}) included. Addition of Ir^{+3} did not change the fit of X$_\mathrm{Ru}$=0.25, and the fraction of Ir^{+3} was found to be zero.

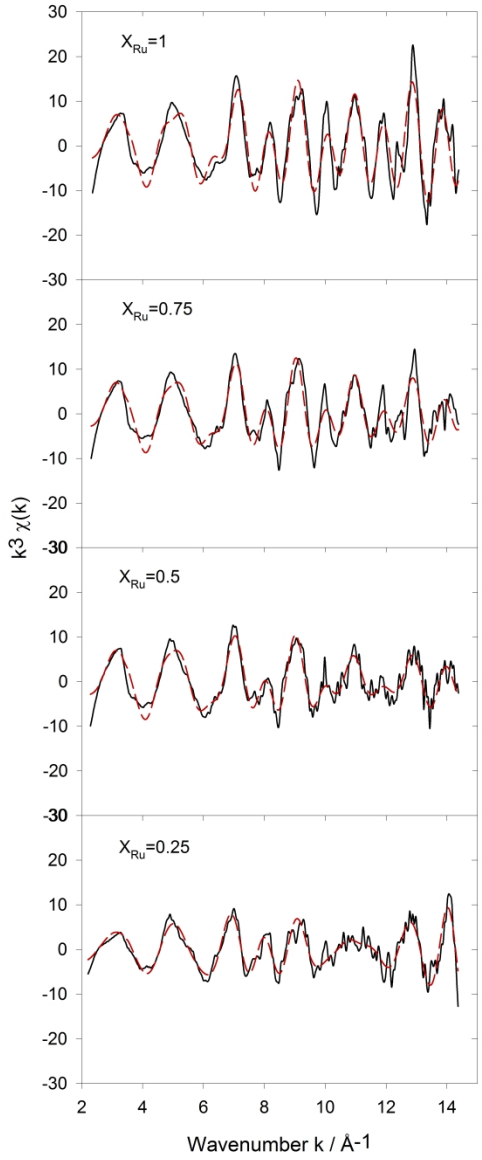

Experimental (-) and least squares refined (-\,-) of (a) k^3 χ(k)

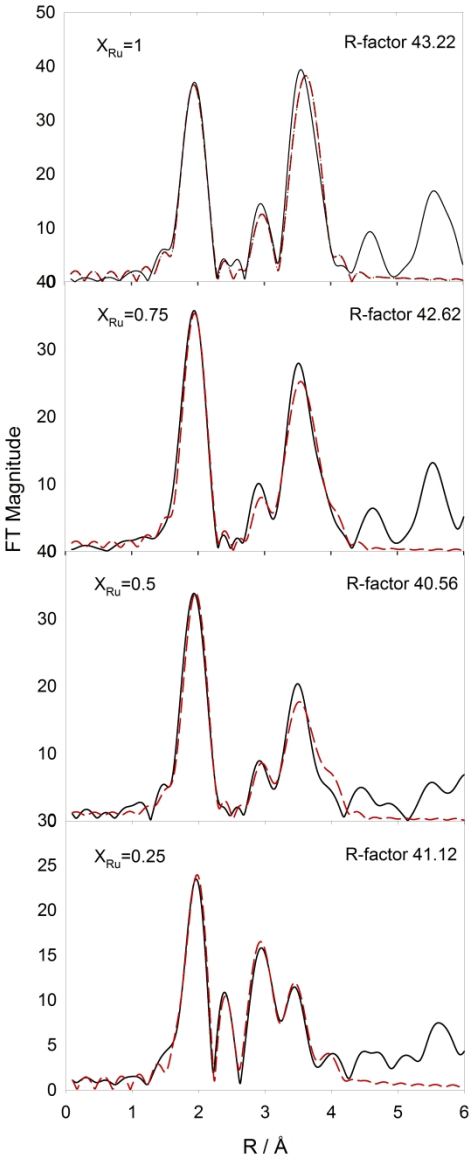

EXAFS Fourier transforms of all spectra recorded at the Ru-edge and refined with the mixed-site approach.

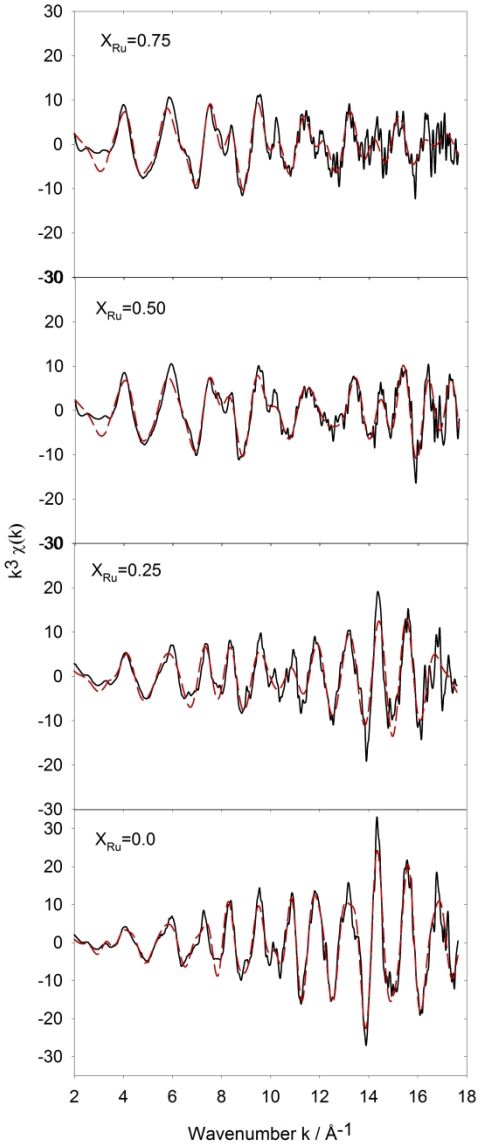

Experimental (-) and least squares refined (-\,-) of (a) k^3 χ(k)

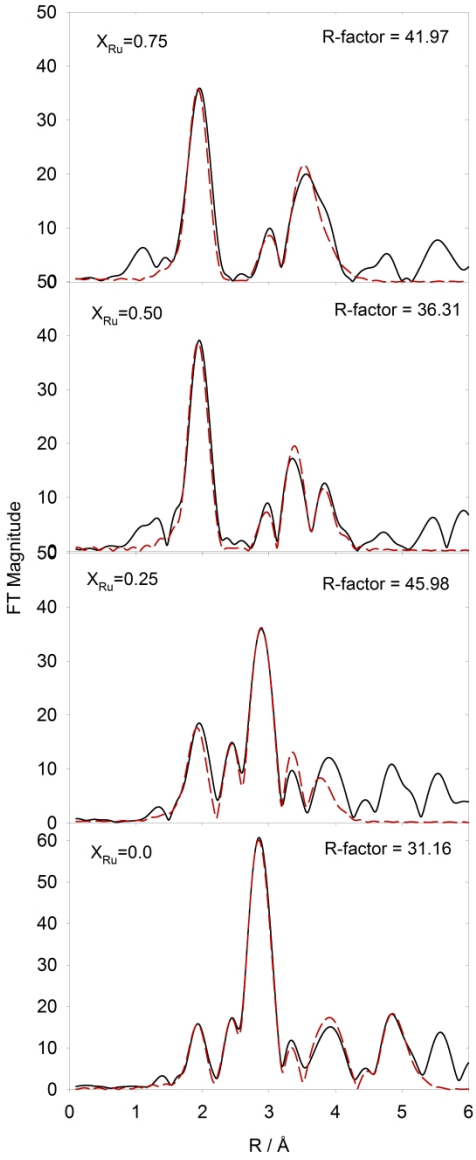

EXAFS Fourier transforms of all spectra recorded at the Ir-edge and refined with the mixed-site approach.

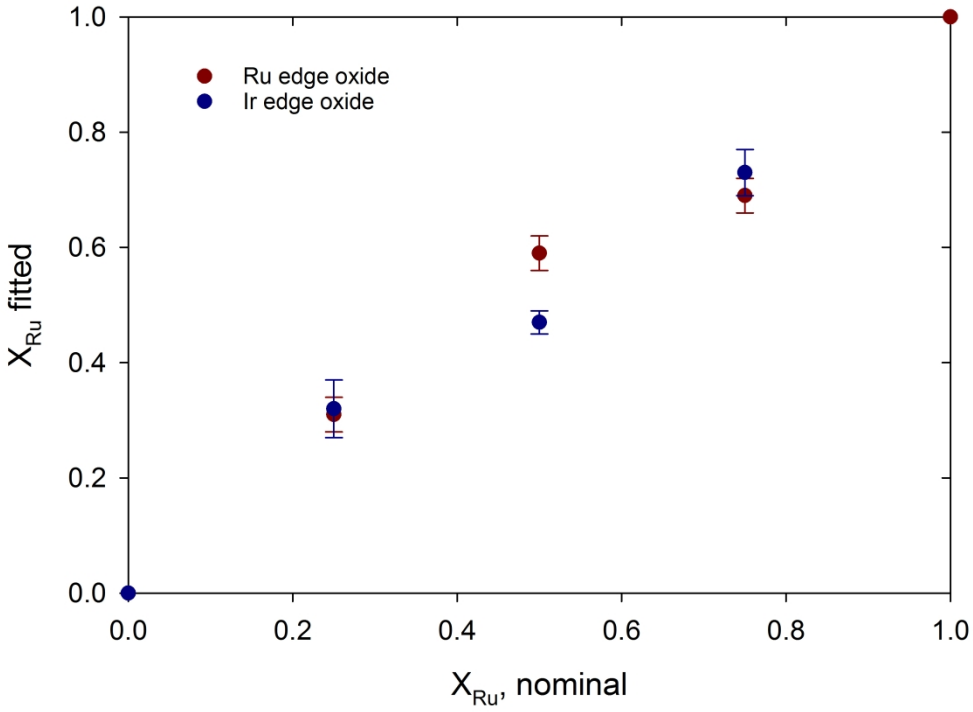

The obtained partial occupancy of Ru of (a) the oxide phase

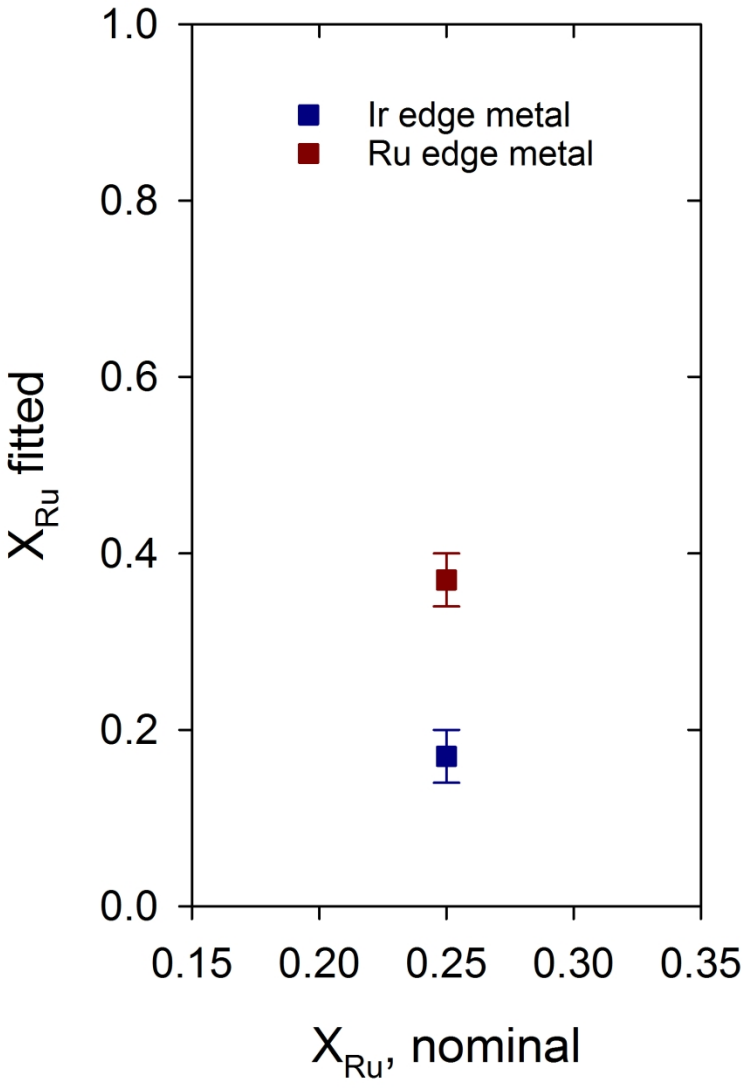

the metal phase evaluated from both Ir- and Ru-edges as function of nominal Ru fraction.

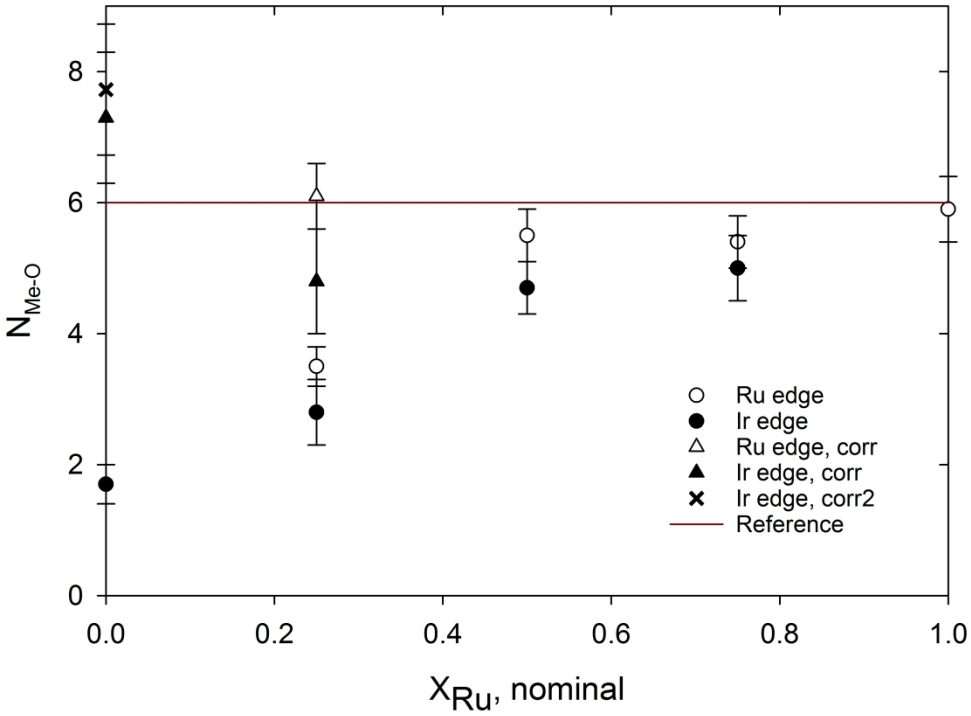

Experimentally obtained coordination numbers for (a) the oxygen shell, \revisedssone{N$_{\mathrm{Me-O}}$}

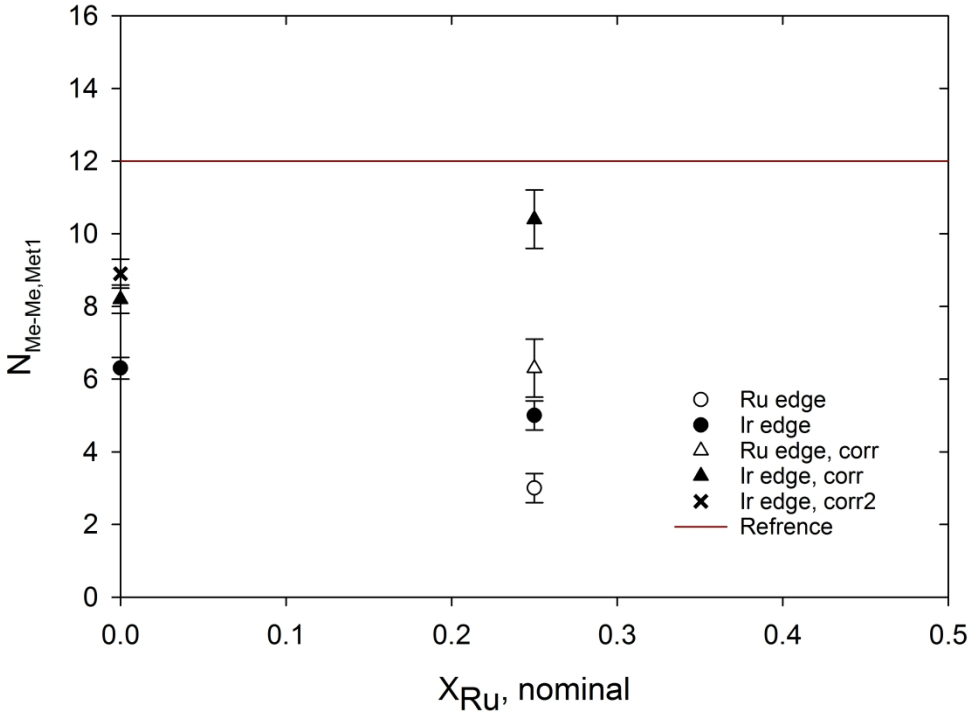

the first metal-phase shell, \revisedssone{N$_{\mathrm{Me-Me,Met1}}$},

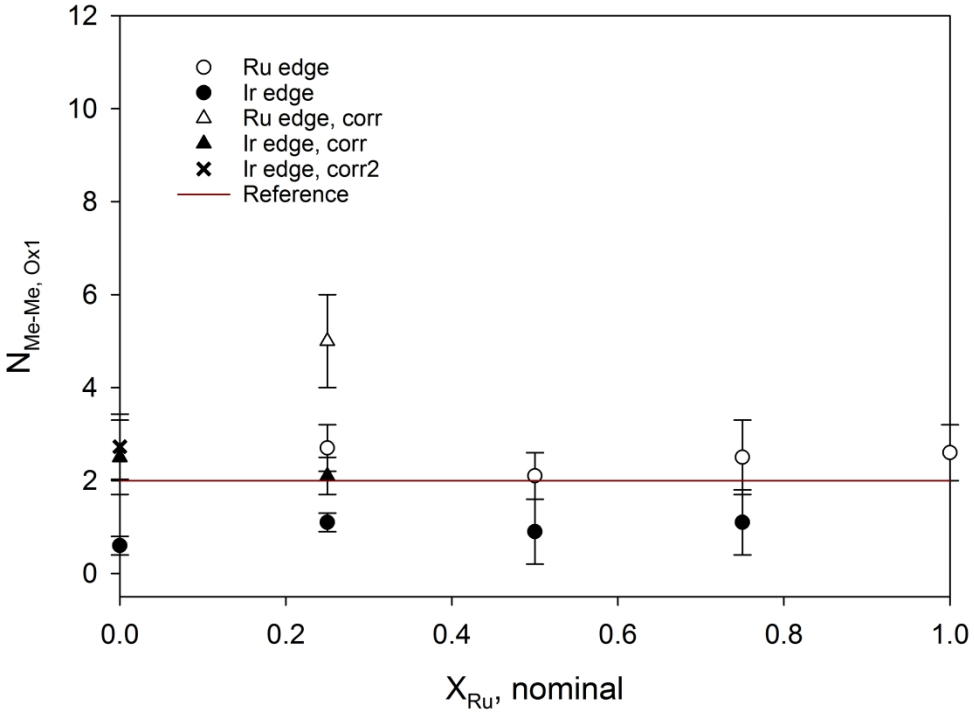

the first metal oxide shell, \revisedssone{N$_{\mathrm{Me-Me,Ox1}}$ (shell 3 in Table~\ref{tab:CNbondlengthpureoxides})},

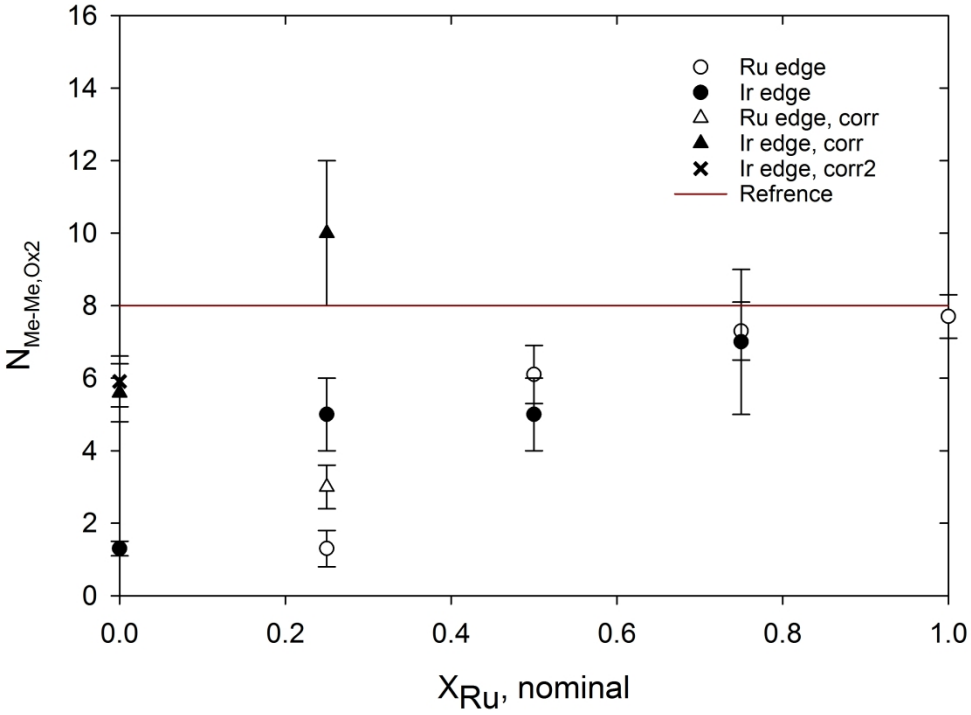

the second metal oxide shell, \revisedssone{N$_{\mathrm{Me-Me,Ox2}}$ (shell 4 in Table~\ref{tab:CNbondlengthpureoxides})}, as function of nominal ruthenium fraction. The reference coordination numbers are indicated with red lines in the figures. For phases which are mixes of oxide and metal-phases the corrected multiplicities are also included. For X$_\mathrm{Ru}$=0 different metal-phase fractions were obtained whether Ir^{+3} was included in the LCF of XANES or not, both are indicated. Fractions obtained without Ir^{+3} are named \revisedssone{``corr''} (triangles), and with named \revisedssone{``corr2''} (crosses).

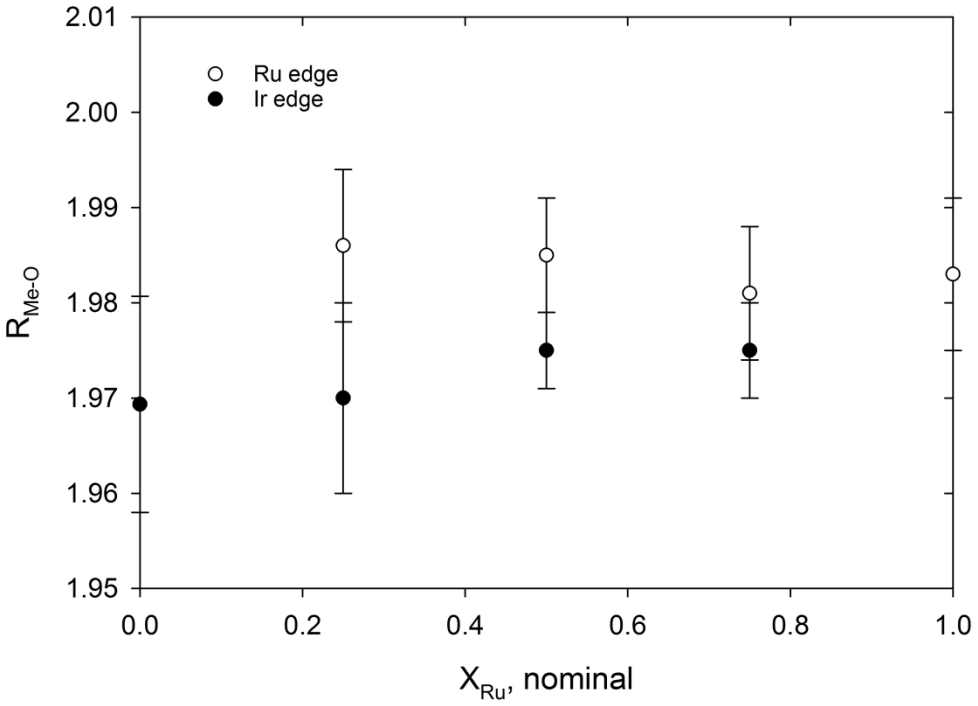

Experimentally obtained bond lengths in {\angstrom} for the (a) oxygen shell

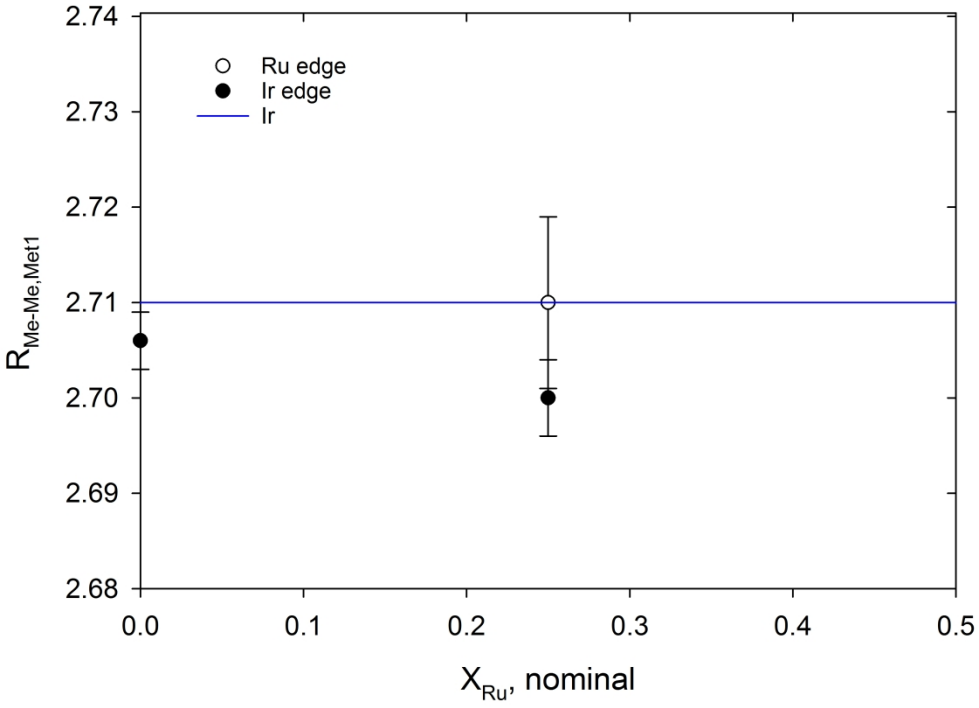

first metal-phase shell, \revisedssone{R$_{\mathrm{Me-Met1}}$}

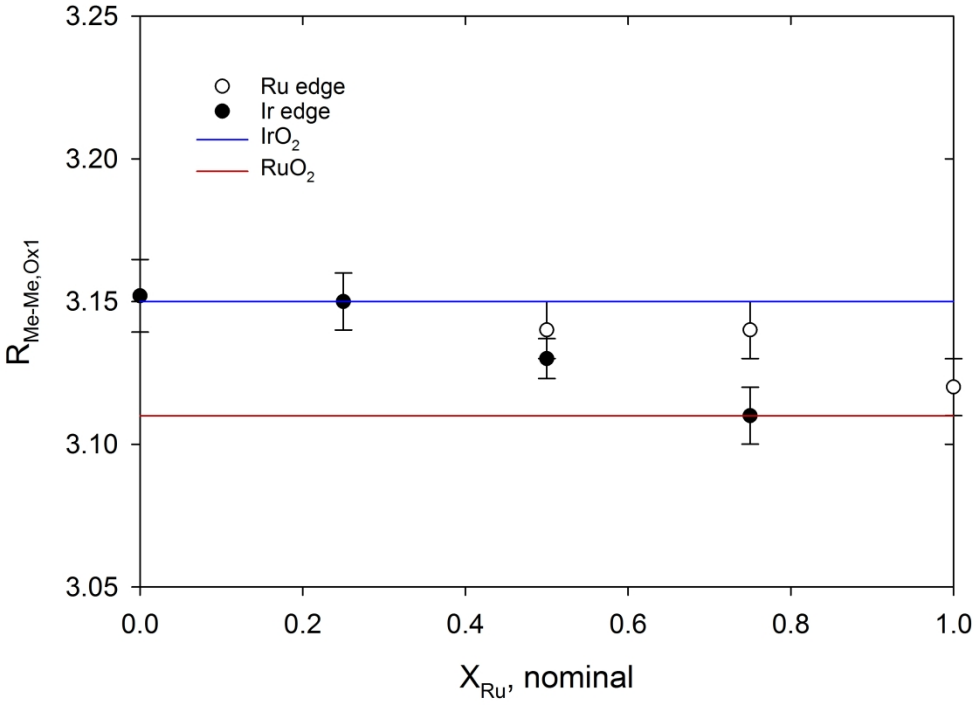

first metal oxide shell, \revisedssone{R$_{\mathrm{Me-Ox1}}$}

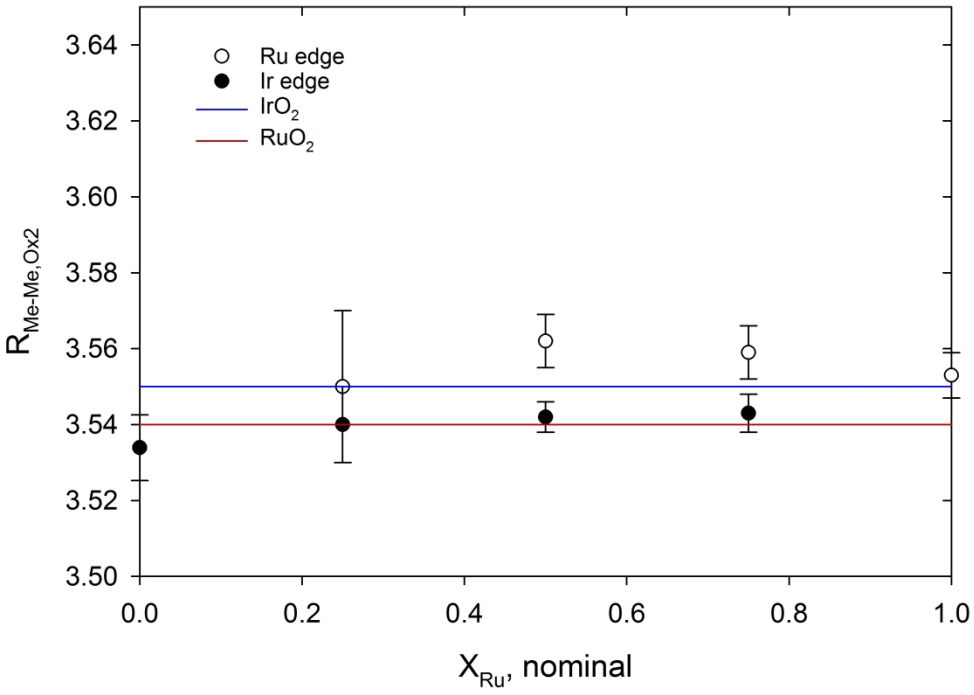

second metal oxide shell, \revisedssone{R$_{\mathrm{Me-Ox2}}$}, as function of nominal ruthenium fraction. The reference bond length is indicated in the figures for IrO$_2$ and Ir in blue and RuO$_2$ in red.

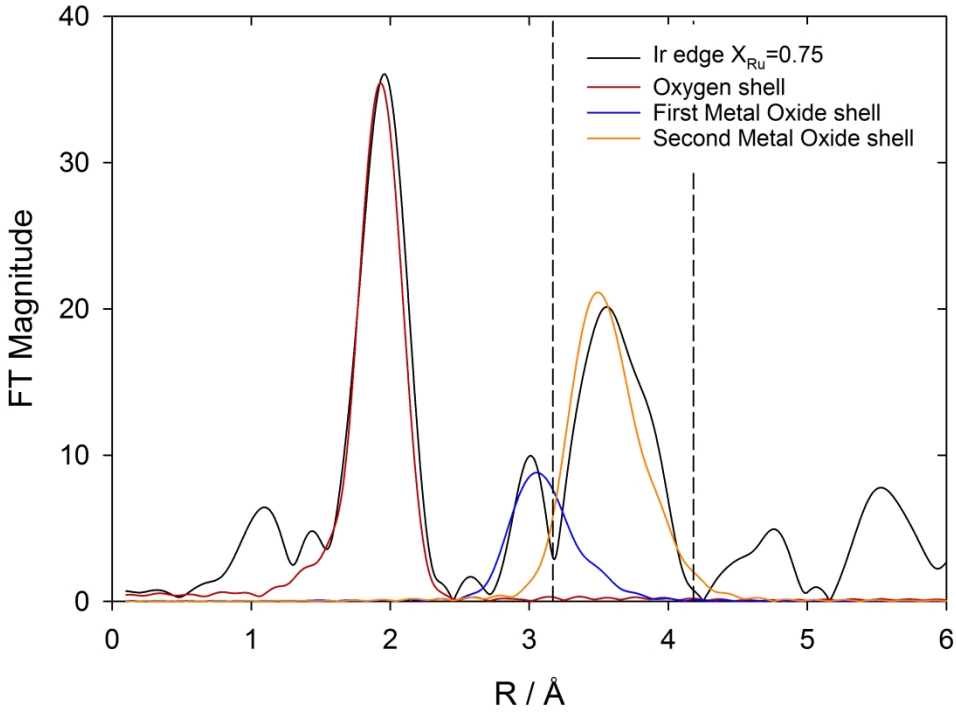

Contributions from individual shells for X$_\mathrm{Ru}$=0.75 recoded at Ir-edge.